POLITECNICO DI TORINO

Environmental and Land Engineering

Master's Degree Thesis

Statistical evaluation of drought indices in CMIP6 projections for the Mediterranean region

Supervisors

Prof. Jost Hardenberg

Candidate

Esmaeil Pourjavad

July 2024

ACKNOWLEDGMENTS

I would like to express my heartfelt gratitude to my supervisor, Professor Jost Hardenberg, for his unwavering support throughout this research. His deep-rooted expertise in the field and innovative approach to problem-solving have been invaluable, guiding me every step of the way.

I am also profoundly thankful to Dr. Bellomo for her insightful advice during the initial stages of this research. Her guidance helped shape the foundation of this study.

Special thanks go to my partner, Taraneh Rajabi, for her steadfast support through the ups and downs of this research journey. Her presence and encouragement have been a constant source of strength. I also wish to extend my deepest appreciation to my parents for their endless love and financial support throughout my academic path. Their belief in me has been my greatest motivation.

I am grateful to all the professors and administrative staff of the Department of Environmental, Land and Infrastructure Engineering at the Polytechnic University of Turin. Their dedication to education and research has provided me with the resources and environment necessary to complete this thesis.

Lastly, I extend my thanks to everyone who has contributed to this work, directly or indirectly. Your support has been crucial in the successful completion of this research.

Abstract

The Mediterranean region has recently become a critical hotpot regarding accelerated climate change, with an increasingly shifting pattern in precipitation and rising temperatures that, in turn, worsen the frequency and intensity of extreme events. Drought events are particularly important, as they are among the most severe and wide-reaching natural disasters involving significant socio-economic and ecological impacts. Strong projections of drought trends are urgently needed for active adaptation strategies, which will underline the need to assess the reliability of the climate models.

This study statistically assesses the capability of CMIP6 models to simulate drought characteristics in the Mediterranean zone. The Standardized Precipitation Index (SPI) was used as the primary metric for evaluating drought characteristics during both the historical period (1950-2014) and the future period (2070-2099). Reanalysis data from ERA5 served as the observational dataset for this research. The study focuses on the worst-case scenario (RCP8.5) to determine potential alterations in drought conditions in the future. Despite some inter-model variability, the multi-model mean analysis confirms an increase in the frequency of dry months in the present compared to 30 years ago, with a substantial projected growth for the last 30 years of the current century under high RCP8.5 emission scenarios. The results indicate a consistent increase in dry months frequency from northern Europe toward the Mediterranean Sea, highlighting that countries at significant risk include Italy, Greece, and those with Mediterranean coastlines.
This work evaluates the performance of CMIP6 models in realistically simulating historical drought characteristics and the statistical reliability of the signals over the Mediterranean region using a method called bootstrapping. This method ensures that the obtained signals are not false alerts and are not due to chance or any random populations.

Table of Contents

Chapter 1

Introduction

1.1 Climate Change in the Mediterranean Region

The Mediterranean zone, named for its proximity to the Mediterranean Sea, is characterized by a Mediterranean climate, also known as a dry summer climate according to the Köppen climate classification system[1]. This climate is characterized by hot summers, and wet winters standing alone from other climates. Geographically, the Mediterranean region contains areas located within the Mediterranean Sea basin. This includes countries such as Spain, France, Italy, Greece, Turkey, Egypt, Tunisia, Algeria, and Morocco, among others.

The Mediterranean climate strongly influences the weather patterns and climates of the majority of South European and North African countries. This region, home to approximately 542 million people, serves as a significant hot spot for climate impacts. This climate not only affects the temperature and precipitation patterns but also impacts the socio-economic sector of many countries[2].

Given the socio-economic importance of the Mediterranean region and the increasing vulnerability of its communities to climate change, there is a pressing need for comprehensive research and analysis. Future projections indicate that the Mediterranean climate will continue to undergo significant changes, with potentially far-reaching consequences for both human societies and the environment.

For these reasons and many others, studying the climate of the Mediterranean region and projecting its future is essential for policymakers. This will enable them to prepare and take actions to mitigate and adapt to any potential future challenges.

Figure 1.1: Map of the Mediterranean Sea and surrounding lands. In order to conduct a more thorough analysis, a particular geographic region within the Mediterranean region was selected. This area covers latitudes from 30.5 to 60.5 and longitudes from 0 to 40, therefore all models will accurately depict the Mediterranean region to better capture and study the patterns of precipitation in the Mediterranean region by choosing this slice of latitude and longitude [3].

1.2 Droughts in the Mediterranean

1.2.1 Drought Definition

The definition of drought, as outlined in the Sixth Assessment Report by the Intergovernmental Panel on Climate Change (IPCC), delineates it as a period of exceptional water scarcity affecting both ecosystems and human populations, primarily due to decreased rainfall and heightened temperatures [4]. This definition underscores the transient nature of droughts and emphasizes the role of precipitation deficiency and evaporation, distinguishing them from long-term aridity. Additionally, droughts can be exacerbated by human activities such as over-extraction of water resources and poor land management, further intensifying water scarcity and its impacts.

Moreover, droughts are characterized by a shortfall in precipitation, leading to

water scarcity across various activities [5]. This scarcity affects agriculture, reducing crop yields and leading to food shortages; it impacts water supply for domestic and industrial use, and can cause significant ecological damage by stressing water-dependent ecosystems.

Droughts can be categorized based on several parameters, including duration, intensity, and frequency, each warranting distinct treatment. Meteorological droughts, lasting from hours to a few weeks, primarily stem from precipitation deficits, affecting weather patterns and immediate water availability [6]. These short-term droughts can disrupt daily activities and influence short-term agricultural practices. Agricultural droughts, extending from three to nine months, significantly impact soil moisture, vegetation, and the agricultural sector, contingent upon additional precipitation deficiencies and soil moisture content [6]. These droughts can lead to reduced crop yields, increased soil erosion, and a decline in livestock productivity, causing significant economic losses for farmers and affecting food supply chains. Lastly, hydrological droughts, exceeding nine months, entail prolonged water shortages in streams or reservoirs, with profound implications for the hydrology of the region and posing formidable socioeconomic challenges [7]. These droughts can deplete water reserves, restrict water supply for domestic, industrial, and agricultural use, and cause long-term ecological damage.

Recent observations highlight a discernible trend towards a warmer climate across the Mediterranean Basin and its sub-regions, precipitating shifts in rainfall patterns and adversely impacting numerous Mediterranean ecosystems [8]. These drier conditions have not only fostered an uptick in extreme events like wildfires but have also expanded the regions susceptible to such occurrences. Consequently, there's a growing interest in comprehending drought events, encompassing their frequency, duration, and severity.

Since the 1980s, the Mediterranean region has witnessed atmospheric warming exceeding the global average, accompanied by a notable escalation in the intensity, frequency, and duration of temperature extremes and heatwaves, particularly during the summer months [9]. Projections indicate a continuation and exacerbation of these trends, driven by a combination of increased evaporative demand and modest reductions in precipitation. Models further anticipate a progression towards more severe, frequent, and prolonged droughts under moderate emission scenarios, with even graver repercussions under severe emission scenarios [10].

The Mediterranean region finds itself confronting significant vulnerability in the face of warming-induced challenges, including prolonged and intensified heatwaves, heightened drought risks in already arid zones, and amplified susceptibility to

coastal inundation [11]. Freshwater resources, crucial for agricultural sustainability a cornerstone of Mediterranean economies are under mounting pressure due to climate change-induced stressors and escalating agricultural demands. For instance, in Spain, 11 out of 15 river basin districts grapple with water stress attributed to agricultural usage, while Greece's primary agricultural region relies heavily on groundwater and faces similar challenges [12].

The population growth prevalent in Mediterranean countries further compounds the strains on food demand, as climate change threatens to undermine regional food production, necessitating augmented imports. Droughts, in particular, pose substantial challenges to densely populated urban hubs and coastal locales, exacerbating vulnerabilities among impoverished populations residing in substandard housing conditions [13].

1.3 Literature Review

The Mediterranean region is intensely vulnerable to changes in climate. Pronounced alterations to the precipitation patterns and rising temperatures are leading to more frequent and intense droughts. Therefore, projections of drought trends have a great necessity for the preparation of good adaptation plans. The focus of this literature review is mainly on a similar discussion, evaluating recent studies with a focus on how well CMIP6 models reflect the Mediterranean drought characteristics and what background it offers toward understanding the performance of these models in drought trend simulation and future climate scenarios.

After the release of the sixth version of CMIP models, limited studies have assessed the drought representation capacity. Spioni et al.(2020)[14] conducted one of the most comprehensive evaluations assessing CMIP6-based drought projections over Europe. Their findings suggest an increase in the frequency and magnitude of drought over Southern Europe and the Mediterranean basin. Using a multi-model ensemble is essential in this study to make robust projections with reduced uncertainties caused by individual models. Since two RCPs (Representative Concentration Pathway) were taken into consideration, 4.5 and 8.5, both SPI (Standard Precipitation Index) and SPEI (Standardized Precipitation-Evapotranspiration Index) were chosen in the measurement of their analysis, giving continued measurement to be compared in past and future projected drought conditions. They extensively used CORDEX simulations.

Douville et al.(2021)[15] conducted their research focusing on the hydrological cycle, with particular interest in the current state of the droughts based on the

CMIP6 scenarios; they emphasize a global scale. They reported a significant decrease in soil moisture and an increase in the number of extreme drought events under the RCP8.5 scenario. This study will lead to important conclusions about the amount of strategy among most adaptive strategies, particularly for risks in near-future global drought types.

H. Essa et al.(2021)[16] tried to address the physical properties of various drought types in near-future climates in the Mediterranean. They applied the multi-model mean of the bias-adjusted and downscaled product from five Earth System Models participating in CMIP6 under four shared socioeconomic pathways: SSP1–2.6, SSP2–4.5, SSP3–7.0, and SSP5–8.5; SPEI; and reanalysis "WFDE5" for the reference period 1980–2014. Their work proved that the projection depicts drought frequencies between ’12 percent and 25 percent for the period 2021–2060, depending on the region and the climate scenarios. It reveals an upward trend in the frequency of droughts, especially in southern countries rather than in the northern ones.

Papalexiou et al.(2020)[17] assessed the skill of 285 CMIP6 historical simulations, applying 17 models for reproducing drought duration and severity in three observation-based datasets using the Standardized Precipitation Index (SPI). They employed summary statistics and developed a new probabilistic framework based on the Hellinger distance to quantify the difference between the observed versus simulated drought characteristics. It remains true that no single model has shown consistent improvement in performance over large regions, but these studies highlight the importance of statistical evaluation of CMIP6 performance in drought simulation.

All researchers agree that droughts will become more severe and frequent in Southern Europe and the Mediterranean area within various scenarios and for different climate models. No study commented, however, on the reliability of such simulations or if signals of much higher frequency of droughts are even statistically reliable. Are these changes and trends significant, or would they occur again if the data were resampled entirely randomly?

To address these questions, in this paper, we use the well-established statistical approach called "Bootstrap". By applying the said methods, we evaluate the statistical reliability of CMIP6 model projections for drought characteristics in the Mediterranean region, where the observed trends are significant. It is within this framework that the following analysis will take place, providing critical insights into drought projection robustness and adaptation strategies for the mitigation of future drought impacts in the Mediterranean.

Chapter 2

Models and Datasets

2.1 CMIP6 climate models

2.1.1 What is CMIP?

CMIP stands for Coupled Model Intercomparison Project. it's a global modeling project and frame work used in climate research so that all scientists from all around the world would be able to better address the past and future of Earth's climate system. A climate model is a complex computer code that creates a digital analog to Earth. This model digitizes the processes and interactions between parts of Earth's climate system: the atmosphere, ocean, land surface, cryosphere, and biosphere. We use models to experiment with how future changes in human activities will impact the Earth's future climate, how much it warms, and how floods, droughts, and other extremes will change.However, many processes in our climate occur on such small scales, that models are not able to exactly represent them in models, and therefore some simplifications are required. How we simplify the climate system is unique to each model. Therefore comparing simulations from different models is useful for understanding which results are consistent across models, and which results are less agreed upon. Since 1995, CMIP has been coordinating this model intercomparison across the climate science community.

In practice global climate models operate in a grid system dividing earth's surface into discrete grid cells each representing distinct geographical area. The geographical grid sizes vary model by model and experiment by experiment. They use three-dimensional grids of cells, in both horizontal and vertical and since mathematical equations are computed at every grid point, and data is exchanged with adjacent cells to simulate the exchange of mass and energy throughout the system as time progresses. This approach allows us to be able to scale down for regional analysis as well. These resolutions can be altered by interpolation methods to a

coarser and finer resolutions.

This multi-model approach helps to evaluate climate models, leads to improvements in the model simulations and provides a better understanding of past, present and future climates. One additional strength of CMIP lies in its global infrastructure which has gathered the data and gives open access to a growing global research community.CMIP has grown from a modest scientific research initiative in the early nineties to become a global enterprise: more than 50 modeling centers around the world are participating in the sixth phase of CMIP, CMIP6. Many hundreds of scientific papers have already been published and the results are taken into account for policy decisions.

CMIP is a project of the World Climate Researcher Programme (WCRP), providing climate projections to understand past, present, and future climate changes. It is part of the WCRP Earth System Modelling and Observations (ESMO) Core Project, which was formed to coordinate all modeling, data, and observation activities across WCRP and its key partners.

2.1.2 Coupled Model Intercomparison Project 6

In this discussion the CMIP6 (last updated model) has been used to interpret the analysis and there are several clear updates in CMIP6 with respect to CMIP5 is that CMIP6 represents a substantial expansion over CMIP5, in terms of the number of modelling groups participating, the number of future scenarios examined and the number of different experiments conducted and These models are running a number of new and updated emission pathways that explore a much wider range of possible future outcomes than were included in CMIP5. So far Many modeling groups that contribute to CMIP6 (Coupled Model Intercomparison Project phase 6) have found a larger equilibrium climate sensitivity (ECS) with their latest model versions compared to the values obtained with earlier versions for CMIP5. [13]. CMIP6 includes over 100 models developed by more than 50 different modelling centers. A modelling center is a research institution or organization that specializes in creating and running climate models. Each center contributes its own unique models to the CMIP6 project, which allows for a diverse range of simulations and projections. These models vary in their approaches and methodologies, reflecting the expertise and focus areas of their respective institutions.

Typically, HighResMIP high-resolution CMIP6 projections have a horizontal resolution of about 25 km or less in the atmosphere and 10 km or less in the ocean. This is in contrast to more standard resolutions of approximately 100 km in the atmosphere and 50 km in the ocean seen in lower-resolution models.

CMIP6 simulations encompass two main categories: historical simulations and scenario future simulations. Historical simulations aim to reproduce the past climate conditions of the earth by forcing climate models with observed historical changes in atmospheric composition such as GHG concentration in atmosphere, land use, and aerosols with temporal coverage from 1850 to 2014 for these historical experiments and temporal resolutions can be vary from hourly to monthly. For CMIP6 projections and simulations they project future climate changes under different emissions scenarios driven by different socioeconomic assumptions These are the Shared Socioeconomic Pathways (SSPs).

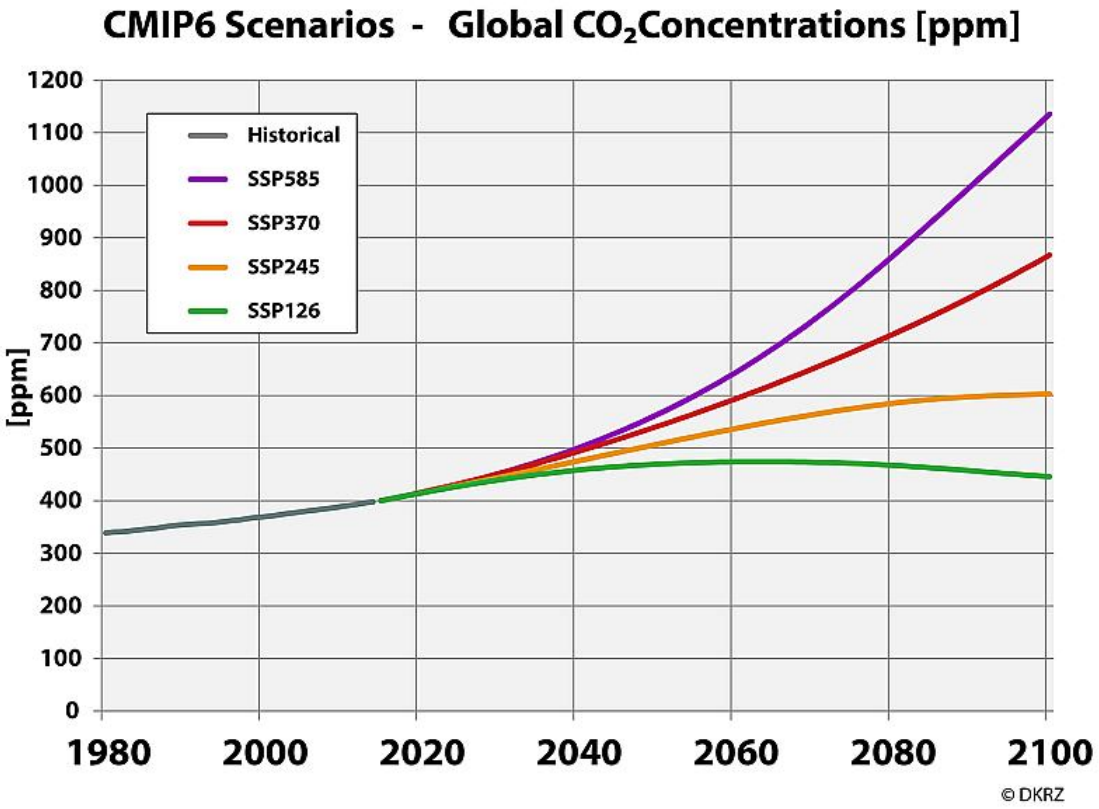

Figure 2.1: The gray line depicts the past increase in the mean CO2 concentration; the colored lines show the development of the mean CO2 concentration corresponding to the SSP scenarios [21]

The IPCC AR5 featured four Representative Concentration Pathways (RCPs) that examined different possible future greenhouse gas emissions. These scenarios – RCP2.6, RCP4.5, RCP6.0, and RCP8.5 – have new versions in CMIP6. These

updated scenarios are called SSP1-2.6, SSP2-4.5, SSP4-6.0, and SSP5-8.5, each of which result in similar 2100 radiative forcing levels as their predecessor in AR5 and Temporal coverage are from 2015 to 2100 for SSP experiments[22].

2.2 Materials

To meet the objective of assessing CMIP6 models in predicting drought, an observational dataset was necessary. For this purpose, ERA5, a dataset created by the European Centre for Medium-Range Weather Forecasts (ECMWF), was selected. ERA5 is a reanalysis dataset, meaning it integrates historical observations from diverse sources like weather stations, satellites, and ocean buoys with a numerical weather prediction model. This process produces a coherent and thorough depiction of Earth's atmosphere over a defined time span.

For this analysis, ERA5-Land monthly averaged total precipitation data spanning from 1950 to 2023 was chosen as observational data to evaluate CMIP6 historical simulations. ERA5-Land offers a consistent depiction of surface-level water and energy cycles over multiple decades, starting from 1950 and featuring a temporal resolution of 1 hour. The native spatial resolution of the ERA5-Land reanalysis dataset is 9km on a reduced Gaussian grid (TCo1279), but the data in the CDS has been regridded to a regular lat-lon grid of 0.1x0.1 degrees[15]. Total precipitation was selected due to its ability to encompass both large-scale precipitation driven by synoptic weather systems and convective precipitation generated by localized convection processes. This inclusive representation captures the entirety of precipitation events contributing to the water balance and potential drought conditions in a given region.

A table provided with all model's name and information in Table 2.1. The selection of the CMIP6 models was done in such a way that all the models are r1i1p1f1, which means they are the first realization (r1), using the initial condition (i1), physics (p1), and forcing (f1) configurations. This consistent selection ensures that the simulations are comparable and eliminates variability that could arise from different initial conditions, physics, or forcing scenarios, thereby providing a more reliable and standardized basis for analysis[23].

Table 2.1: List of models used for the study, modeling center, and variant label

Models	Modeling center
NorESM2-MM	Norwegian Climate Center
MRI-ESM2-0	Meteorological Research Institute
AWI-CM-1-1-MR	Alfred Wegener Institute
CanESM5	Canadian Centre for Climate Modelling and Analysis
CAMS-CSM1-0	Chinese Academy of Meteorological Sciences
TaiESM1	Research Center for Environmental Changes, Academia Sinica
IITM-ESM	Indian Institute of Tropical Meteorology
FGOALS-g3	Chinese Academy of Sciences
CAS-ESM2-0	Chinese Academy of Sciences
FGOALS-f3-L	Chinese Academy of Sciences
BCC-CSM2-MR	Beijing Climate Center
MIROC6	Japan Agency for Marine-Earth Science and Technology
E3SM-1-0	U.S. Department of Energy
E3SM-1-1-ECA	U.S. Department of Energy
E3SM-1-1	U.S. Department of Energy
IPSL-CM6A-LR	Institut Pierre-Simon Laplace
CIESM	Tsinghua University
ACCESS-CM2	Commonwealth Scientific and Industrial Research Organisation
MPI-ESM1-2-LR	Max Planck Institute for Meteorology
FIO-ESM-2-0	First Institute of Oceanography
CMCC-ESM2	Euro-Mediterranean Center on Climate Change
CMCC-CM2-SR5	Euro-Mediterranean Center on Climate Change
ACCESS-ESM1-5	Commonwealth Scientific and Industrial Research Organisation
EC-Earth3	EC-Earth Consortium
EC-Earth3-CC	EC-Earth Consortium
EC-Earth3-Veg	EC-Earth Consortium
EC-Earth3-Veg-LR	EC-Earth Consortium
CESM2	National Center for Atmospheric Research
CESM2-WACCM	National Center for Atmospheric Research
KACE-1-0-G	National Institute of Meteorological Sciences
NESM3	Nanjing University of Information Science and Technology

Chapter 3

Methodology

3.1 Climate Indices

To evaluate drought characteristics, the first step involves selecting a climate index, which provides a numerical representation of drought features and relies on climatic or hydrometeorological data such as precipitation, temperature, streamflow, and soil moisture. In this study, the Standardized Precipitation Index (SPI) was chosen for analysis. The SPI, a widely used meteorological drought index, compares precipitation anomalies to long-term climatological norms using empirical probability distributions. This approach allows for comparisons of dryness or wetness across regions with diverse climate patterns [24].

The Standardized Precipitation Index (SPI-n) is a statistical indicator that compares the total precipitation received at a specific location over an n-month period with the long-term rainfall distribution for the same duration at that location. Calculated monthly for a moving window of n months, where n represents the accumulation period, typically ranging from 1 to 48 months, SPI values like SPI-1, SPI-3, SPI-6, etc., are derived. For this study, the 6-month Standardized Precipitation Index (SPI-6) was selected, serving as a meteorological drought indicator for monitoring precipitation anomalies over 6-month accumulation periods. Unlike averaging over 6 months, SPI-6 considers precipitation from the current month and the previous five months, providing a cumulative measure over a rolling 6-month window. Thus, each SPI-6 value reflects the conditions over the preceding 6-month period .

Calculating the SPI involves fitting a probability density function to the frequency distribution of precipitation totals for a specific station or grid point over a given accumulation period. Typically, the gamma probability density function is

utilized for this purpose. The statistical parameters of the frequency distribution are determined based on a reference period, often spanning at least 30 years of precipitation data.

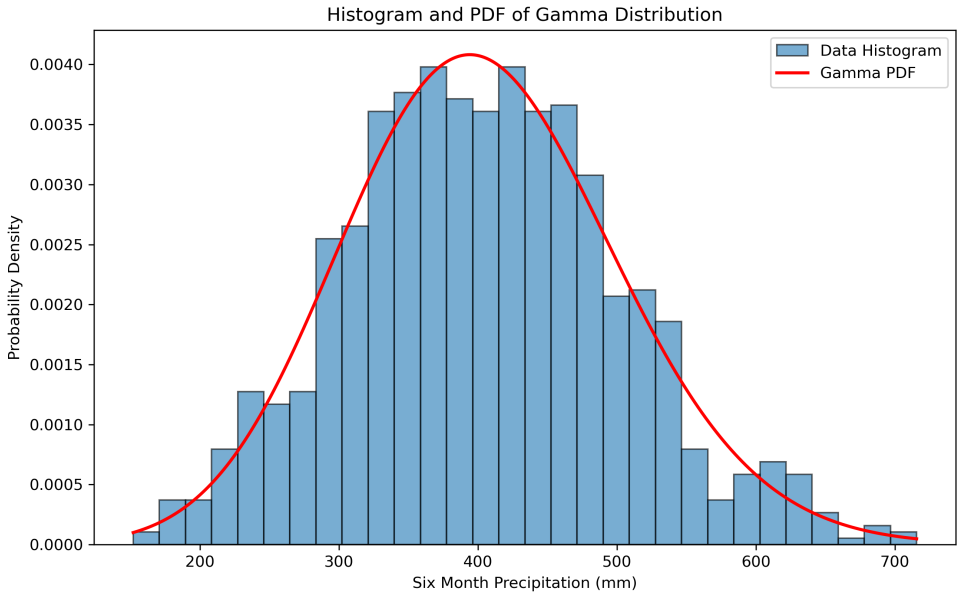

Figure 3.1: Histogram and Probability Density Function (PDF) of Gamma Distribution for Six-Month Precipitation Data. The histogram (blue bars) shows the frequency distribution of six-month precipitation values, while the red curve represents the fitted Gamma distribution, highlighting the probability density across the range of observed precipitation values.

Next, the parameters of the probability density function are employed to compute the cumulative probability of the observed precipitation for the desired month and temporal scale. This cumulative probability is then standardized to the normal distribution with a mean of zero and a variance of one, resulting in the SPI value. The process of transforming observed rainfall using the cumulative distribution functions (CDF) of the Gamma distribution and standardizing it to the SPI is depicted in the Figure 3.2.
Most global centers opt for the Gamma distribution as the basis for SPI calculations. This model, defined by only two parameters, offers substantial flexibility in shaping distribution, spanning from an exponential to a Gaussian form. What sets the Gamma distribution apart is its left-bound characteristic at zero, effectively eliminating the chance of negative precipitation values. Furthermore, its positively skewed nature, coupled with an elongated tail to the right, proves particularly

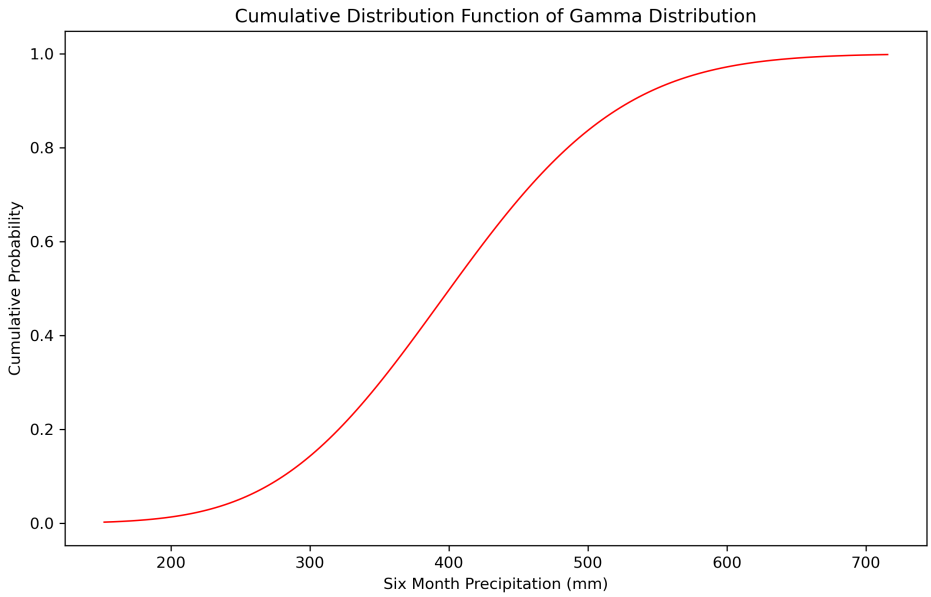

Figure 3.2: Cumulative Distribution Function (CDF) of Gamma Distribution for Six-Month Precipitation Data. The graph illustrates the cumulative probability (y-axis) of receiving a given amount of six-month precipitation (x-axis). The red curve represents the fitted Gamma distribution, indicating the cumulative likelihood of various precipitation levels.

advantageous for regions characterized by low mean precipitation and high variability. This attribute is especially crucial for SPI assessments in arid areas, where capturing extreme dry conditions accurately is paramount.
Drought events are identified when SPI values consistently dip below zero and reach a critical threshold of -1 or less, signaling the onset of dry conditions. These dry conditions persist until the SPI rebounds to a value of 0. While McKee et al. (1993) set the threshold for drought initiation at an SPI of -1 or lower, there's variation among researchers in selecting thresholds. Some may opt for a threshold slightly below zero, while others may classify drought at values below -1. In this study, a threshold below -1 has been chosen for identifying drought events.

The most beneficial of SPI calculation is that enables us to use a distribution parameter from one population dataset to compute SPI values for another dataset. The first dataset that we get our distribution parameters from is called the calibration period or reference period so once the distribution parameters are determined for the calibration period, they serve as a basis for estimating the SPI values for the

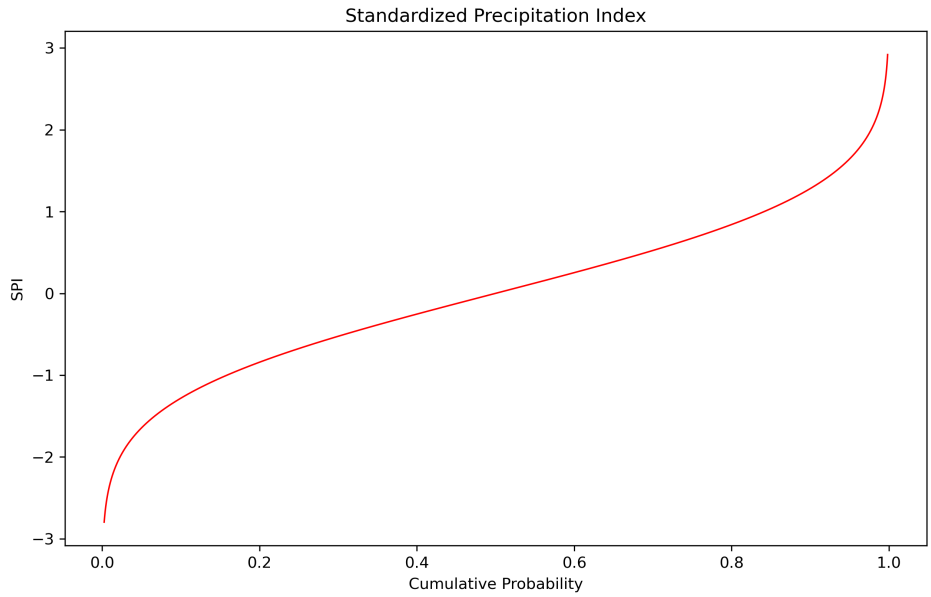

Figure 3.3: This graph shows the inverse of the Standard Normal Distribution's Cumulative Distribution Function (CDF) to transform the observed six-month precipitation data into a standard normal distribution.

second dataset , With these distribution parameters were calculated, SPI values can be computed for different datasets, even those with different time periods or locations. By applying the same distribution function and parameters to new datasets, SPI values are standardized, allowing for meaningful comparisons of precipitation anomalies across diverse regions and time frames.
For instance, consider a precipitation dataset from 1985 to 2014 that has a calibration period from 1950 to 1979. This dataset reveals that the baseline or reference conditions for that particular area are established using historical precipitation data from 1950 to 1979 when calculating the SPI. The parameters of the gamma distribution function that best characterize the precipitation patterns throughout the calibration period are estimated using this period as a base. Through this procedure, the historical variability and precipitation patterns for the particular location under study are reliably reflected in the SPI results.

3.2 Pre-processing of the data

Both the historical models and the observational ERA5 data require pre-processing of the data before the SPI-6 values can be computed. For analysis and interpretation to be useful, it is imperative to ensure a same standard format in terms of both temporal and spatial characteristics. The data's temporal resolution must first be aligned, which is crucial. To guarantee uniformity in the time steps utilized for analysis, this entails harmonizing the time intervals across all datasets. In this way, the data can be efficiently compared and synchronized for precise SPI-6 value computation.
Furthermore, methods for data quality control are put in place to find and address any anomalies or inconsistencies that may exist in the datasets. To guarantee the accuracy and dependability of the data used for SPI computation, this may entail eliminating outliers, fixing mistakes, and interpolating missing values.

The Max Planck Institute for Meteorology's CDO library utility provides a set of command line operators for basic climate data processing, making manipulation of the data easy and efficient for spatial conversion needs[20]. Additionally, the smmregrid python library utility is used to improve processing performance and maintain weight integrity. In contrast to CDO, smmregrid applies pre-calculated weights within CDO using sparse matrix multiplication rather than being an interpolation technique.

The latitude and longitude spatial dimensions are interpolated onto a grid with a consistent resolution of 1° x 1° in all models. The average grid resolution of all models was found to be very near to 1°, which led to the decision to regrid into a coarser resolution. Bilinear interpolation is computationally efficient and only uses four surrounding grid points, hence it is preferred over finer resolutions. Bicubic interpolation, on the other hand, uses 16 surrounding points and adds complexity without significantly increasing accuracy. It was determined that the most appropriate option for preserving accuracy and consistency among models is the cautious remapping approach, which takes into account all source grid points.

Additionally, we need the third dimension time to be constant across all of the models. For this reason, the analysis can be broadly divided into two sections: historical analysis and future analysis of CMIP6 simulations of drought characteristics. For the historical portion, a time coverage spanning from 1950 to 1979 is taken into consideration as a baseline or reference period, and a time coverage spanning from 1985 to 2014 is used to examine changes in the precipitation pattern relative to the reference period. WMO (2012) recommended taking into account at least 30 years of continuous monthly precipitation data, which is valid in our analysis. for

the analysis in the future To determine how precipitation might change throughout a 30-year period from 2070 to 2099 at the end of the century, the second era (1985–2014) can be utilized as a reference.

3.3 Precipitation data from models

A Preliminary study was done on the average yearly values over a 30-year period of the models' simulated precipitation patterns. Comparing these simulated values to matching averages calculated from ERA5 precipitation data was the aim of the study. Overall, with a difference of about ±2 mm/month, the mean average precipitation values derived from the models were found to be similar to those from ERA5. Still when the models were examined more closely using the accompanying Figure 2.5 as a visual aid, significant differences between them were found. In example, some projections overstated the deficiencies in precipitation, especially in the summer, especially in July.

It is noteworthy that although these discrepancies among simulations are expected, the models were not subjected to any bias adjustment. Since SPI is a normalized index of precipitation deficit, these impacts can be ignored in SPI analysis. The only goal was to see how CMIP6 models would replicate precipitation patterns.

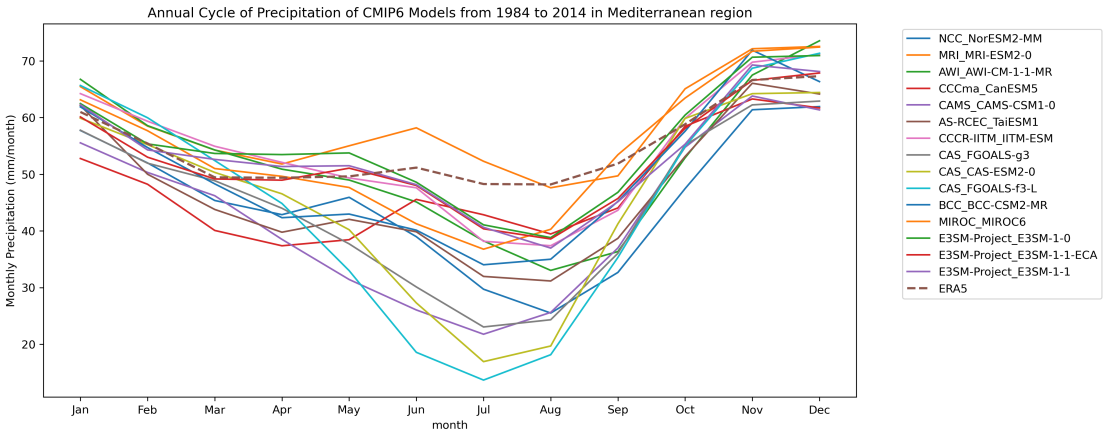

Figure 3.4: Annual cycle of precipitation from CMIP6 models and ERA5 for the period 1984 to 2014 in the Mediterranean region.

The Figure 3.4 represents the annual cycle of precipitation for different CMIP6 model simulations with observed ERA5 data over the Mediterranean region from

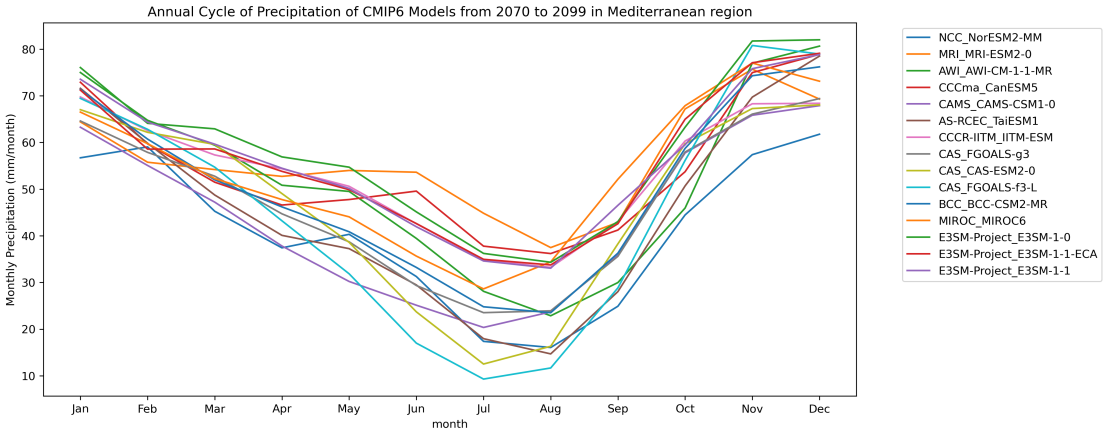

Figure 3.5: Annual cycle of precipitation from CMIP6 models for the period 2070 to 2099 in the Mediterranean region under 8.5 scenario

1984 to 2014. The colored lines show CMIP6 models, and the dashed line refers to the ERA5 observational data. This allows us to determine how good the models are and how close they come to the observed seasonal patterns in precipitation. For some models, this overestimation of the precipitation deficit, especially during the summer months, June to August, carries out a steeping deviation from ERA5 that suggests an overestimation of the dry condition. On the contrary, other models depict precipitation trends more or less mimicking the ERA5 data and thus represent the observed seasonal cycle better. About the comparison of the ERA5 results to some of the model simulations, this will underscore which models might be more robust toward future projections in the region. Understanding these discrepancies is an essential key for better model performance in climate projection studies.

3.4 SPI and Drought

3.4.1 SPI time series

The Standardized Precipitation Index (SPI), which has a mean of zero and a standard deviation of one, is used to assess drought based on precipitation excess or deficit, as was covered in the section on climatic indicators. SPI values typically fall between -3 and +3. A threshold of -1 was chosen for this discussion, designating as dry months any month with SPI values less than -1.

It's possible that monthly precipitation anomalies don't always indicate the presence

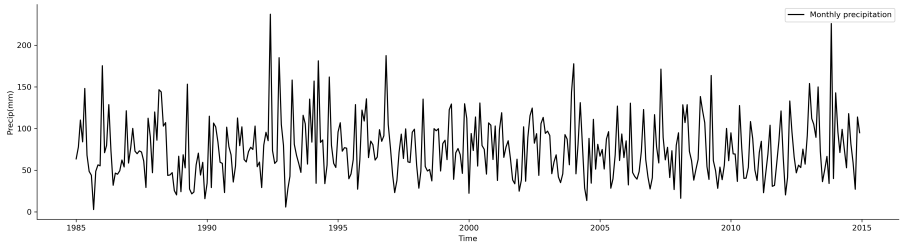

Figure 3.6: Monthly precipitation anomalies for a specific coordinate in the Mediterranean region from 1984 to 2015.

of a drought. On the other hand, the matching SPI values provide a clearer picture of the wet and dry seasons. Key drought features, including intensity, length, and the number of dry months for each location, can be interpreted using SPI analysis. Because of this, it's a useful tool for comprehending and tracking drought.

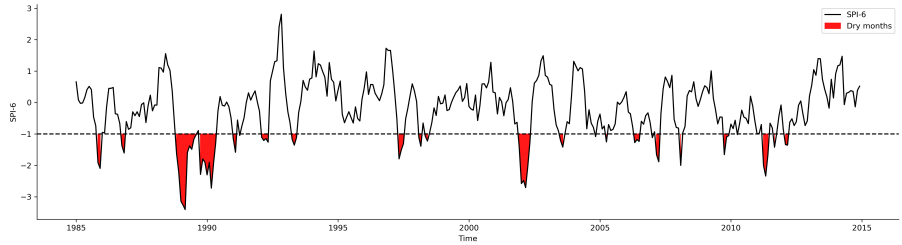

Figure 3.7: Identification of dry months based on the Standardized Precipitation Index (SPI-6). The plot shows the SPI-6 values over time, with values below -1 (indicated by the red shaded areas) representing dry periods.

The SPI does, however, have certain drawbacks. Notably, while evapotranspiration is predicted to rise in the future, its applicability in estimating future drought changes is limited due to the exclusion of this factor. Also, the SPI does not represent true variations in the statistical characteristics of precipitation when comparing model simulations with observations. Therefore, two time series may produce very different SPI values but similar results overall. Because of its ease of use it simply requires precipitation data and its capacity to distinguish between wet and dry periods, the SPI continues to be the most used drought indicator in spite of these shortcomings. Additionally, compared to other commonly used drought indicators like the Palmer Drought Severity Index, the SPI is more comparable across various locations.

3.4.2 SPI Spatial Distribution

Because the datasets are three-dimensional, each coordinate in the Mediterranean region has to have its SPI calculated. By using this technique, the final SPI representation is guaranteed to be a comprehensive map of SPI values, where each grid point represents an SPI value for a certain month of the year. This leads to a detailed and thorough geographic examination of drought conditions. ERA5 observational monthly precipitation data are used to offer an example of how SPI values depict drought conditions regionally in Figure 3.8. This graphic provides a clear visual representation of the severity of the drought for a given month in the Mediterranean area.
To create these SPI maps, the Cartopy mapping library in python was used, which includes features such as country boundaries to enhance the geographical context. Notably, ocean regions were not masked in this research. This choice was taken in light of the knowledge that seas have a big impact on drought conditions. For example, a dry spell over the Mediterranean Sea can change local climatic patterns and moisture availability, which can have a major effect on neighboring land regions. Representing three-dimensional data in a two-dimensional map format requires careful consideration of grid resolution. A 1° x 1° grid size is commonly used as a standard for regional climate studies, including those focused on the Mediterranean area.
Figure 3.8 is an illustration of how the Standardized Precipitation Index is distributed in space for August 2003, which is calibrated in period 1950-1979. It has been selected to show the diversity in dry and wet months across the Mediterranean Basin. The blue colors indicate wetter-than-average conditions, while red colors indicate drier-than-average conditions. The SPI values help to identify regions experiencing significant deviations from typical precipitation patterns for the selected month.

3.5 Reference Drought Signal

The aim of this analysis is to examine how models represent drought conditions in past and future forecasts, as was indicated in the section on climatic indicators. In order to compute SPI values in relation to a baseline climatology spanning from 1950 to 1979, we utilized the historical analysis to compare the ERA5 observational data from 1985 to 2014. This baseline era serves as a benchmark for assessing the degree of human forcing-induced changes in climate and drought since it is typical of preindustrial circumstances in historical simulations.
By examining the ERA5 reanalysis precipitation data, we can observe how drought conditions have evolved from the baseline period (1950-1979) to the more recent period (1985-2014). This analysis allows us to establish a clear and valid signal of

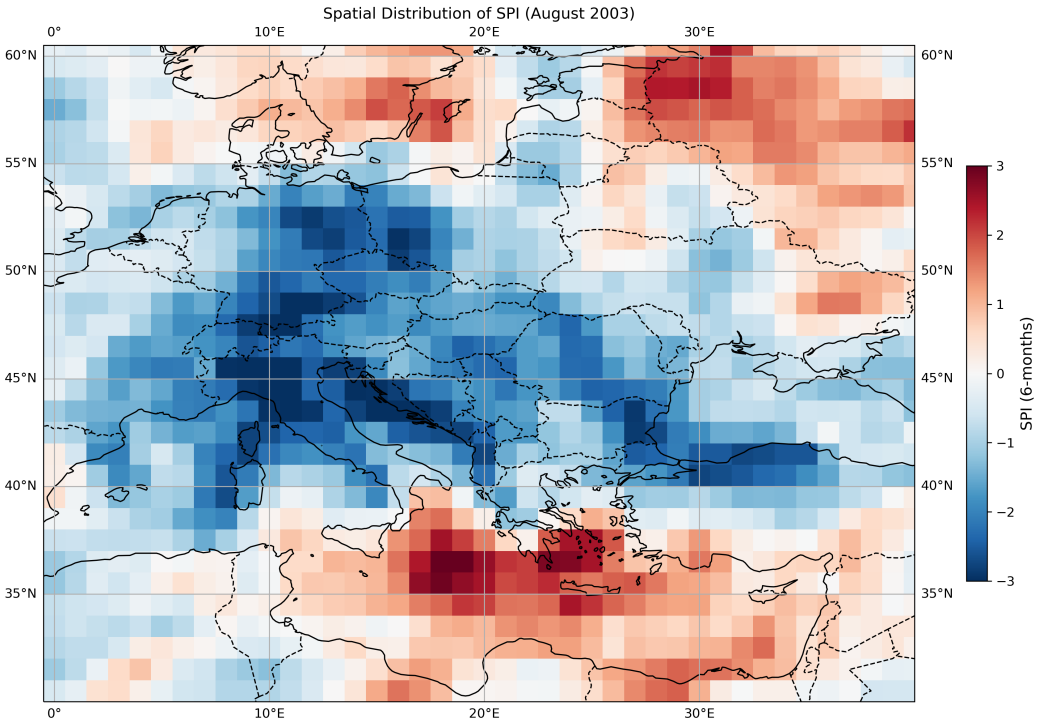

Figure 3.8: SPI-6 values for Mediterranean region for August of 2003 as an example derived from monthly precipitation of ERA5

drought changes over time. The ERA5 data provides a comprehensive and consistent representation of atmospheric conditions, which is crucial for understanding real-world drought patterns and their temporal shifts.
By comparing it to the CMIP6 simulations, we can evaluate how well the models capture the observed changes using this distinct signal from the historical past. As seen in the ERA5 data, comparable patterns and indicators of drought conditions are anticipated to be captured by the CMIP6 models. In order to assess the models' accuracy and dependability in modeling drought under historical conditions and thus increase trust in their future forecasts, this comparison is essential.

To assess changes in drought occurrence, SPI-6 values were computed for two periods of ERA5 data using the following steps:

For this purpose, SPI-6 values for ERA5 in the period 1950-1979 were calculated by fitting a gamma distribution to the monthly precipitation data and deriving the distribution parameters. Then, the same distribution parameters from the 1950-1979 period were utilized to calculate SPI-6 values for ERA5 in the subsequent

period of 1985-2014.

To analyze drought frequency, a threshold of -1 was defined to identify dry periods. Months with SPI-6 values below this threshold were considered dry, and the number of dry months was tallied across the entire time span for both periods (1950-1979 and 1985-2014).

Finally, the count of dry months in the 1985-2014 period was subtracted from the count for the 1950-1979 period for each pixel, revealing changes in drought frequency. This comparison highlights shifts in drought occurrence over time.

When examining the number of dry months in ERA5 during the periods 1950-1979 and 1985-2014 separately, distinct patterns emerge. As anticipated, the analysis for the earlier period shows a relatively uniform distribution of dry months across the Mediterranean area, However, this result is expected and primarily serves as a baseline for comparison Figure 3.9. Conversely, the examination of ERA5 data

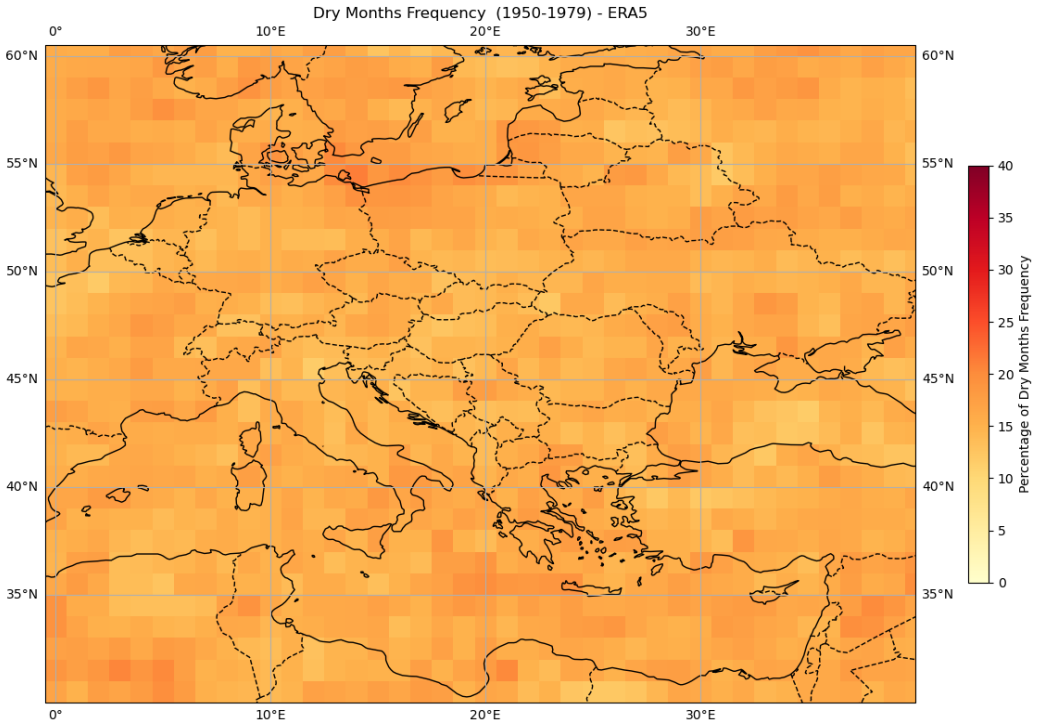

Figure 3.9: Spatial distribution of dry months frequency from 1950 to 1979 over 30 years period based on ERA5 data. Since the distribution of dry months follows a Gaussian distribution, 16% of the observations (months) fall below one standard deviation from the mean (-1σ) in the left tail of the distribution.

from 1985-2014 reveals notable fluctuations in the number of dry months across different geographical locations. This variability underscores the dynamic nature of drought occurrence during this period, with some areas experiencing a significant increase in dry months while others show a decrease (Figure 3.10).

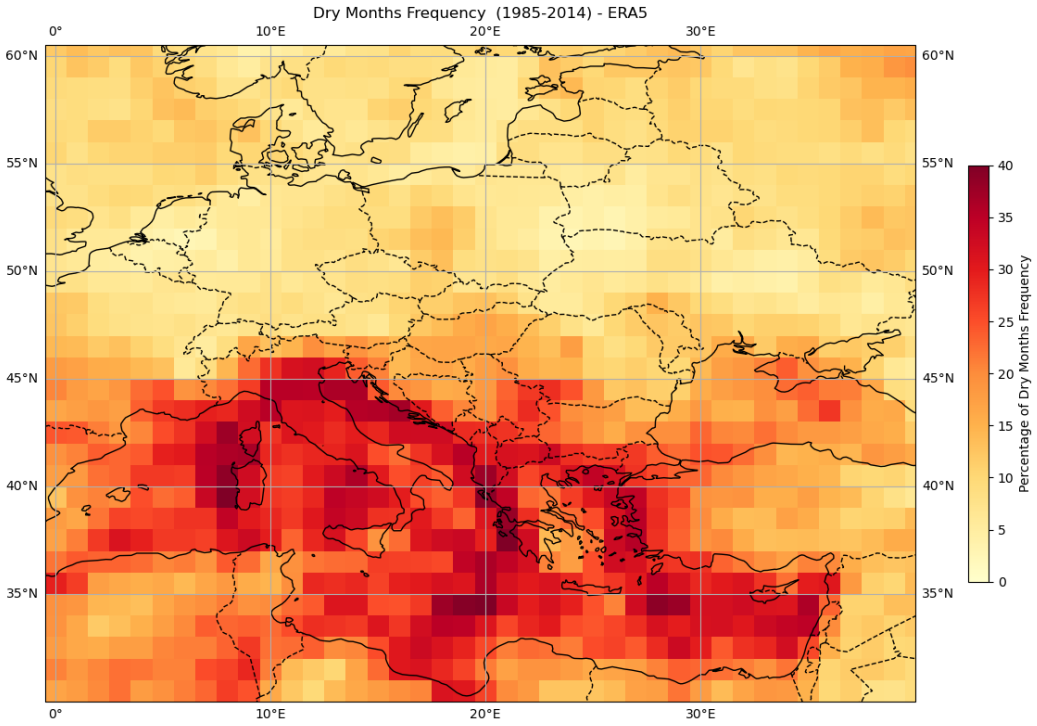

Figure 3.10: Spatial distribution of dry months frequency from 1985 to 2014 over 30 years period based on ERA5 data.

When compared to the reference era of 1950–1979, the ERA5 reanalysis data offers strong evidence of a notable rise in the frequency of drought occurrence in the Mediterranean area, especially in recent decades. Greece and Italy, two nations that border the Mediterranean Sea, are among those where this trend is most noticeable. The data shows an almost 30 percent increase in the frequency of dry months, suggesting a long-term trend in these locations' climate toward drier conditions (see figure 3.11).
In addition, the drought frequency's spatial distribution reveals a clear gradient effect, with southern regions going through longer and more frequent dry spells than their northern counterparts. As we move to higher latitudes, the number of dry months decreases significantly. This latitudinal gradient highlights the varying impact of changing climatic conditions across the Mediterranean region, with southern areas like Greece, and Italy experiencing a more pronounced increase

in drought frequency compared to northern regions. This pattern indicates that southern Europe is becmming increasingly vulnerable to prolonged dry periods, whereas northern areas are less affected.

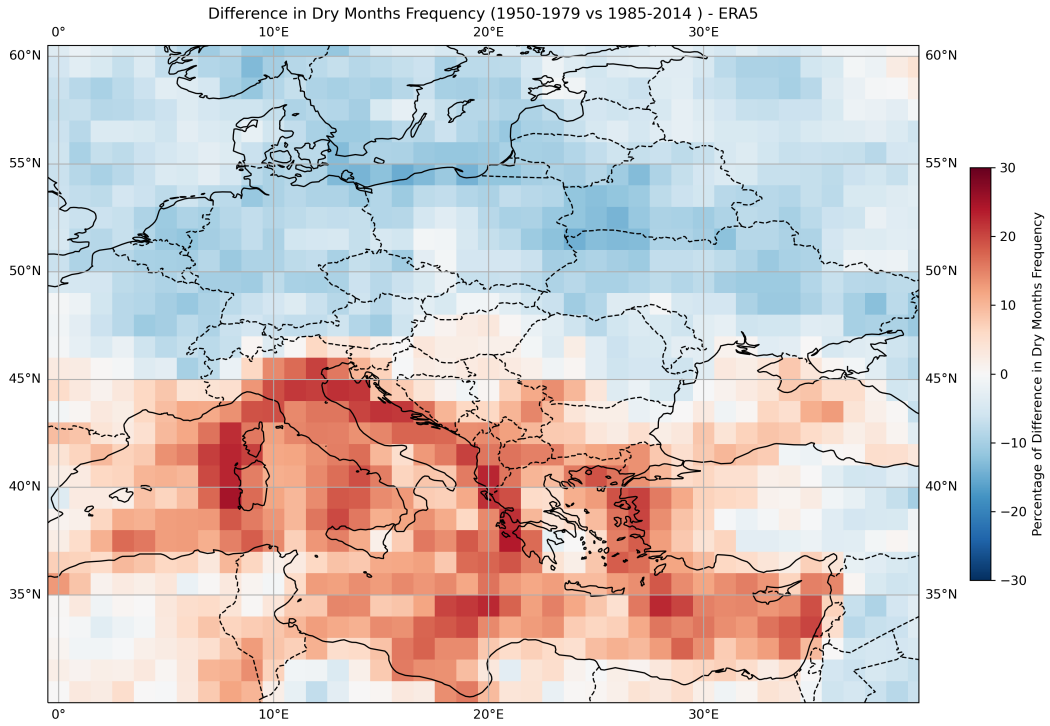

Figure 3.11: Difference in dry months frequency between the periods 1950-1979 and 1985-2014 based on ERA5 data. The color bar indicates the percentage change in dry months frequency, with red shades representing an increase and blue shades representing a decrease.

3.6 Bootstrapping

Bootstrapping is a fundamental statistical method that revolutionized the approach to data analysis and inferential statistics. In this method, introduced in 1979 by Bradley Efron, sampling distribution estimation for almost any statistic is possible using simple resampling methods. The most important and valuable property of bootstrapping is that it is a non-parametric method and requires no assumption about the form of the population from which the sample might be coming.

The concept of bootstrapping can be linked to the late 1970s when Bradley Efron pinpointed the weaknesses in existing statistical methods that relied predominantly

on parametric assumptions. He outlined a procedure that involves drawing observations from the observed data by replacement, creating a huge number of pseudo-datasets. This method made it possible to estimate the empirical sampling distribution of a statistic without having to assume any distributional form.

This seminal paper by Efron (1979)[25], "Bootstrap Methods: Another Look at the Jackknife," led to the inception of bootstrapping and opened a new way of statistical analysis. Ever since, the method has been polished and further extended into a firm set of tools that are now extremely useful across almost all fields of research.

The bootstrapping process is relatively simple and comprises the following vital steps: Resampling involves generating a large number of bootstrap samples from the original dataset by drawing with replacement. Each bootstrap sample is the same size as the original dataset but may have duplicate observations. Calculating a statistic entails determining the statistic of interest, such as the mean, median, or regression coefficient, for each bootstrap sample. Distribution estimation is achieved by applying the distribution of the bootstrap statistics to approximate the sampling distribution of the statistic. Inference is derived from the bootstrap distribution to obtain confidence intervals, standard errors, and p-values for hypothesis testing. This method is particularly useful when working with small sample sizes or when the theoretical distribution of the statistic is unknown. It provides a non-parametric way to estimate the variability and distribution of a statistic, which is essential for making robust statistical inferences [26].

One of the most widely used applications of bootstrapping is in climate science to evaluate the significance and reliability of model signals. Climate models are quite elaborate and often result in significant variability in their outcomes. Therefore, the application of bootstrapping helps evaluate the statistical significance of observed changes or predicted future changes in climate variables such as temperature, precipitation, and wind patterns.
For example, when assessing projections related to drought conditions from climate models, researchers would use bootstrapping to generate a large number of bootstrap samples from the model outputs. For each of these bootstrap samples, they would calculate the mean duration or severity of drought conditions. This process would produce a distribution of these mean values, which could then be employed to estimate confidence intervals or conduct hypothesis tests concerning future drought occurrences.

The use of bootstrapping also provides insight into the uncertainty associated with climate model predictions. Given the great complexity and inherent biases

in climate models, bootstrapping offers a robust methodological framework for quantifying the variability and reliability of model outputs. This approach is particularly valuable for making more reliable and accurate predictions in the context of climate science [27].

Bootstrapping is used as an alternative to traditional statistical methods because of the following distinct advantages. One significant benefit is its non-parametric nature. Since bootstrapping makes no assumptions regarding the nature of the data, it is very flexible and applicable to a large number of problems. Additionally, it can be applied in cases where traditional methods are inapplicable due to the complexity of the statistics and the estimators involved. The method is also easy to implement with modern computational tools and software, making it accessible to researchers in all fields. Furthermore, bootstrapping is essentially immune to violations of assumptions such as normality and homoscedasticity, which are often problematic for parametric methods [28].
Even though bootstrapping has numerous advantages, there are a few drawbacks to the approach. Bootstrapping can be computationally intensive, especially if the dataset is extensive or if the model being used is highly complex. It requires significant computing power to generate many bootstrap samples and compute a statistic for all the samples. Moreover, the quality of bootstrap estimates depends on the nature of the original sample. If the original sample is biased or not representative of the population, then the bootstrap estimates will also be biased. Sometimes bootstrapping can lead to overfitting, especially when dealing with small sample sizes, as resampled datasets may not adequately represent the variability of the population.

Early in this research, it was discussed that drought frequency would be evaluated based on monthly precipitation data. To determine whether the signals from the CMIP6 models in both the historical period and scenario projections were significant or merely occurred by chance, a bootstrapping method was applied. This method involved selecting 30 random years of precipitation data for each of the 31 CMIP6 climate models. For the historical period, spanning from 1950 to 2014, this random selection ensured a robust analysis by capturing a wide range of possible climatic conditions.

For each climate model, two random models were required: one served as the reference model, and the other was calibrated based on the first model. It was critical to ensure that no pair of models shared the same year of data, thereby maintaining the independence and validity of the bootstrapping process. This step was crucial to prevent artificial correlations that could bias the results.

Furthermore, each random model contains a different 30-year block of precipitation data, ensuring that the historical variability was captured without overlap between the paired models. This selection without overlaps between the paired models has captured the historical variability, allowing for a comprehensive analysis of drought frequency signals. The random year selection is independent for each model, ensuring that the historical variability is well represented across all models.

This procedure was iterated 1000 times, yielding 1000 pairs of models or a total of 2000 random models of precipitation data. This large number of resamples provides the conditions for a robust estimation of the sampling distribution, allowing meaningful statistical inference from the results at hand. The full extent of natural variability is captured, thereby providing a solid foundation for evaluating the significance of the observed drought frequency signals.

After obtaining 1000 pairs of random models, the precipitation data from the first model in each pair was used as a reference level to calculate the SPI-6 values for the second random model. This process was repeated for each pair of random models, ensuring consistency with the methodology applied to the original CMIP6 models' data.
By using the first model in each pair as a reference, the difference in drought frequency could be determined. Specifically, the number of dry months in the second model was subtracted from the number of dry months in the first (reference) model. This calculation provided the final output, which was the difference in drought frequency between the two models.

This allows for the method used for the original CMIP6 models to be carried forward and makes a meaningful statistical evaluation possible. Through a comparison of drought frequencies from the randomized paired models, insights were drawn about the significance of changes in observed drought frequencies.

A similar process was then applied to the future projections of the CMIP6 models for randomly selected years between 1985 and 2014 and 2070 and 2099. As such, the reader can see that direct comparison was made between the randomly generated models for the scenario projections and the original CMIP6 model results. By this approach, the random results were synchronized with the original models' timescale, allowing for a meaningful comparison of the respective drought frequency changes of the original models and random ones simulating outcomes of the same climate model under the same climate scenario.

After obtaining all the random models for the 31 original CMIP6 models, the final output consisted of 1000 random drought frequency values for each pixel grid

of our data. These 1000 random values for each grid cell formed a distribution, allowing the probability of the original drought frequency value for the corresponding grid cell to be assessed within this randomly generated distribution.
This distribution served as a reference to determine whether the original drought frequency values were statistically significant or merely a product of random variability. By comparing the original drought frequency values to the distribution of the 1000 random values, it was possible to calculate the probability that the observed drought frequencies occurred by chance.
In turn provided a robust statistical context within which the impact of the changes in drought frequency could be judged, ensuring that the results were sound and reliable given the scatter represented by the bootstrapped distributions.

Evaluating the significance of a drought signal in this study was conducted by determining a confidence interval for the distribution of random values generated through bootstrapping. Specifically, if the original drought frequency value exceeded the upper 97.5th percentile of this distribution, it indicated that the observed value fell within the upper 2.5% tail of the random values Figure 3.12. This statistical threshold was used to assess the rarity of the observed signal, providing a robust measure of its significance.

If the original drought frequency value was found to be in the upper 2.5% tail of the distribution of random values, it implied a very low probability of the drought signal being a result of random variability. In other words, the likelihood of such an extreme value occurring by chance was minimal. This finding suggested that the drought signal identified by the CMIP6 models for a particular coordinate was statistically significant and could be attributed to climatic factors rather than random fluctuations. Thus, the application of this method allowed for a rigorous evaluation of drought signals, confirming their validity and importance in the context of climate change research.

To give a sense of the extensive database being dealt with, it should be noted that 2000 random models were created for each of the 31 original CMIP6 models in both the historical part and the scenario projections. This process resulted in approximately 124,000 simulations, highlighting the substantial computational effort and time-consuming nature of applying bootstrapping to such a large dataset of climate models. This large number of simulations underscores the complexity and computational demands associated with ensuring robust statistical analysis in climate model evaluations.

To overcome the time-consuming issue of running this vast number of simulations, parallel computation was employed. Since all the processes were performed in Python, Dask, a flexible parallel computing library for analytics, was utilized to

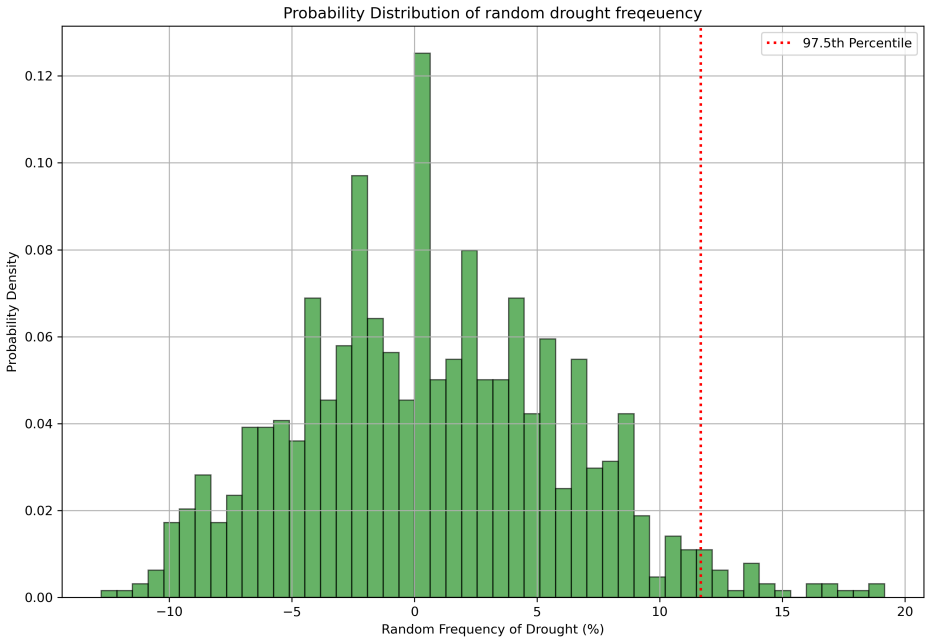

Figure 3.12: The graph illustrates the probability distribution function of random drought frequency values at a specific latitude and longitude. The red dotted vertical line marks the 97.5th percentile, indicating the threshold beyond which the upper 2.5% of the data lies.

manage the workload efficiently. Dask enables parallel computing by breaking down large datasets into smaller chunks and processing them concurrently across multiple CPU cores. This approach significantly reduces computation time and makes it feasible to handle large-scale data processing tasks, such as our bootstrapping analysis of climate models.

Dask operates by creating a task graph that outlines the operations to be performed on each chunk of data. These tasks are then distributed across the available computing resources, allowing for simultaneous execution. By leveraging Dask's capabilities, the large dataset was divided into manageable pieces, and each piece was processed independently and in parallel. This method not only sped up the computations but also optimized the use of memory and CPU resources.

In our study, Dask was used to chunk the precipitation data from the CMIP6 models into smaller subsets. Each subset was then subjected to the bootstrapping

process, where random models were generated, and drought frequency values were calculated. By processing these chunks in parallel, the overall time required to complete the 124,000 simulations was drastically reduced. Additionally, Dask's ability to scale computations across multiple machines further enhanced our capacity to handle the extensive dataset efficiently.
Overall, the use of Dask and parallel computing techniques enabled us to manage the computational demands of the bootstrapping process effectively. This approach ensured that the analysis could be completed within a reasonable timeframe, allowing us to derive meaningful insights from the extensive climate model data without being hindered by computational constraints.

Another significant challenge encountered during the calculation of SPI-6 for the random models was dealing with the non-standard time frames created by the random selection of years. Unlike a typical climate model that follows a chronological order, our random models could include years such as 1961, 2001, 1958, 1973, and 2014, without any sequential order. This randomness posed a particular problem when calculating the SPI-6 values, which require the cumulative precipitation of a given month plus the precipitation of the previous five months.

For instance, to calculate the SPI-6 value for January of a randomly chosen year, say 1958, it is necessary to include the precipitation data from August, September, October, November, and December of the previous year (1957). In the context of our randomly ordered years, this backward reference is not straightforward because the preceding year might not be in a chronological sequence. To address this issue, we had to develop an additional layer of data manipulation to ensure that when calculating the SPI-6 values for each month, the integrity of the theoretical foundations and calculation principles of the SPI were preserved. This involved meticulously aligning and referencing the appropriate months from the random dataset to maintain the continuity required for accurate SPI-6 calculation, ensuring that each month's value was based on the correct historical precipitation data.

```
In [1]: import dask.array as da
        arr = da.random.random((2000, 2000, 2000))
        arr
```

Out[1]:

	Array	Chunk
Bytes	59.60 GiB	119.21 MiB
Shape	(2000, 2000, 2000)	(250, 250, 250)
Count	512 Tasks	512 Chunks
Type	float64	numpy.ndarray

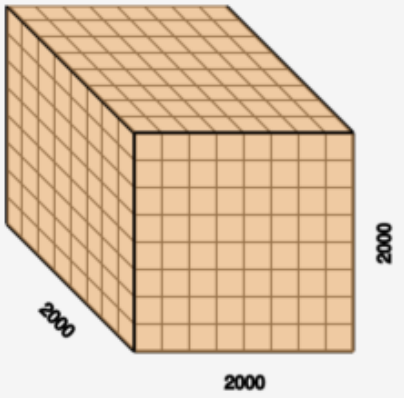


```
In [2]: arr.chunksize
Out[2]: (250, 250, 250)

In [3]: arr.chunks
Out[3]: ((250, 250, 250, 250, 250, 250, 250, 250),
         (250, 250, 250, 250, 250, 250, 250, 250),
         (250, 250, 250, 250, 250, 250, 250, 250))
```

Figure 3.13: The image demonstrates how a large array with a shape of (2000, 2000, 2000) and a total size of 59.60 GiB can be divided into smaller, manageable chunks of (250, 250, 250), creating 512 tasks and chunks. This chunking process facilitates parallel computation and efficient data processing.

Chapter 4

Results and Discussion

4.1 Historical period

In the historical period, changes in drought frequency from 1985 to 2014, as simulated by the CMIP6 models, were analyzed and compared to the earlier period of 1950 to 1979 (Figure 4.1). An increase in the frequency of dry months in the Mediterranean region was indicated by a few models. However, the majority of models displayed scattered signals across Europe. It was noted that none of these models produced a drought frequency signal that matched the expectations derived from the ERA5 reanalysis data for the same period (Figure 3.11).

This inconsistency highlights a critical challenge in climate modeling: the inability of the current generation of CMIP6 models to consistently replicate observed historical drought patterns, particularly those documented by ERA5 data. The scattered and varied signals across different models suggest that there are underlying differences in how these models simulate key climatic processes that influence drought conditions. Consequently, this variability underscores the need for further refinement and calibration of climate models to improve their reliability in regional drought simulations. This is a reminder of historical intervariability amongst CMIP6 models, due to which it becomes necessary to rely on the Multi-Model Mean (MMM) approach. The MMM approach is simple; the mean of multiple climate models are calculated to derive a best estimate. The MMM approach eliminates the biases and uncertainties of individual models by taking into account both averages and differences from its counterparts. This helps the models to use their individual areas of strengths while keeping less reliance on areas where they are relatively weak, thereby resulting in a more predictive and generalized skill that captures other energy part (climate phenomena).

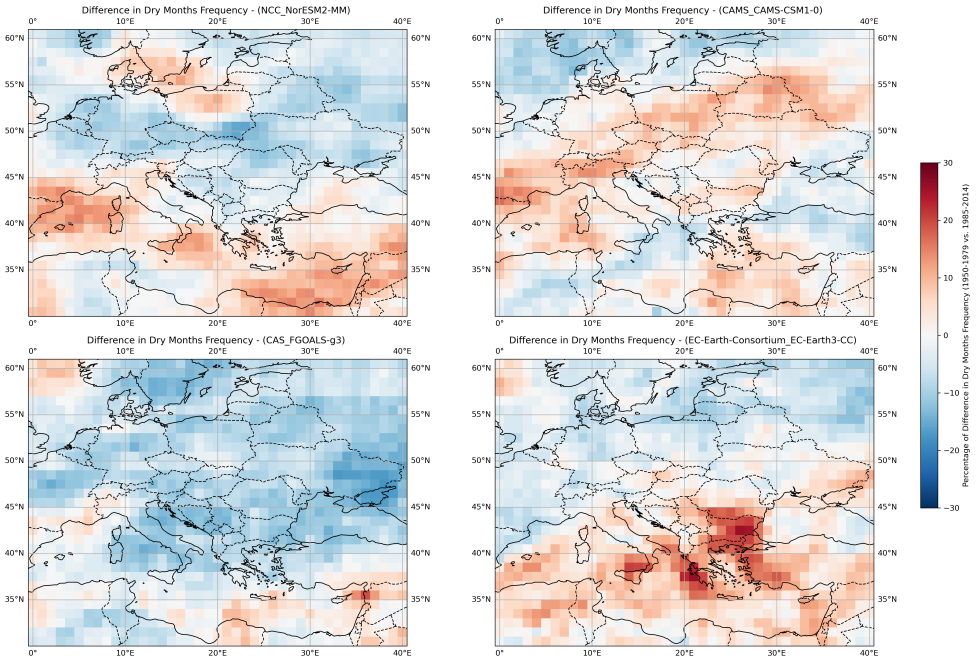

Figure 4.1: figure shows the difference in the number of dry months according to four different CMIP6 models: CAMS CAMS-CSM1-0, CAS FGOALS-g3, NCC NorESM2-MM, and EC-Earth-Consortium EC-Earth3-CC for the period 1985-2014 compared to 1950-1979. The color indicates where the number of dry months differs: red indicates an increase, and blue indicates a decrease. The maps highlight the variability and lack of consensus among the models regarding changes in drought frequency over the European area.

In this study, the application of the MMM approach can significantly enhance our understanding of drought frequency changes. By averaging the results from all CMIP6 models, a more coherent and consistent signal of drought frequency trends across Europe can be obtained. This aggregated result is less susceptible to the anomalies and extreme variations seen in individual models, providing a clearer picture of the overall climatic trends. Furthermore, the MMM approach helps in reducing the noise from inter-model variability, thus offering a more dependable basis for evaluating future drought risks.

In Figure 4-2, the Multi-Model Mean (MMM) of 31 CMIP6 simulations is provided, indicating the average signal for the difference in drought frequency in the present compared to the period 1950-1979. The MMM approach revealed a clear signal of an increase in the number of dry months in the Mediterranean region, predominantly in southern Europe. However, the signal was weak and did not completely mimic

the patterns observed in the ERA5 reanalysis data.

The MMM model still conveyed a similar narrative in Northern Europe, for latitudes above 50°, there was either a decrease in drought frequency or no significant change compared to the past period (1950-1979). In contrast, most grid cells in southern Europe, particularly in the Mediterranean area, experienced an increase in drought frequency. Although the historical simulations from the CMIP6 models did not capture the intensity observed in the ERA5 model, the overall trend was consistent. The intensity of the increase, as highlighted by the darker red shades in Figure 3.11, indicating a noticeable rise in the number of dry months, was not as prominent in the MMM model. Regions such as northern Italy and the eastern coastal borders of countries like Croatia, Albania, and Greece showed less pronounced changes in the MMM model compared to the ERA5 reanalysis. This discrepancy suggests that while the MMM approach provides a more coherent signal, it may still underrepresent certain regional intensities observed in the ERA5 data.

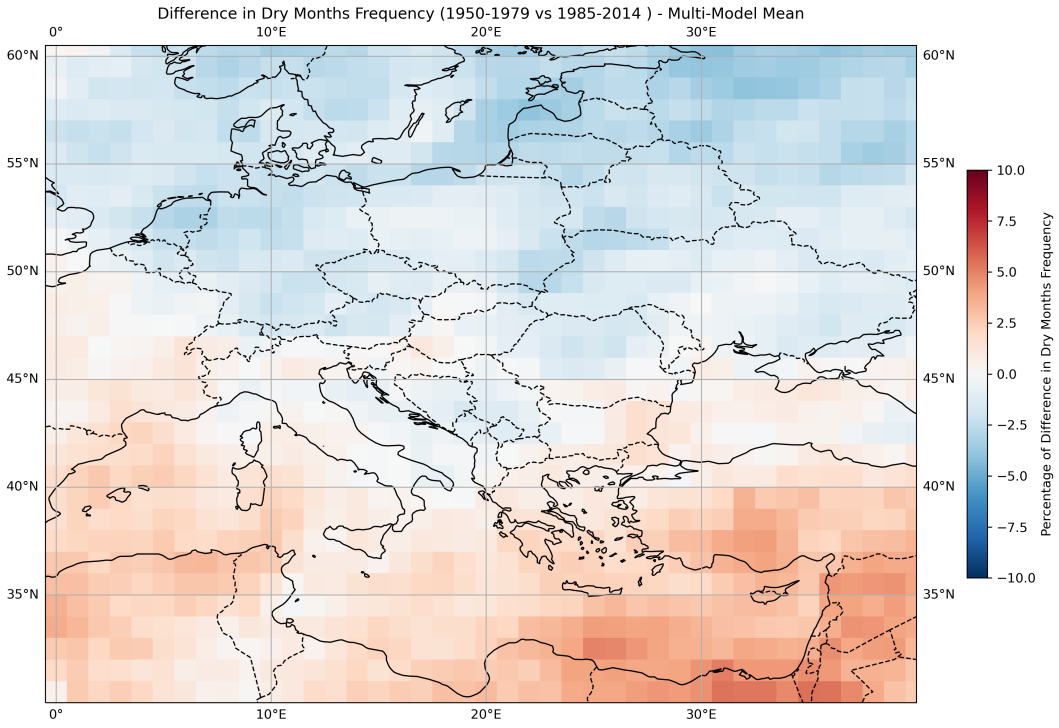

Figure 4.2: Multi-Model Mean Difference in Number of Dry Months (1950-1979 vs 1985-2014): This figure shows the percentage change in the number of dry months across Europe, highlighting increased dryness in southern regions and reduced dryness in northern regions, based on multi-model mean data.

As discussed in the Bootstrapping section, regardless of the parameters and modeling configurations used for climate simulations, models will always generate signals. The importance and significance of these signals can be assessed through a statistical approach known as bootstrapping. To validate our approach, bootstrapping was applied to the ERA5 model to evaluate the significance of its signal regarding the increase in drought frequency in the Mediterranean area (Figure 3.11).
Through the creation of completely random models, a probability distribution was obtained. Each pixel of the ERA5 drought frequency model that indicated an increase in drought frequency was evaluated to determine if the corresponding signal could be produced by a random population or if it represented a meaningful signal. The results of this evaluation are presented in Figure 4.3, demonstrating the effectiveness of bootstrapping in distinguishing significant drought frequency signals from random variability.

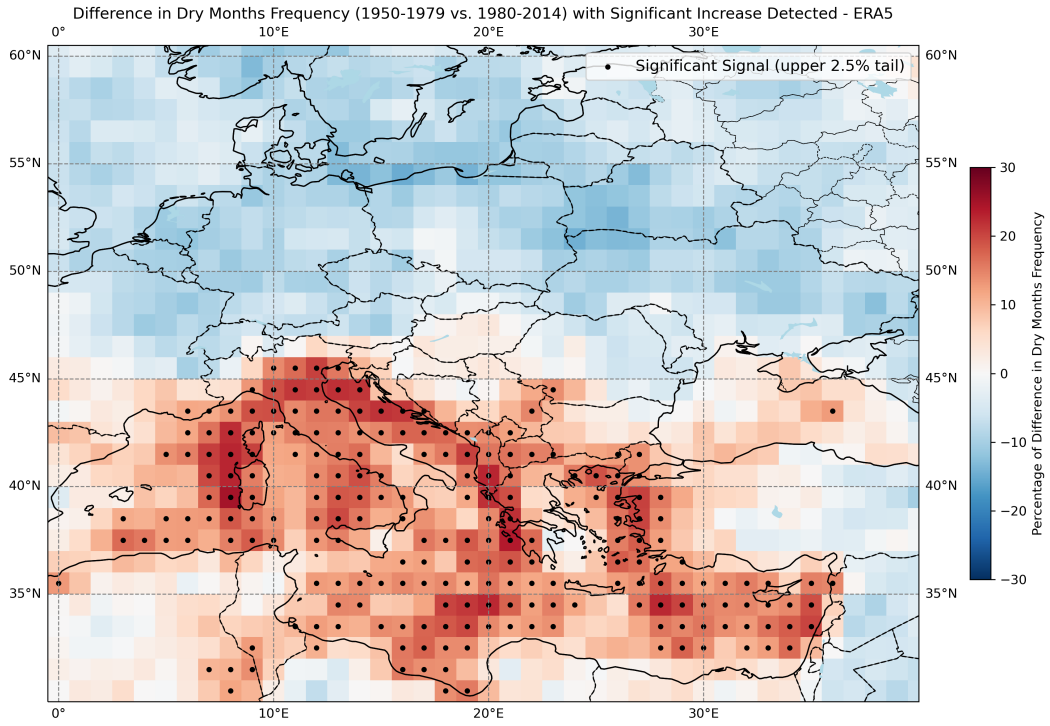

Figure 4.3: This figure shows the difference in dry months frequency between the periods 1950-1979 and 1980-2014 as observed in the ERA5 dataset. Areas marked with black dots indicate regions where a significant increase in drought frequency was detected, corresponding to the upper 2.5% tail of the random distribution, highlighting meaningful signals of increased drought conditions in the Mediterranean region.

As seen in Figure 4.3, the statistical method used in this research correctly detects signals that express a significant increase in drought frequency for the observational ERA5 model. As expected, most of the signals obtained from ERA5 are significant and are not merely the result of random variability and chance. This validation confirms that the applied bootstrapping technique effectively distinguishes meaningful drought frequency increases in the Mediterranean region, showcasing the reliability of the analysis method used in this study.

Bootstrapping was applied to each individual CMIP6 model in the historical period. However, the significant variability among the models meant that evaluating each climate model individually did not yield meaningful results. As demonstrated in Figure 4.1, where a few examples of CMIP6 simulations are shown (The results of the evaluation for each individual CMIP6 model are provided in the Appendix) the signals for differences in drought frequency, the resulting maps from the statistical evaluation revealed only a few significant signals or none at all. This was consistent across the historical simulations of drought characteristics among the 31 CMIP6 models (Figure 4.4).

The lack of significant signals in the individual model evaluations highlights the challenge posed by the high inter-model variability. Each model's unique configuration and parameterization lead to diverse outcomes, making it difficult to draw robust conclusions from any single model's output. Consequently, the application of bootstrapping to individual models did not effectively capture the drought frequency signals, reinforcing the need for a multi-model approach to enhance the reliability and robustness of the findings.

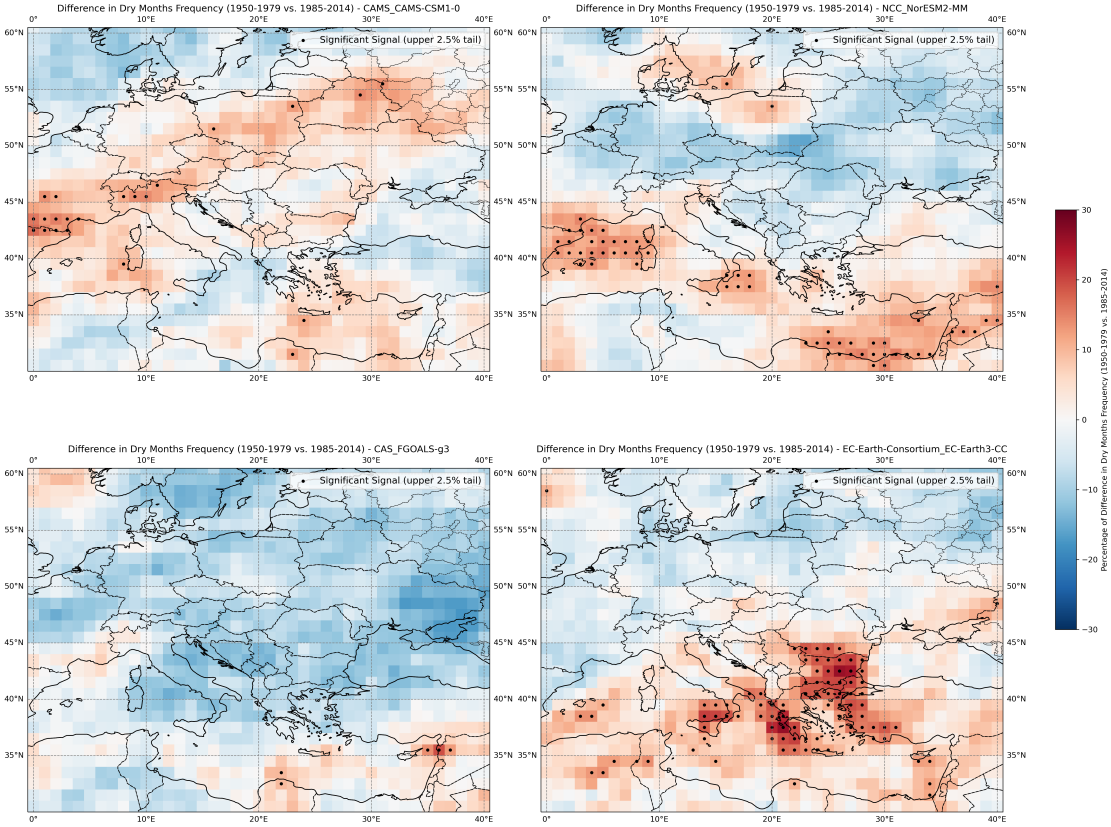

Figure 4.4: This figure shows the difference in dry months frequency between the periods 1950-1979 and 1985-2014 for four CMIP6 models (CAMS-CSM1-0, NorESM2-MM, FGOALS-g3, and EC-Earth3-CC). Areas marked with black dots indicate regions where significant signals (upper 2.5% tail) were detected. Despite some indications of changes in drought frequency, the multi-model mean approach reveals generally weak signals, highlighting the challenge of achieving consistent drought characteristic simulations among the models.

Applying bootstrapping to the multi-model mean output of historical simulations (Figure 4.5) further underscores the weakness of the signals obtained from these models, with no significant signals detected in this step. This outcome suggests that the CMIP6 models were unable to accurately simulate the drought characteristics in the Mediterranean area for the historical period. Despite the weak signal observed in the multi-model mean (Figure 4.2), bootstrapping confirmed that this signal is not significant and could easily be generated by chance from any random configuration of climate models.

The fact that no meaningful signals were found using bootstrapping suggests that the CMIP6 models as a whole are unable to replicate the patterns of drought that have been observed in the Mediterranean during the historical period. This result suggests that the models are unable to adequately represent the complex dynamics of droughts due to their inherent variability and possible structural biases. Thus, the findings emphasize the necessity of additional model enhancements and potentially novel methodologies to more accurately replicate localized drought attributes and their underlying causes. Additionally, future investigation is needed to check the ability of the models in capturing changes in other statistics of precipitation.

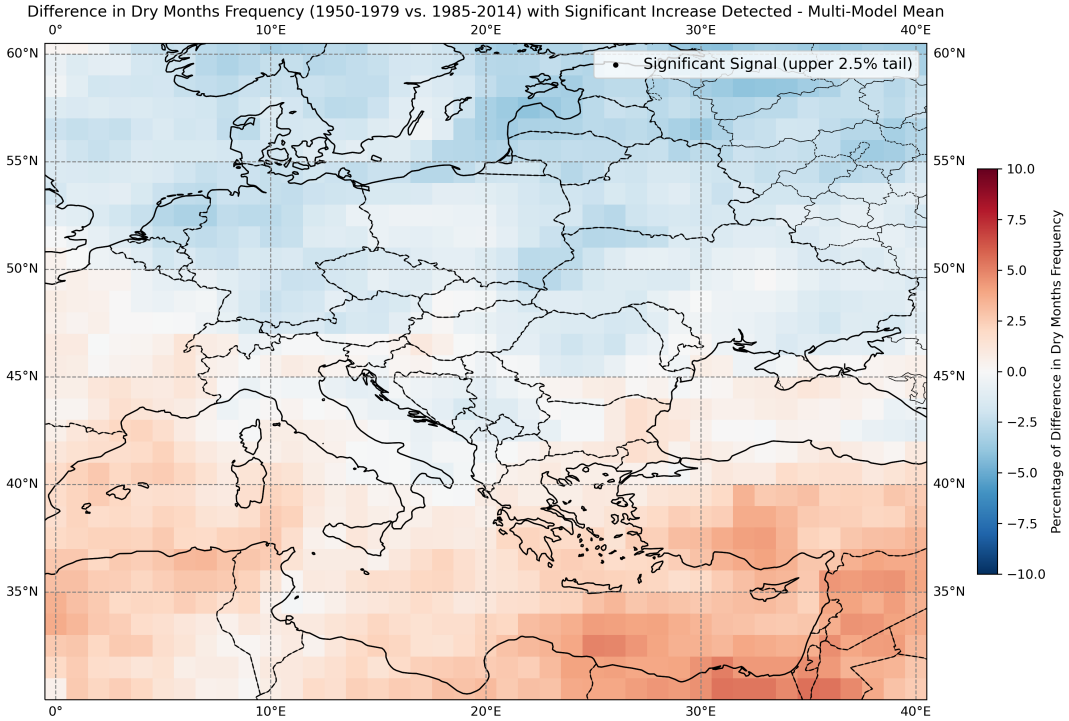

Figure 4.5: This figure presents the difference in dry months frequency between the periods 1950-1979 and 1985-2014, as derived from the Multi-Model Mean (MMM) of 31 CMIP6 models. Areas marked with black dots indicate regions where significant increases in drought frequency (upper 2.5% tail) were detected. The MMM reveals weak signals with no significance detected, suggesting that the CMIP6 models collectively struggle to simulate historical drought characteristics accurately in the Mediterranean region.

Additionally, the multi-model standard deviation (MMSD) was calculated for the historical period. Standard deviation is a crucial indicator of uncertainty

in simulations for each grid cell. A higher standard deviation indicates greater disagreement among models, whereas a lower standard deviation signifies stronger agreement on the obtained signal. MMSD complements the multi-model mean (MMM), which demonstrated a weak signal in Figure 4.5, by revealing considerable and consistent variability among the models. This MMSD flat map indicates that there were no specific zones where models agreed more than in other zones. Instead, different signals were distributed more or less evenly across Europe, which aligns with the findings from the bootstrapping analysis on historical models.

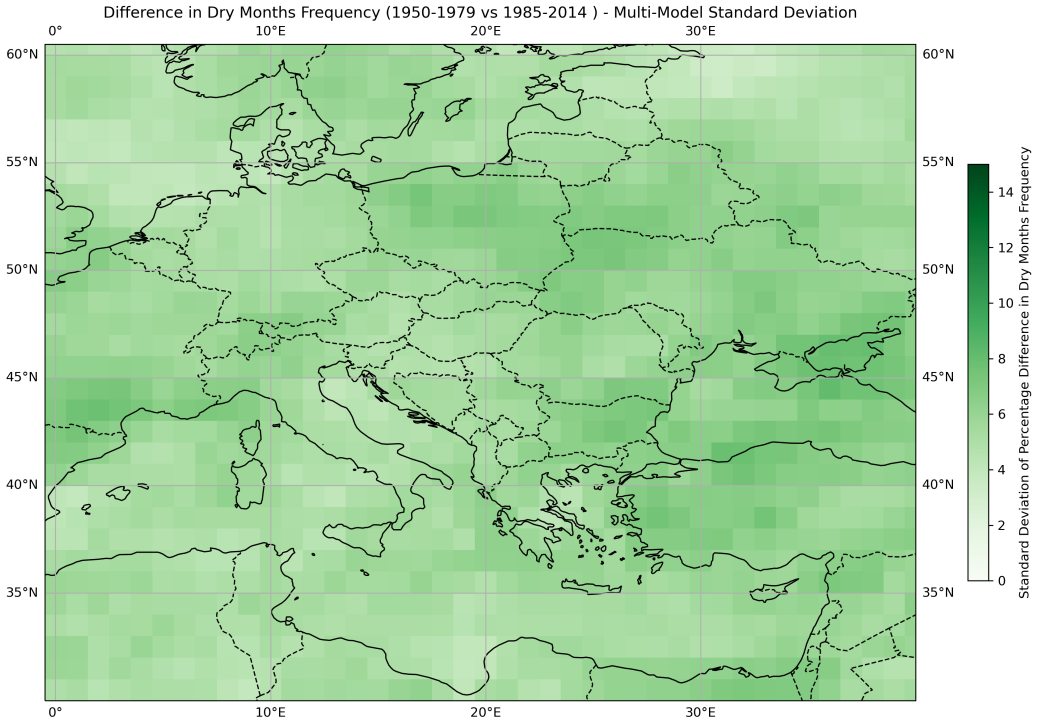

Figure 4.6: Multi-Model Standard Deviation (MMSD) of the difference in dry months frequency between 1950-1979 and 1985-2014, indicating the variability among CMIP6 models. Higher standard deviations highlight regions of greater model disagreement.

4.2 Future period

Looking at the future projections of drought frequency from the CMIP6 scenario models, it is evident that these models exhibit an improved ability to project drought changes in the future compared to their simulations for historical and present periods. In Figure 4.7, several examples illustrate the projected changes in

drought frequency for the last 30 years of the century relative to 1985-2014. Each individual scenario model consistently indicates an increase in dryness frequency in the Mediterranean area, this time with much higher frequency numbers and more extreme conditions (Figure 4.7).

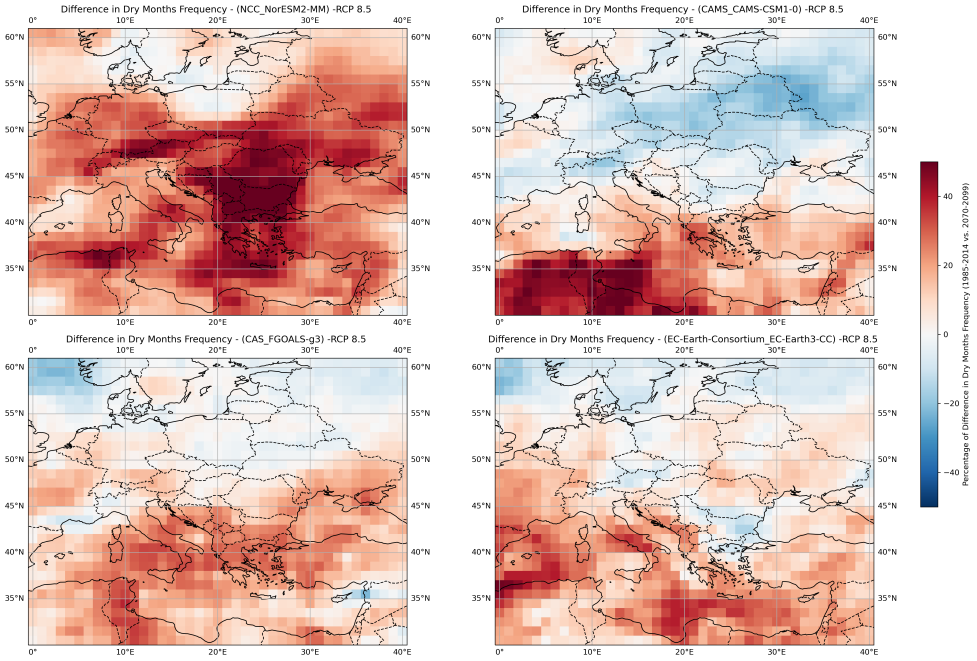

Figure 4.7: This figure illustrates the projected difference in dry months frequency for the period 2070-2099 compared to 1985-2014, as simulated by four CMIP6 models under the RCP 8.5 scenario (NorESM2-MM, CAMS-CSM1-0, FGOALS-g3, and EC-Earth3-CC).

To reduce the effect of intervariability among the scenario models, a Multi-Model Mean (MMM) was created for the 31 future models (Figure 4.8). This approach helps to smooth out noise and allows us to determine if the average signal aligns with those observed in the ERA5 observational model. The MMM is expected to produce a more accurate and harmonious representation, as most of the future models were able to recreate the observational signals with greater consistency. By averaging the outputs of these models, the MMM approach aims to enhance the reliability of the projected drought frequency patterns and provide a clearer understanding of future climatic conditions in the Mediterranean region.

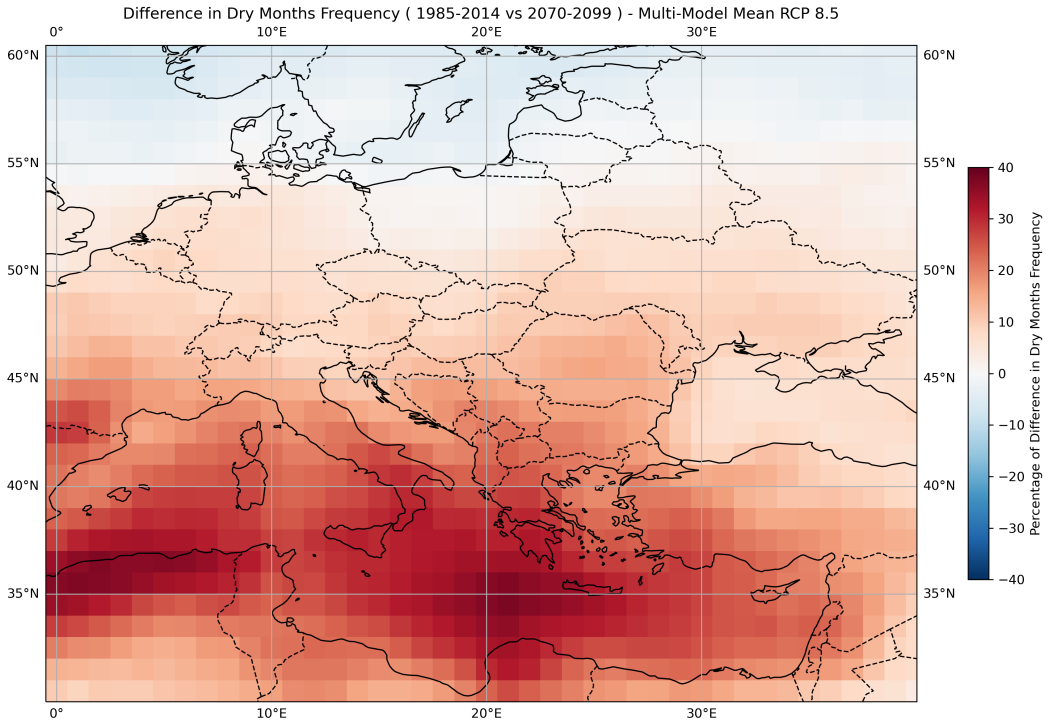

Figure 4.8: This figure shows the projected increase in the frequency of dry months for the period 2070-2099 relative to 1985-2014, based on the Multi-Model Mean (MMM) of 31 CMIP6 models under the RCP 8.5 scenario. The Mediterranean region, particularly southern Europe and North Africa, is expected to experience significant increases in drought frequency, up to 40%.

As expected, the Multi-Model Mean (MMM) of future projections effectively captured the drought frequency, outperforming the simulations for the historical period. The MMM emphasizes an extreme increase in the number of dry months for the period 2070-2099. In particular, Southern Europe, including regions such as southern Italy, Greece, Albania, and countries in North Africa bordering the Mediterranean Sea, is projected to experience almost a 40% increase in drought occurrence. This projection is strikingly similar to the signal observed in Figure 4.3 for the ERA5 model, though with even higher frequency and a more extensive coverage of the catastrophic conditions across Europe compared to the historical drought coverage.

In the historical period, Northern Europe was largely spared from drought, with some regions even experiencing a decrease in drought frequency. However, future projections indicate that almost all countries in Europe are likely to experience an increase in drought frequency. Exceptions include the north of Poland, which shows no significant changes, and Norway, Sweden, and Finland, where a decrease

in the number of dry months is anticipated compared to the past. This comprehensive outlook underscores the pressing need for adaptive strategies to mitigate the heightened risk of drought across the European continent, particularly in the vulnerable Mediterranean region.

The main question remains: although these signals are close to the reality of the signals obtained from the ERA5 model, and most models agree on a strong increase in drought frequency in the Mediterranean area, are these signals significant?
The results from the bootstrapping evaluation of each individual scenario model reveal that the signals are indeed significant. The statistical performance of all 31 CMIP6 models, detailed in the bibliography section, indicates that most of the observed signals stem from a profound precipitation pattern. The drought frequency change values predominantly fell within the upper 2.5% tail of the random values distribution (Figure 4.9), suggesting that the increases in drought frequency are not due to random chance but represent significant climatic trends.

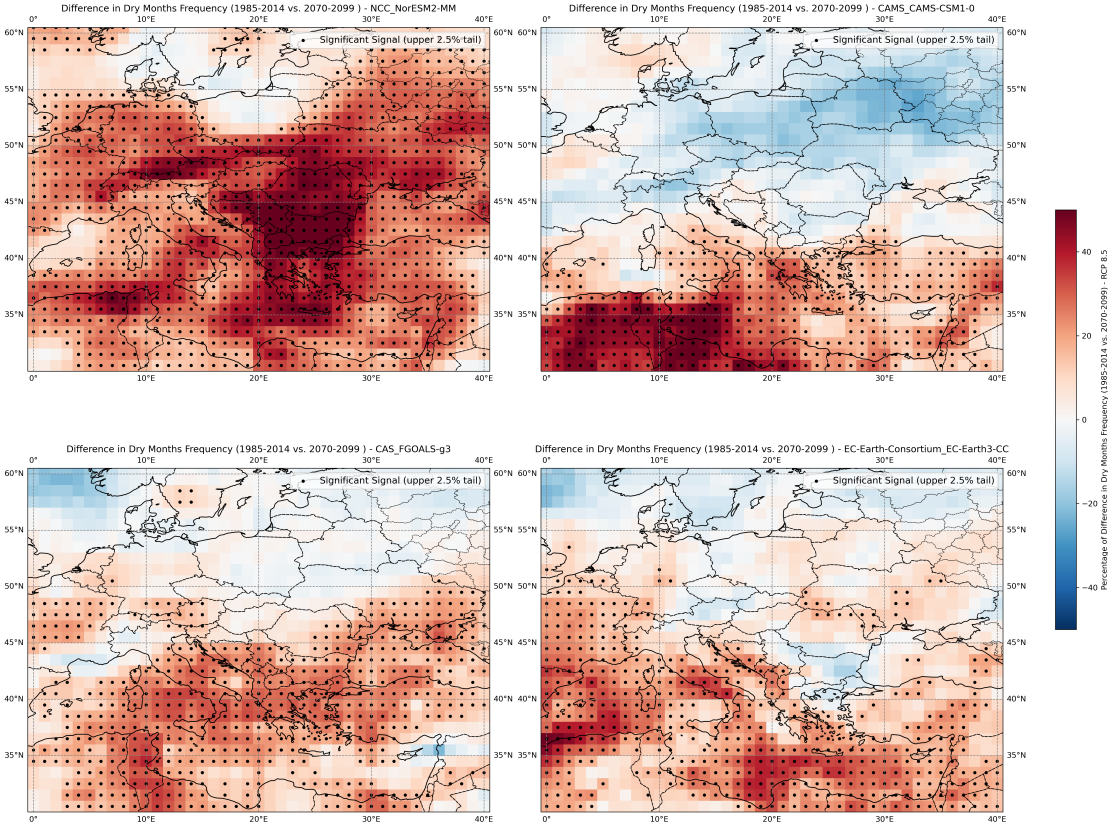

Figure 4.9: This figure shows the difference in dry months frequency between the periods 1950-1979 and 1985-2014 for four CMIP6 models (NorESM2-MM, CAMS-CSM1-0, FGOALS-g3, and EC-Earth3-CC). Areas marked with black dots indicate regions where the changes are significant, falling within the upper 2.5% tail of the random values distribution. The significant signals highlight the robustness of the observed increase in drought frequency in the Mediterranean region.

Although significant signals for an increase in drought frequency in the Mediterranean area were not observed in the historical simulations (Figure 4.5), the bootstrapping analysis on future projections (Figure 4.10) reveals a compelling picture. The CMIP6 scenario models not only closely align with the reality depicted by the ERA5 model but also show high agreement on the increase of dry months in the Mediterranean region. Notably, over 90% of the signals indicating a rise in drought frequency in the Multi-Model Mean (MMM) for future projections were detected as significant. This strongly suggests that Southern Europe, especially Italy, is likely to experience an average 30% increase in drought occurrence.

This figure also underscores the improved performance of the CMIP6 scenario models in projecting drought characteristics based on the Standardized Precipitation Index (SPI). The reliable signals provided by these models are crucial for decision-making regarding future hydrological issues. The significant increase in drought frequency projected for Southern Europe, as highlighted by the bootstrapping analysis, validates the use of CMIP6 scenario models in planning and mitigating the impacts of future droughts. This enhanced predictive capability is essential for developing effective strategies to address the anticipated rise in drought conditions in the Mediterranean region.

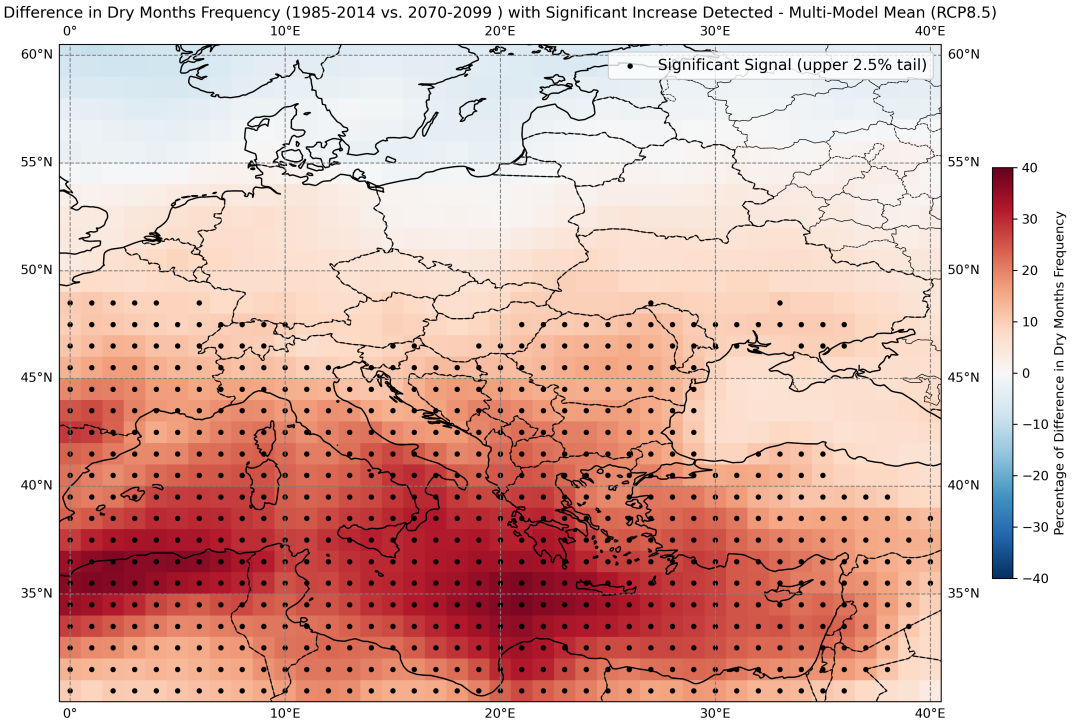

Figure 4.10: This figure illustrates the projected difference in dry months frequency between 1985-2014 and 2070-2099, based on the Multi-Model Mean (MMM) of CMIP6 models under the RCP 8.5 scenario. Areas marked with black dots indicate significant increases in drought frequency, highlighting the expected rise in dry months across the Mediterranean region, particularly in Southern Europe.

As expected, the MMSD plot for Scenario models reveals more fluctuations in standard deviation across Europe. Figure 4.11 showcases zones with a higher intensity increase in dry months frequency, now accompanied by greater disagreement among all models compared to zones characterized by a mild increase in the Mediterranean region. Conversely, there is higher agreement on the signal of decreased drought

frequency in Northern Europe. This comparison draws attention to the areas where the frequency of droughts has changed significantly and the corresponding uncertainties in these forecasts. This result emphasizes the value of additional research employing more sophisticated and reliable statistical techniques.

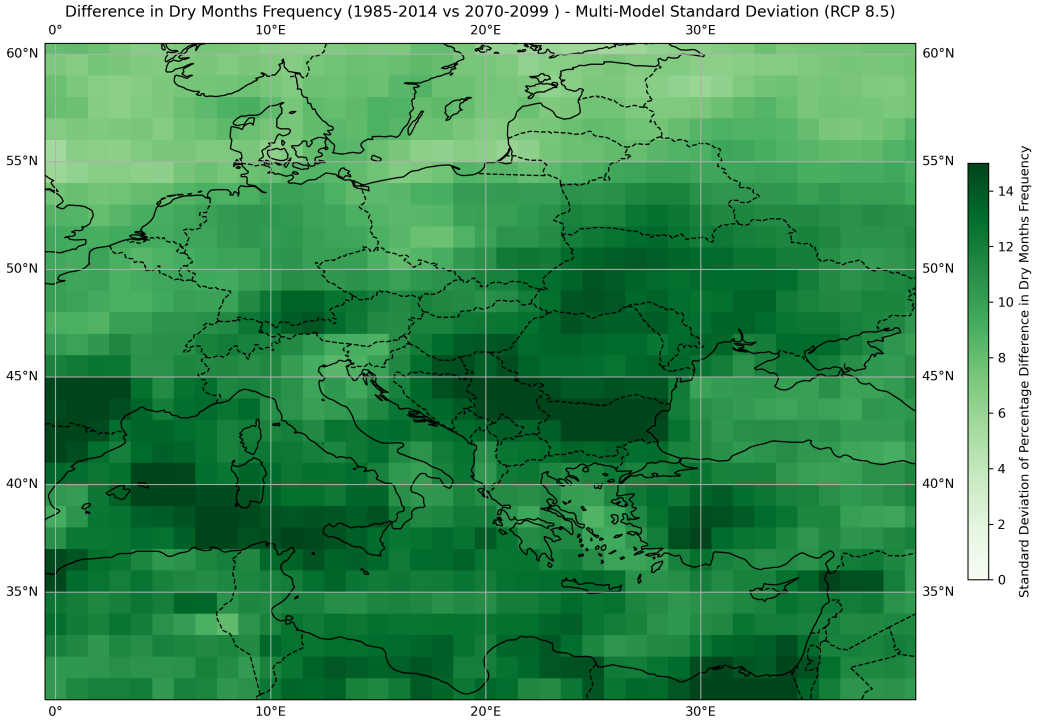

Figure 4.11: Multi-Model Standard Deviation (MMSD) of the difference in dry months frequency between 1985-2014 and 2070-2099 under the RCP 8.5 scenario. Higher standard deviations indicate greater model disagreement, particularly in regions with projected increases in dry months frequency.

Chapter 5

Conclusion

As the Mediterranean region becomes a hotspot for climate change impacts, it is expected to see more frequent and extreme changes in the hydrological cycle, as confirmed by the Intergovernmental Panel on Climate Change (IPCC) with high confidence. This makes it essential to evaluate these changes precisely and measure the extent of these extremes.

ERA5 reanalysis simulations on drought conditions indicate that climate change has significantly affected the Mediterranean region from 1985-2014 compared to 1950-1979. Precipitation patterns during this period show an increased frequency of dry months (SPI $<$ -1), especially in Southern Europe. Regions bordering the Mediterranean Sea, such as Italy, have seen an average increase of 20% in drought frequency, with areas like Piedmont, Lombardy, and Emilia-Romagna experiencing increases up to 30%. Albania and Greece also exhibit the highest rise in drought frequency (Figure 3.11). These findings underscore the necessity of projecting future drought conditions to develop impactful adaptation strategies. Reliable projections from CMIP6 simulations are crucial for this purpose.

CMIP6 historical simulations indicated an increase in the frequency of dry months in the Mediterranean region in a few models, but most displayed scattered signals across Europe. None of these models produced drought frequency signals matching the ERA5 reanalysis expectations. However, the multi-model mean analysis of 31 CMIP6 models provided a more coherent and consistent signal of drought frequency trends across Europe. Although the signal for increased drought frequency in Southern Europe was weak, averaging a 2.5% increase, it highlighted the general trend of increased dry month occurrence moving from Northern to Southern Europe. Bootstrapping analysis suggested that the historical period signals were not significant and could result from any random precipitation pattern (Figure 4.5).

Conversely, the signals obtained from individual CMIP6 models for future scenarios in 2070-2099 compared to 1985-2014, alongside the average signal of all models, indicated a pronounced increase in drought frequency for Southern Europe near the Mediterranean Sea. The intensity and land coverage of these signals are expected to rise significantly in the last 30 years of the 21st century under the RCP8.5 scenario, with over 60% of European countries experiencing increased drought frequency. Even Northern Europe is not exempt from this trend. These projections highlight a widespread and intensifying trend of drought conditions across Europe, with substantial implications for water resources, agriculture, and ecosystems. The reliability of these projections is reinforced by bootstrapping analysis, which confirms that the obtained signals are mostly significant for countries with latitudes lower than 50 degrees (Figure 4.9). Furthermore, the results obtained for changes in drought frequency in both historical and future projections align with other statistical approaches of extremes related to droughts and general reduction of precipitation projected by both global and regional models, as discussed in the literature review chapter. This agreement with previous studies enhances the robustness and validity of the current research findings.

These projections highlight a widespread and intensifying trend of drought conditions across Europe, with substantial implications for water resources, agriculture, and ecosystems. The reliability of these projections is reinforced by bootstrapping analysis, which confirms that the obtained signals are mostly significant for countries with latitudes lower than 50 degrees (Figure 4.10). This statistical validation underscores the robustness of the model projections and the urgent need for adaptive strategies to address these anticipated changes. Additionally, the continued refinement of climate models, including higher-resolution simulations and advanced statistical methods, will be essential for improving the accuracy and reliability of future climate projections, given the high uncertainty observed in CMIP6 simulations. While this study primarily utilized the Standardized Precipitation Index (SPI) to evaluate drought characteristics, this index does not account for the effects of evaporation within the hydrological cycle. This raises pertinent questions about how bootstrapping might respond if evaporation parameters were included in the modeling process. Incorporating additional hydrological parameters could provide a more comprehensive statistical evaluation and a clearer understanding of drought dynamics.

Bibliography

[1] Markus Kottek, Jürgen Grieser, Christoph Beck, Bruno Rudolf, and Franz Rubel. «World Map of the Köppen?Geiger climate classification updated». In: *Meteorologische Zeitschrift* 15.3 (July 2006), pp. 259–263. DOI: 10.1127/0941?2948/2006/0130. URL: http://dx.doi.org/10.1127/0941?2948/2006/0130.

[2] M.A. Caretta et al. «Water». In: *Climate Change 2022: Impacts, Adaptation, and Vulnerability. Contribution of Working Group II to the Sixth Assessment Report of the Intergovernmental Panel on Climate Change*. Ed. by H.-O. Pörtner et al. Cambridge, UK and New York, NY, USA: Cambridge University Press, 2022, pp. 551–712. DOI: 10.1017/9781009325844.006.

[3] O H 237. *Own work*. CC BY-SA 4.0. 2014. URL: https://commons.wikimedia.org/w/index.php?curid=38364150.

[4] IPCC. *Climate Change 2022: Impacts, Adaptation, and Vulnerability. Contribution of Working Group II to the Sixth Assessment Report of the Intergovernmental Panel on Climate Change*. Ed. by H.-O. Pörtner et al. Cambridge, UK and New York, NY, USA: Cambridge University Press, 2022, p. 3056. DOI: 10.1017/9781009325844.

[5] Donald Wilhite and Mickey Glantz. «Understanding: the Drought Phenomenon: The Role of Definitions». In: *Water International - WATER INT* 10 (Jan. 1985), pp. 111–120. DOI: 10.1080/02508068508686328.

[6] J. Lawrence et al. «Australasia». In: *Climate Change 2022: Impacts, Adaptation, and Vulnerability. Contribution of Working Group II to the Sixth Assessment Report of the Intergovernmental Panel on Climate Change*. Ed. by H.-O. Pörtner et al. Cambridge, UK and New York, NY, USA: Cambridge University Press, 2022, pp. 1581–1688. DOI: 10.1017/9781009325844.013.

[7] Sergio Vicente-Serrano, Steven Quiring, Marina Peña-Gallardo, Shanshui Yuan, and F. Domínguez-Castro. «A review of environmental droughts: Increased risk under global warming?» In: *Earth-Science Reviews* 201 (Sept. 2019), p. 102953. DOI: 10.1016/j.earscirev.2019.102953.

[8] IPCC. *Climate Change 2014: Impacts, Adaptation, and Vulnerability. Part A: Global and Sectoral Aspects. Contribution of Working Group II to the Fifth Assessment Report of the Intergovernmental Panel on Climate Change*. Ed. by C.B. Field et al. Cambridge, United Kingdom and New York, NY, USA: Cambridge University Press, 2014, p. 1132.

[9] Intergovernmental Change. «Weather and Climate Extreme Events in a Changing Climate». In: *Climate Change 2023: Impacts, Adaptation, and Vulnerability*. June 2023, pp. 1513–1766. ISBN: 9781009157896. DOI: 10.1017/9781009157896.013.

[10] S.I. Seneviratne et al. «Weather and Climate Extreme Events in a Changing Climate». In: *Climate Change 2021: The Physical Science Basis. Contribution of Working Group I to the Sixth Assessment Report of the Intergovernmental Panel on Climate Change*. Ed. by V. Masson-Delmotte et al. Cambridge, United Kingdom and New York, NY, USA: Cambridge University Press, 2021, pp. 1513–1766. DOI: 10.1017/9781009157896.013.

[11] Haim Kutiel. «Climatic Uncertainty in the Mediterranean Basin and Its Possible Relevance to Important Economic Sectors». In: *Atmosphere* 10 (Jan. 2019), p. 10. DOI: 10.3390/atmos10010010.

[12] «Determination of annual and seasonal daytime and nighttime trends of MODIS LST over Greece - climate change implications». In: *Science of The Total Environment* 616-617 (2018), pp. 937–947. ISSN: 0048-9697. DOI: https://doi.org/10.1016/j.scitotenv.2017.10.226. URL: https://www.sciencedirect.com/science/article/pii/S0048969717329443.

[13] K. Wyser, T. van Noije, S. Yang, J. von Hardenberg, D. O'Donnell, and R. Döscher. «On the increased climate sensitivity in the EC-Earth model from CMIP5 to CMIP6». In: *Geoscientific Model Development* 13.8 (2020), pp. 3465–3474. DOI: 10.5194/gmd-13-3465-2020. URL: https://gmd.copernicus.org/articles/13/3465/2020/.

[14] Jonathan Spinoni, Gustavo Naumann, Jürgen Vogt, and Paulo Barbosa. «The biggest drought events in Europe from 1950 to 2012». In: *Journal of Hydrology: Regional Studies* 3 (Mar. 2015), pp. 509–524. DOI: 10.1016/j.ejrh.2015.01.001.

[15] H. Douville, A. Ribes, B. Decharme, R. Alkama, and J. Sheffield. «Anthropogenic influence on multidecadal changes in reconstructed global evapotranspiration». In: *Nature Climate Change* 6.7 (2021), pp. 627–633.

[16] Yassmin Hesham, Martin Hirschi, Wim Thiery, Ahmed Kenawy, and Chunxue Yang. «Drought characteristics in Mediterranean under future climate change». In: *npj Climate and Atmospheric Science* (Sept. 2023). DOI: 10.1038/s41612-023-00458-4.

[17] Simon Michael Papalexiou, Chandra Rajulapati, Konstantinos Andreadis, Efi Foufoula-Georgiou, Martyn Clark, and Kevin Trenberth. «Probabilistic Evaluation of Drought in CMIP6 Simulations». In: *Earth's Future* 9 (Oct. 2021). DOI: 10.1029/2021EF002150.

[18] H. Hersbach et al. *ERA5 monthly averaged data on single levels from 1940 to present*. Accessed on DD-MMM-YYYY. 2023. DOI: 10.24381/cds.f17050d7.

[19] V. Eyring, S. Bony, G. A. Meehl, C. A. Senior, B. Stevens, R. J. Stouffer, and K. E. Taylor. «Overview of the Coupled Model Intercomparison Project Phase 6 (CMIP6) experimental design and organization». In: *Geoscientific Model Development* 9.5 (2016), pp. 1937–1958. DOI: 10.5194/gmd-9-1937-2016. URL: https://gmd.copernicus.org/articles/9/1937/2016/.

[20] World Meteorological Organization (WMO) and Global Water Partnership (GWP). *Handbook of Drought Indicators and Indices*. Ed. by M. Svoboda and B.A. Fuchs. Geneva: Integrated Drought Management Programme (IDMP), Integrated Drought Management Tools and Guidelines Series 2, 2016.

[21] *Copernicus Drought Factsheet*. https://drought.emergency.copernicus.eu/documents/factsheets/factsheet_spi_ado.pdf. 2022.

[22] *JRC Data*. https://data.jrc.ec.europa.eu/dataset/566c45e3-6372-4ee1-939a-145709b54102. 2022.

[23] *CDO Documentation*. https://wcrp-cmip.github.io/WGCM_Infrastructure_Panel/Papers/CMIP6_global_attributes_filenames_CVs_v6.2.7.pdf. 2022.

[24] Michael Böttinger and Dieter Kasang. *The SSP Scenarios*. https://www.dkrz.de/en/communication/climate-simulations/cmip6-en/the-ssp-scenarios. 2022.

[25] B. Efron. «Bootstrap Methods: Another Look at the Jackknife». In: *The Annals of Statistics* 7.1 (1979), pp. 1–26. DOI: 10.1214/aos/1176344552. URL: https://doi.org/10.1214/aos/1176344552.

[26] A. C. Davison and D. V. Hinkley. *Bootstrap Methods and their Application*. Cambridge Series in Statistical and Probabilistic Mathematics. Cambridge University Press, 1997.

[27] Daniel Wilks. «Statistical Methods In The Atmospheric Sciences». In: *International Geophysics Series* 59 (Jan. 2006). DOI: 10.1016/S0074-6142(06)80036-7.

[28] B. Efron and R.J. Tibshirani. *An Introduction to the Bootstrap*. New York: Chapman and Hall, 1993. DOI: 10.1007/978-1-4899-4541-9. URL: https://doi.org/10.1007/978-1-4899-4541-9.

List of Figures

Appendix A

Historical Simulations

In Appendix A and B, the results of each individual CMIP6 model are presented to illustrate how each model has simulated drought conditions during both the historical and future periods. Additionally, the evaluation of significance for signals indicating an increase in the frequency of dry months is included. This comprehensive analysis allows for a detailed comparison of each single model's performance quality of projected changes in drought conditions.

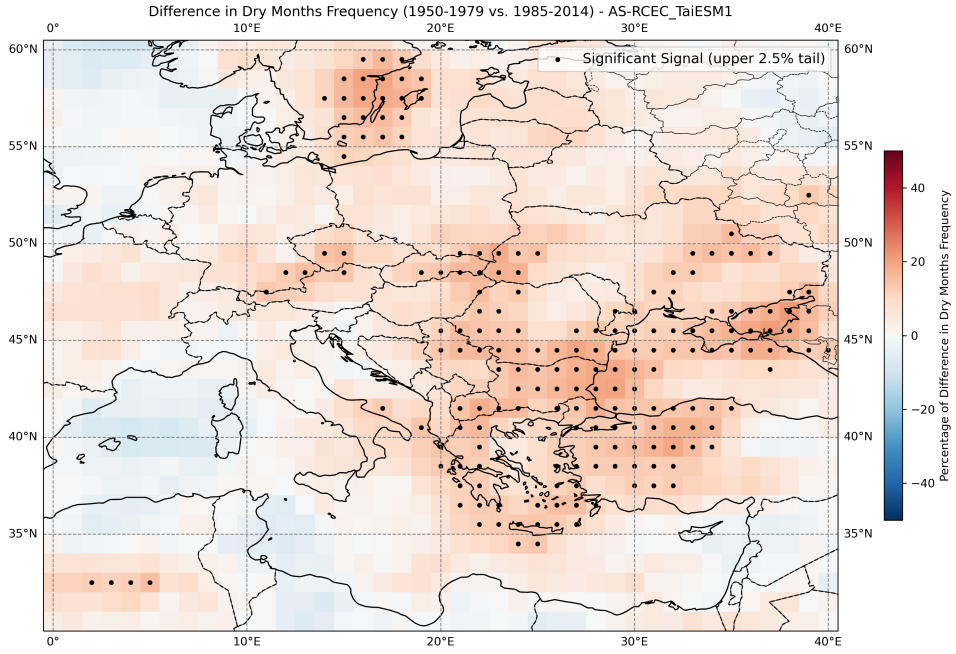

Figure A.1: Difference in dry months frequency for AS-RCEC TaiESM1.

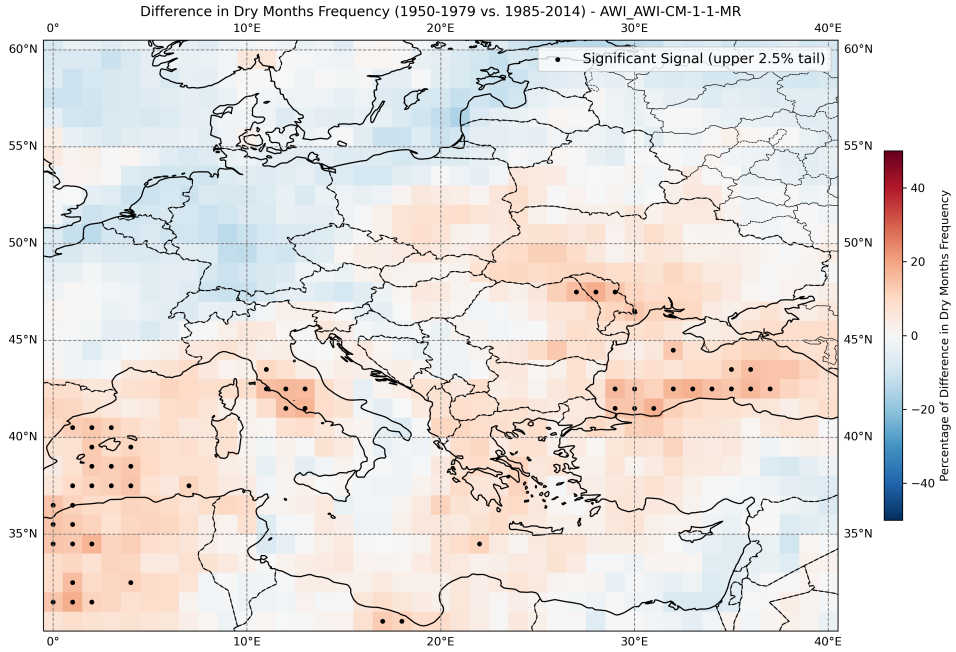

Figure A.2: Difference in dry months frequency for AWI AWI-CM-1-1-MR.

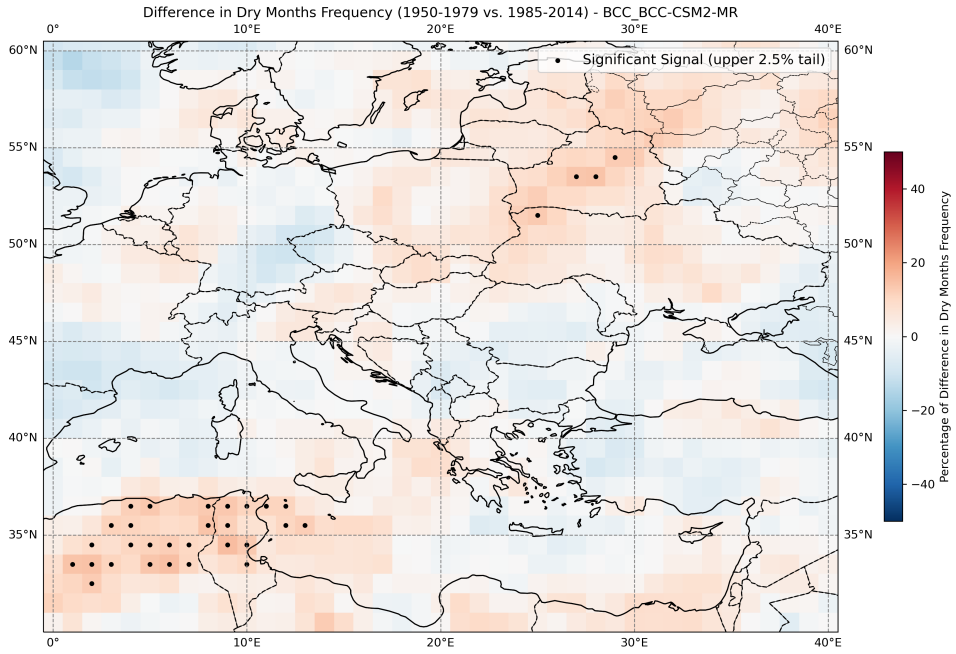

Figure A.3: Difference in dry months frequency for BCC BCC-CSM2-MR.

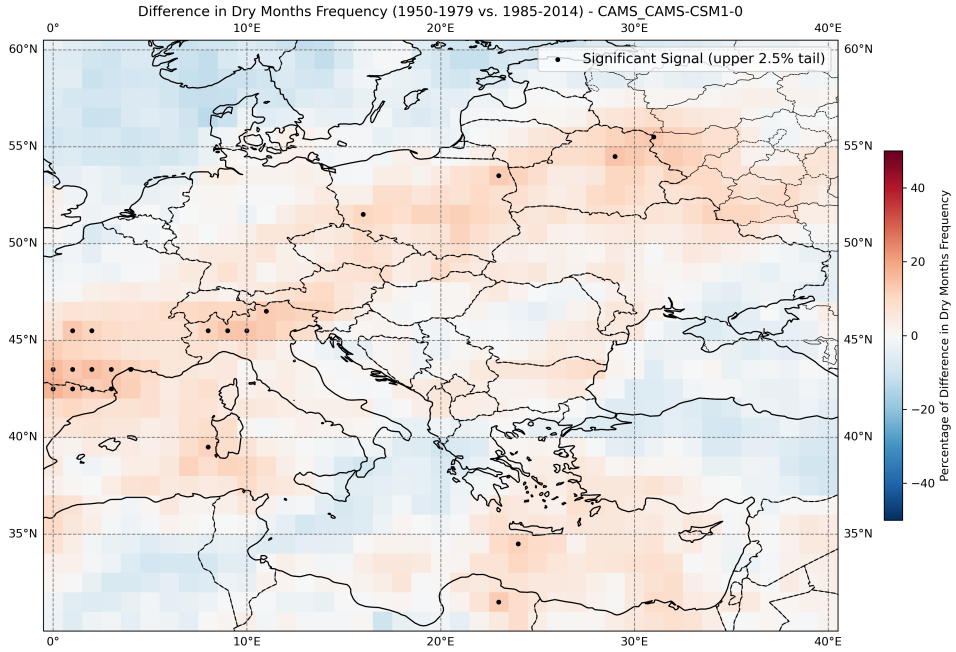

Figure A.4: Difference in dry months frequency for CAMS CAMS-CSM1-0.

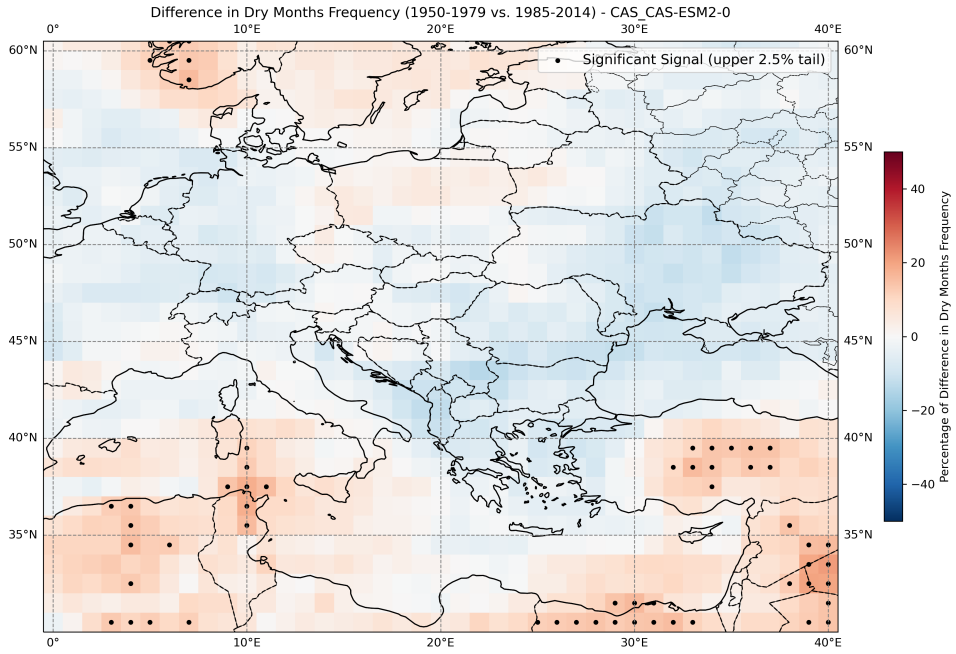

Figure A.5: Difference in dry months frequency for CAS CAS-ESM2-0.

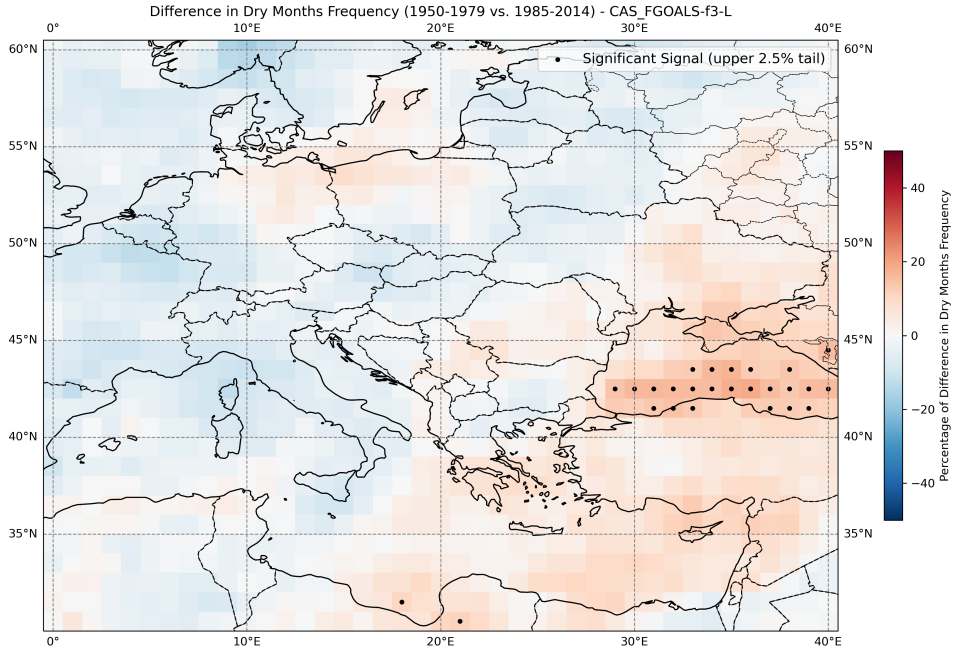

Figure A.6: Difference in dry months frequency for CAS FGOALS-f3-L.

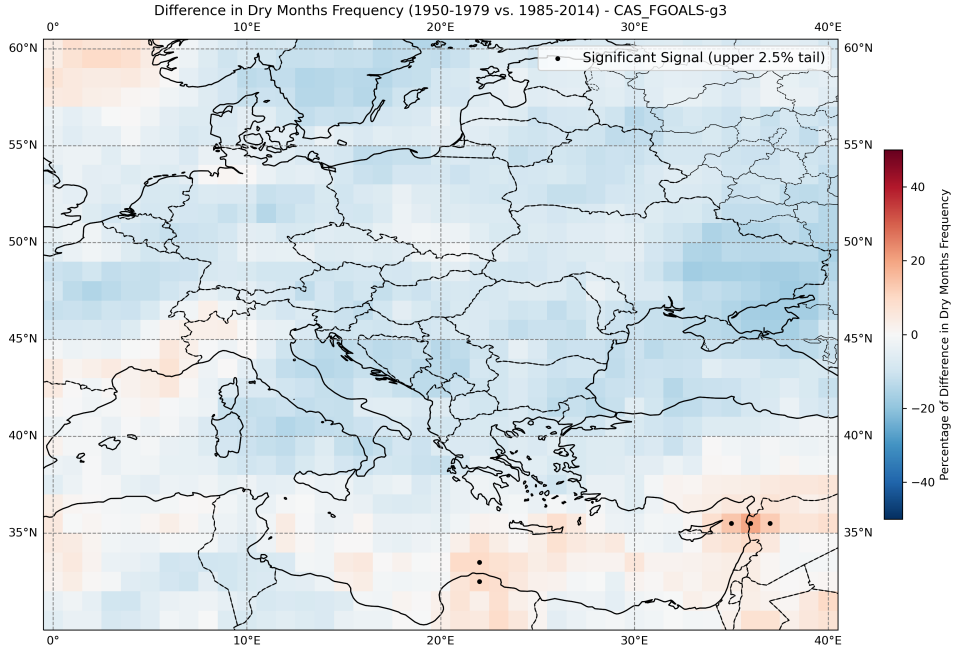

Figure A.7: Difference in dry months frequency for CAS FGOALS-g3.

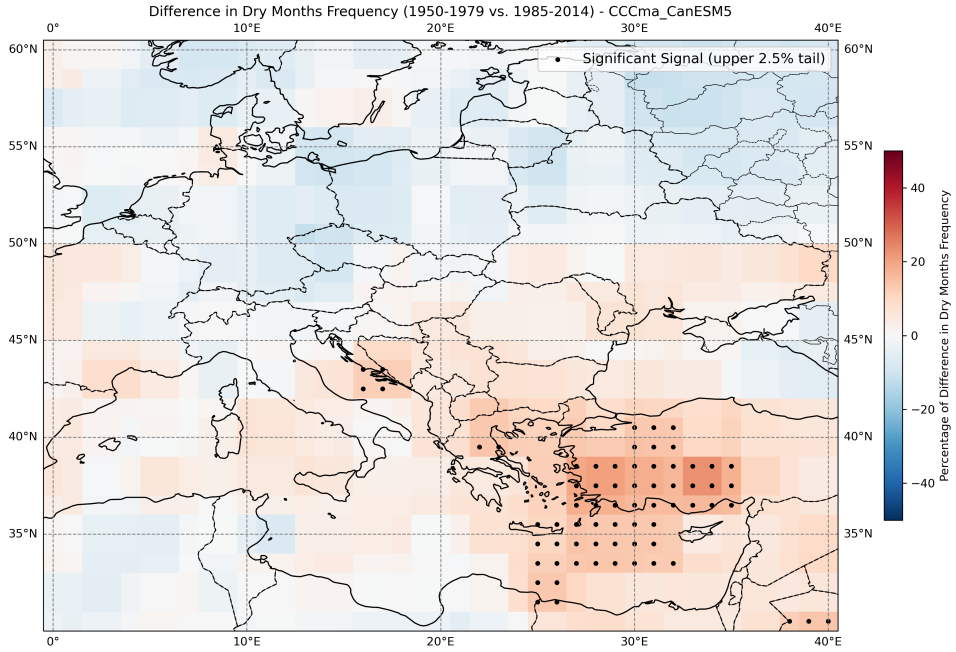

Figure A.8: Difference in dry months frequency for CCCma CanESM5.

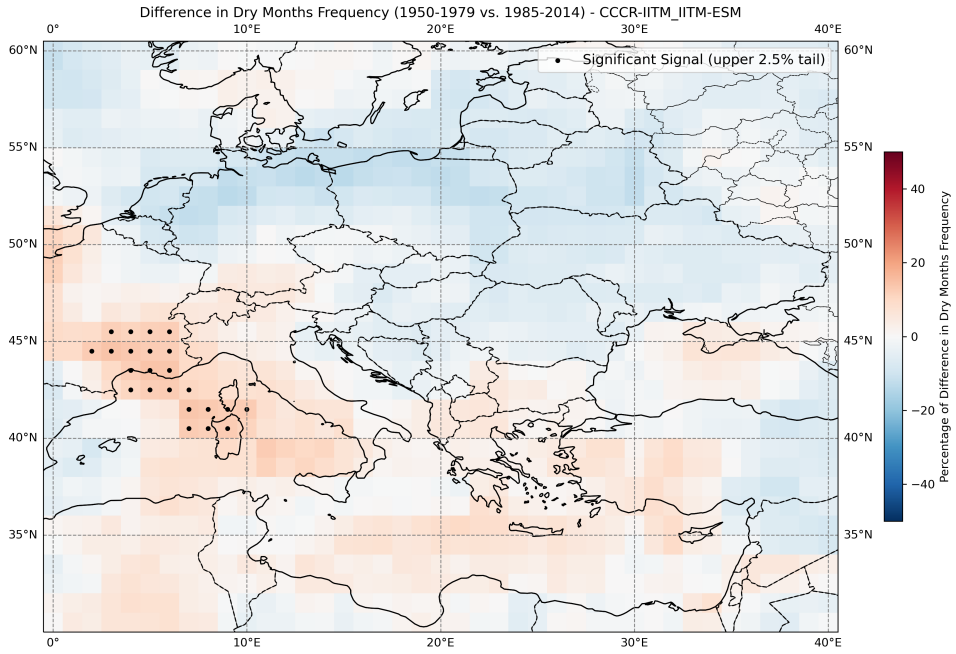

Figure A.9: Difference in dry months frequency for CCCR-IITM IITM-ESM.

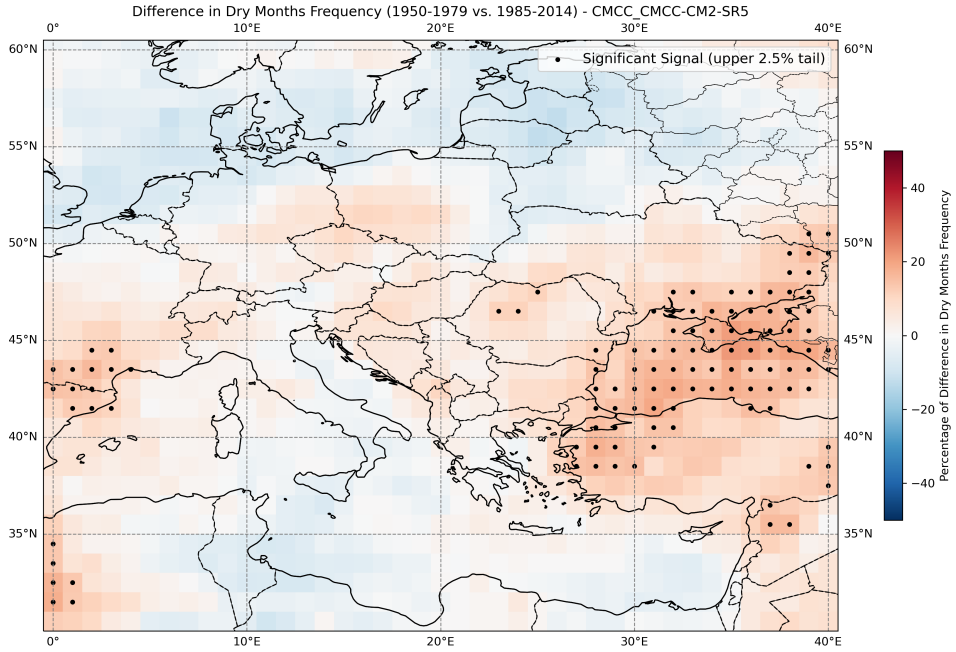

Figure A.10: Difference in dry months frequency for CMCC CMCC-CM2-SR5.

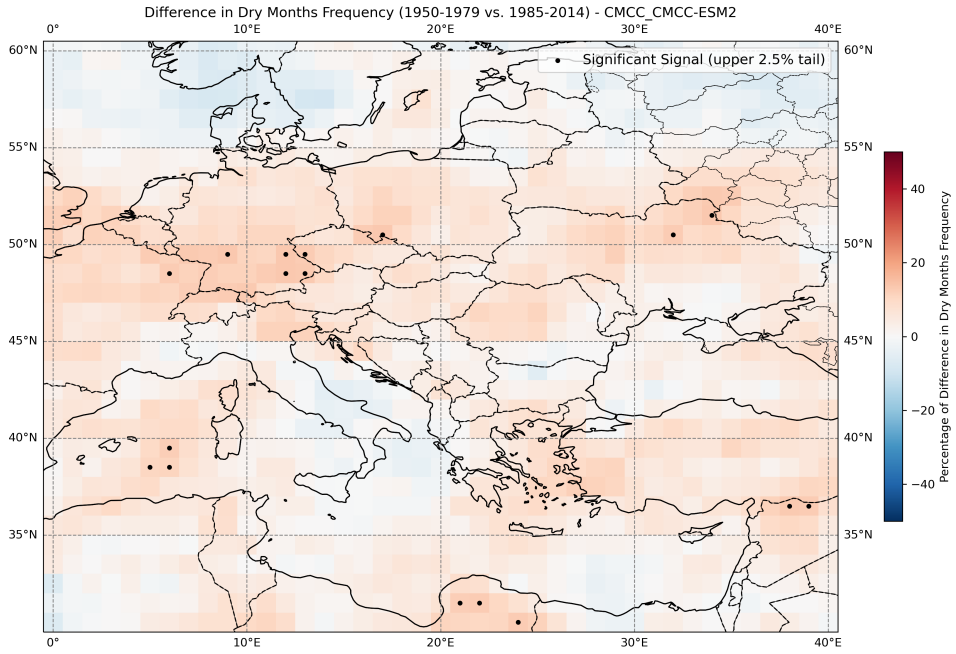

Figure A.11: Difference in dry months frequency for CMCC CMCC-ESM2.

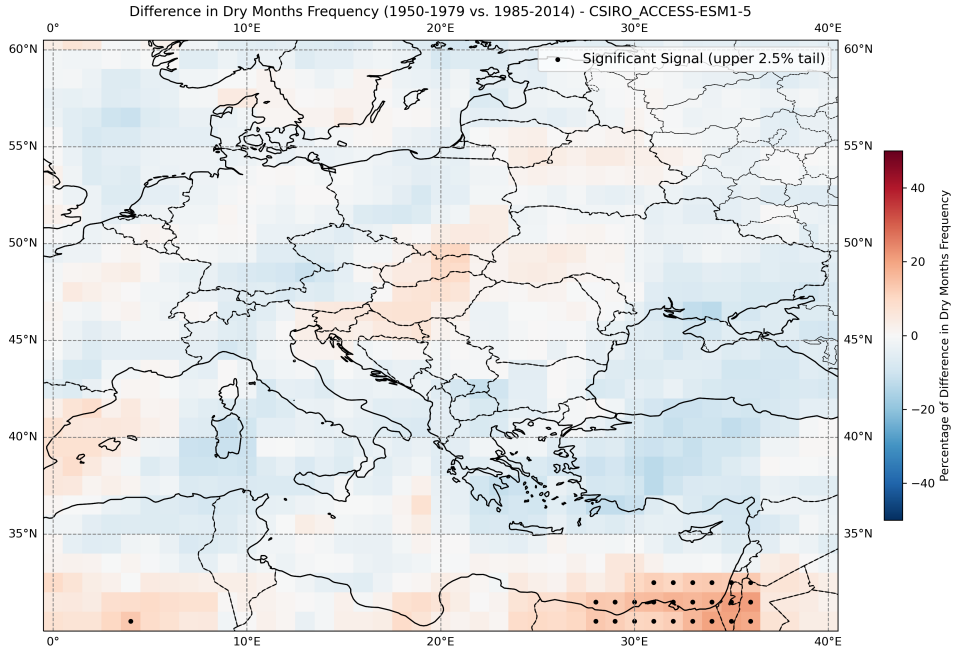

Figure A.12: Difference in dry months frequency for CSIRO ACCESS-ESM1-5.

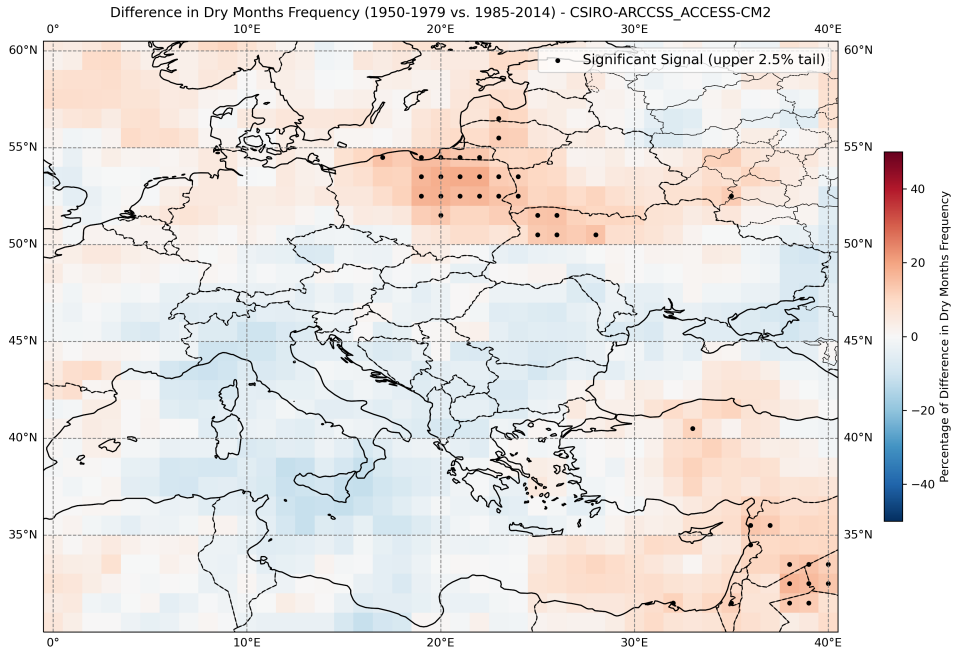

Figure A.13: Difference in dry months frequency for CSIRO-ARCCSS ACCESS-CM2.

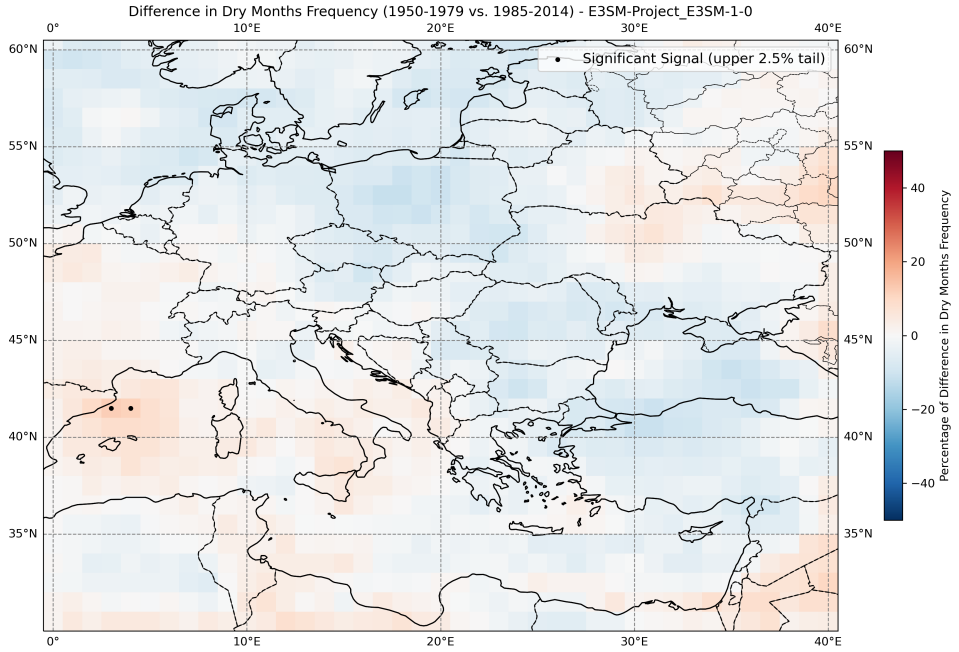

Figure A.14: Difference in dry months frequency for E3SM-Project E3SM-1-0.

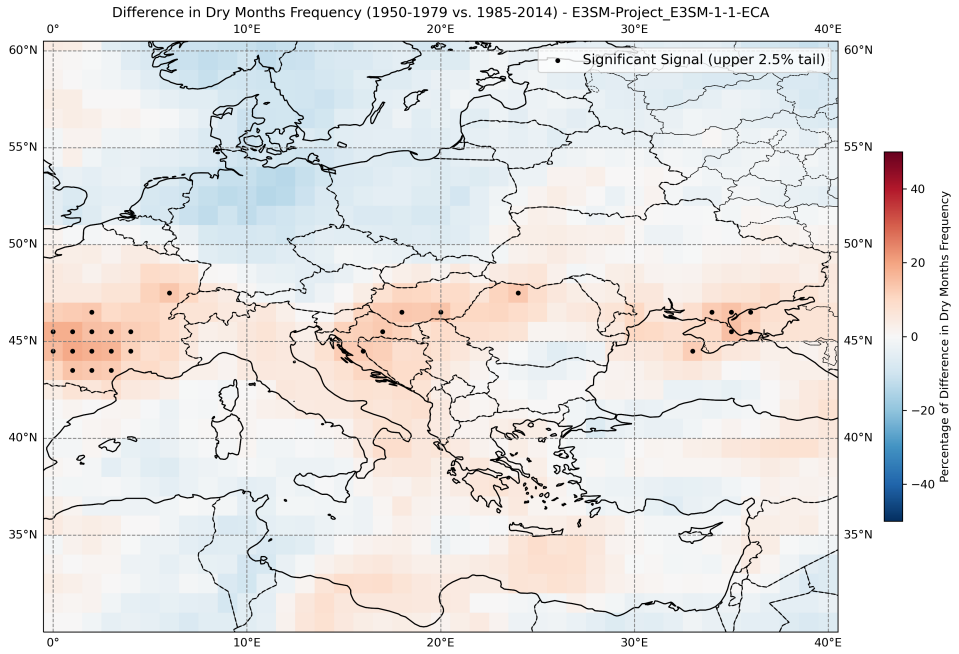

Figure A.15: Difference in dry months frequency for E3SM-Project E3SM-1-1-ECA.

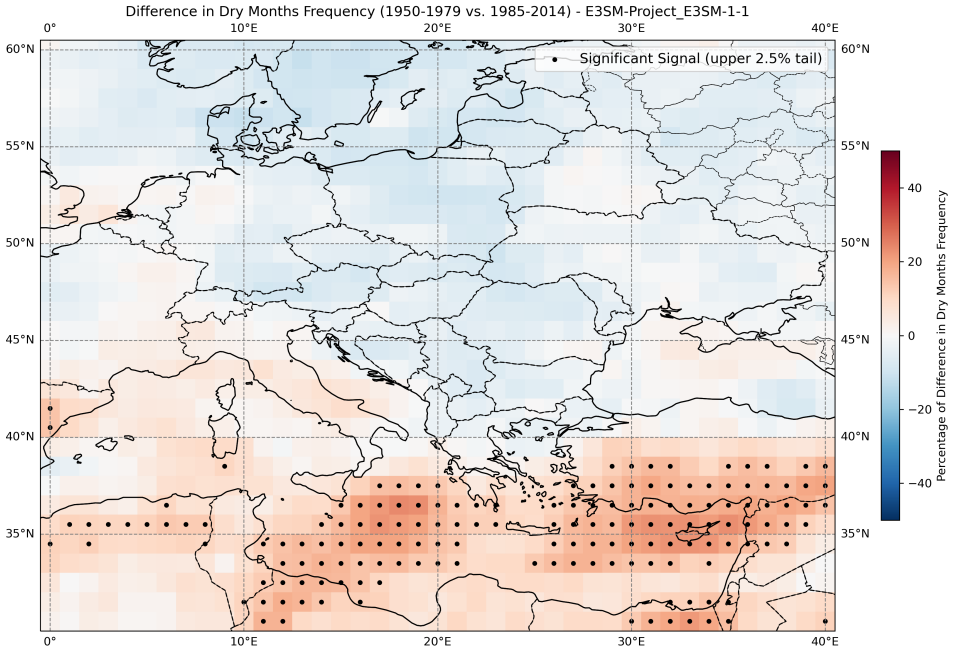

Figure A.16: Difference in dry months frequency for E3SM-Project E3SM-1-1.

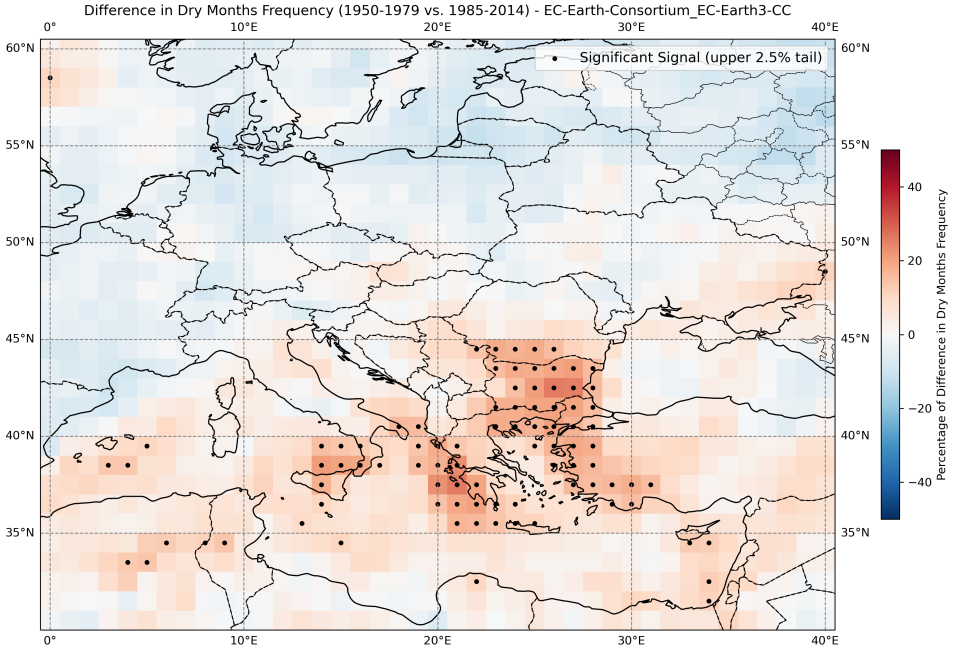

Figure A.17: Difference in dry months frequency for EC-Earth-Consortium EC-Earth3-CC.

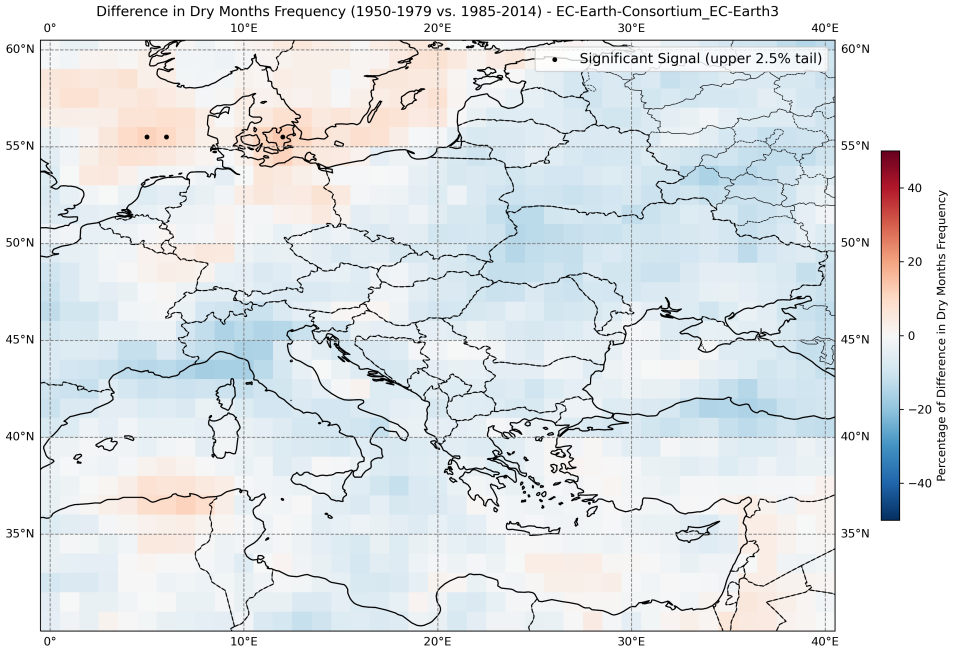

Figure A.18: Difference in dry months frequency for EC-Earth-Consortium EC-Earth3.

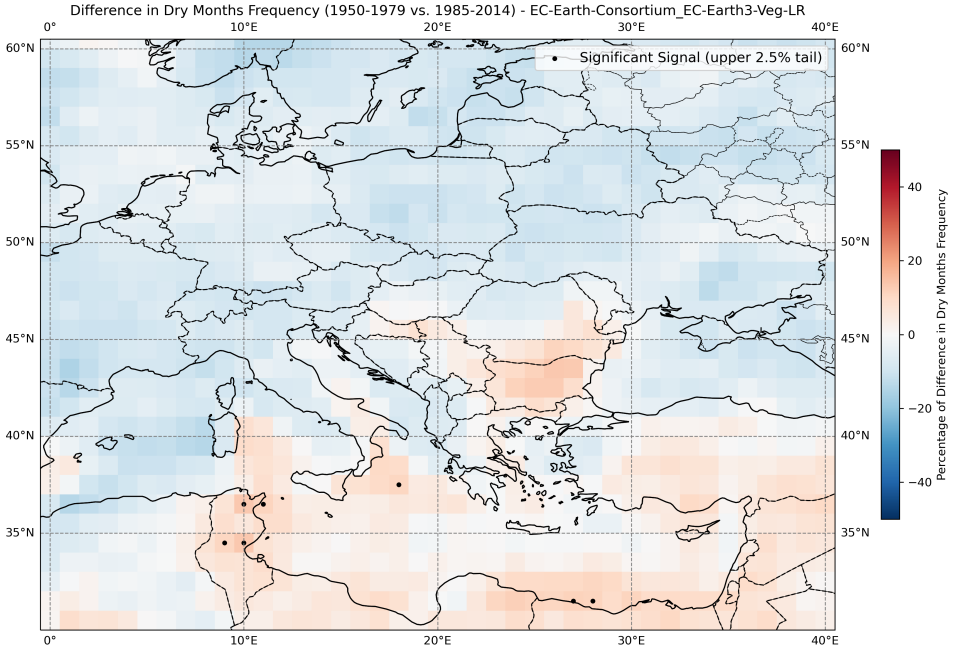

Figure A.19: Difference in dry months frequency for EC-Earth-Consortium EC-Earth3-Veg-LR.

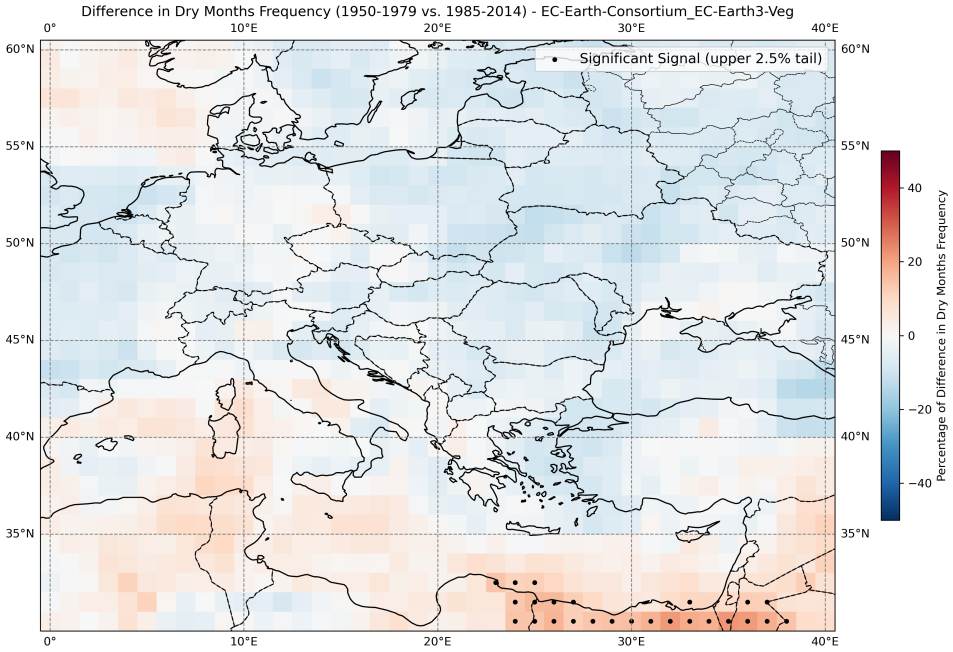

Figure A.20: Difference in dry months frequency for EC-Earth-Consortium EC-Earth3-Veg.

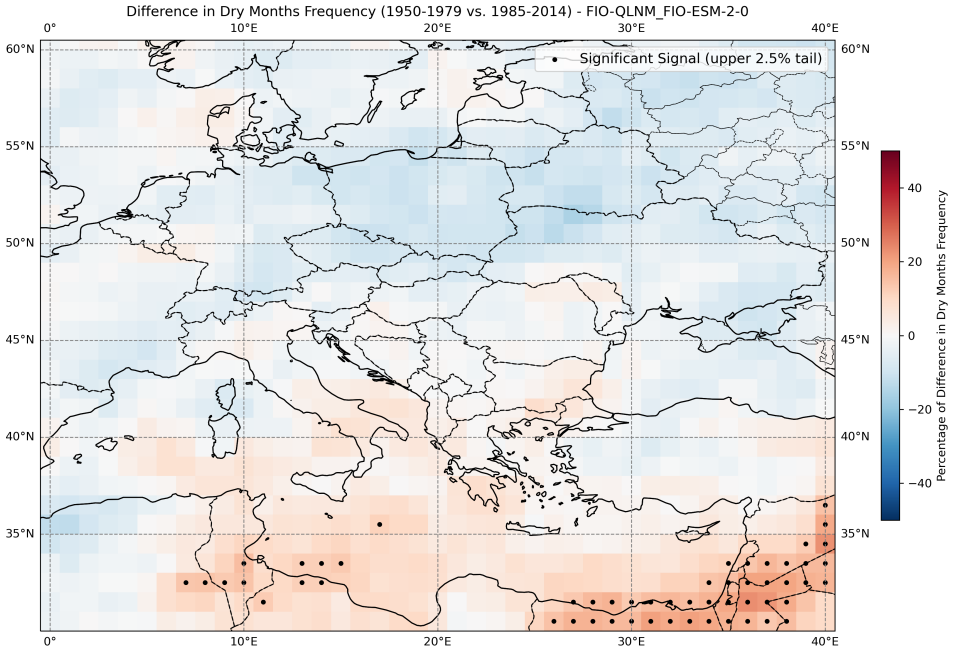

Figure A.21: Difference in dry months frequency for FIO-QLNM FIO-ESM-2-0.

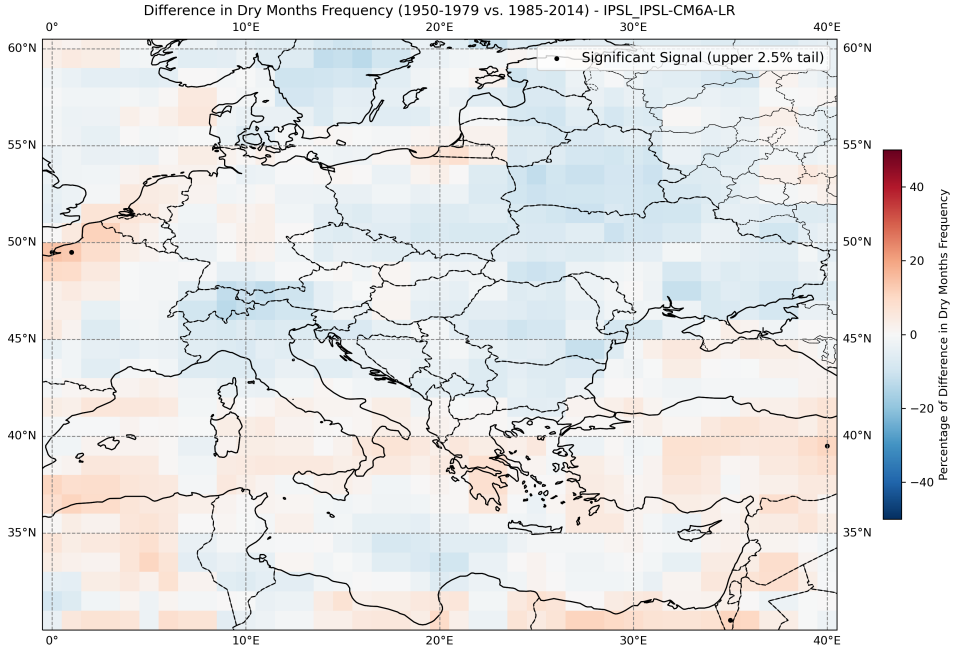

Figure A.22: Difference in dry months frequency for IPSL IPSL-CM6A-LR.

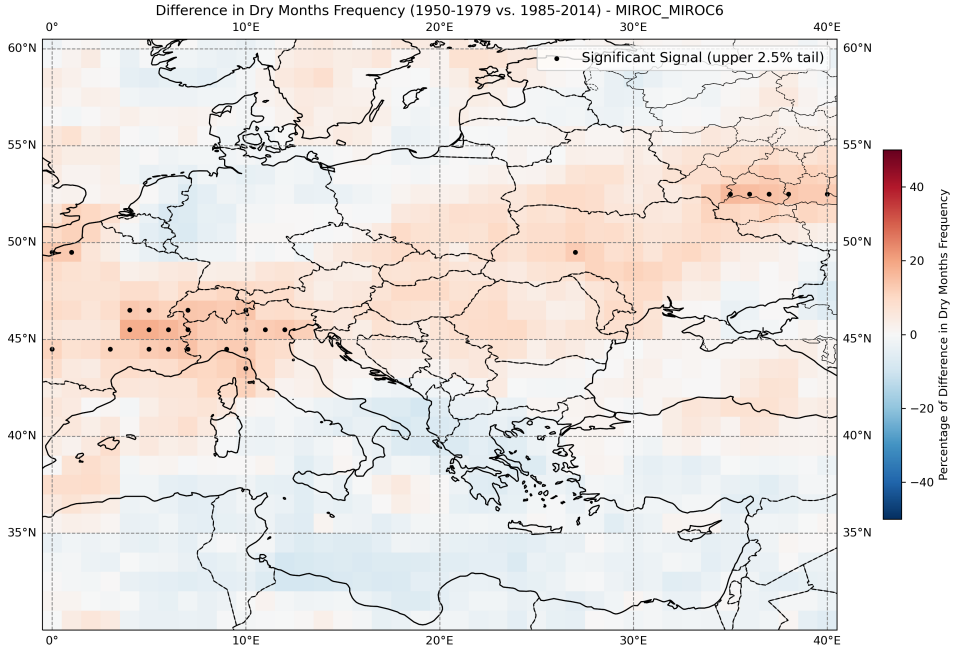

Figure A.23: Difference in dry months frequency for MIROC MIROC6.

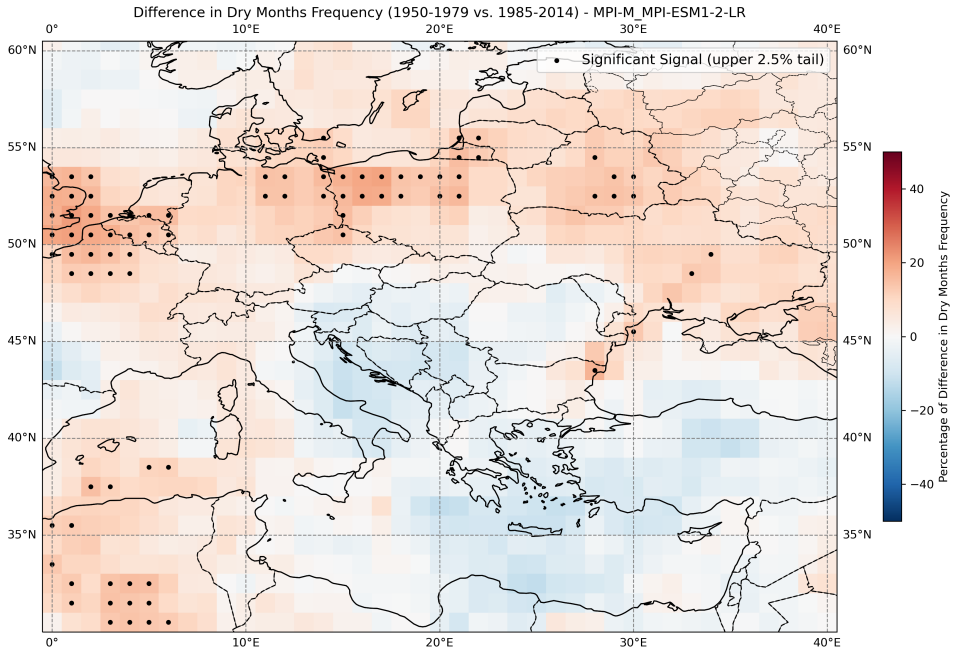

Figure A.24: Difference in dry months frequency for MPI-M MPI-ESM1-2-LR.

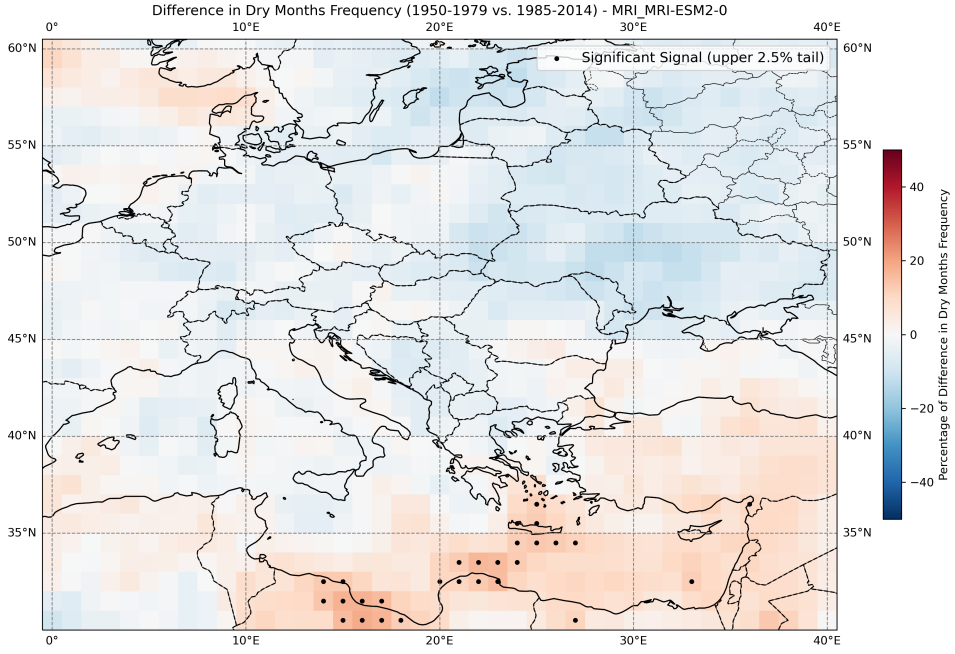

Figure A.25: Difference in dry months frequency for MRI MRI-ESM2-0.

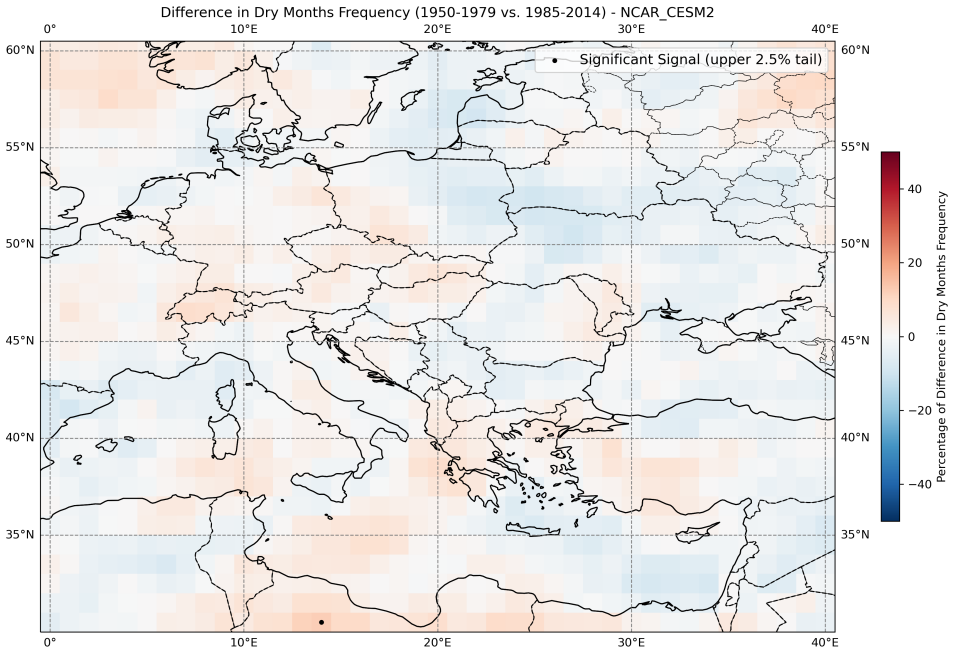

Figure A.26: Difference in dry months frequency for NCAR CESM2.

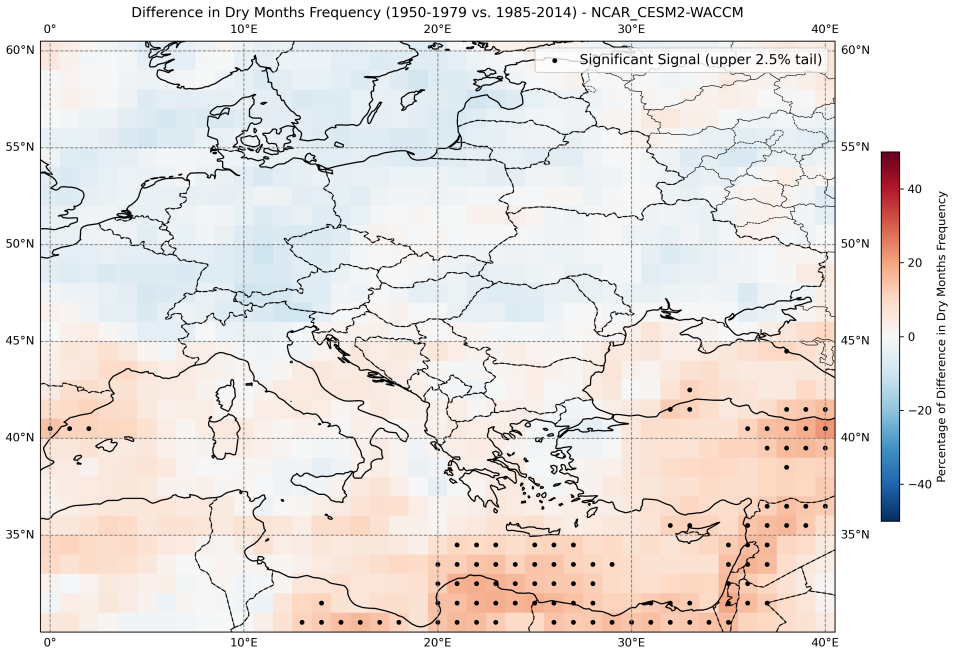

Figure A.27: Difference in dry months frequency for NCAR CESM2-WACCM.

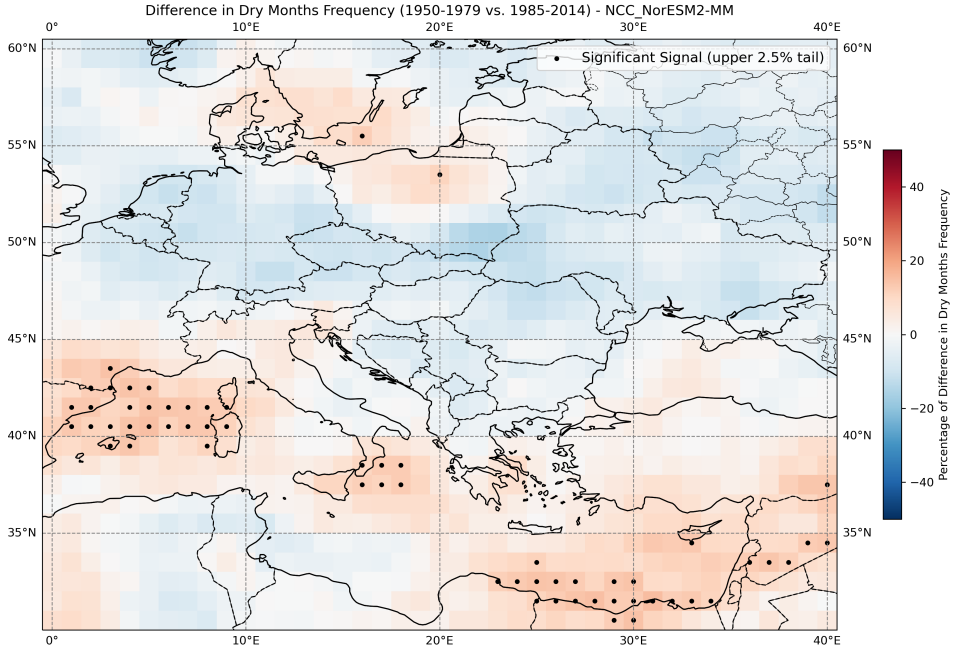

Figure A.28: Difference in dry months frequency for NCC NorESM2-MM.

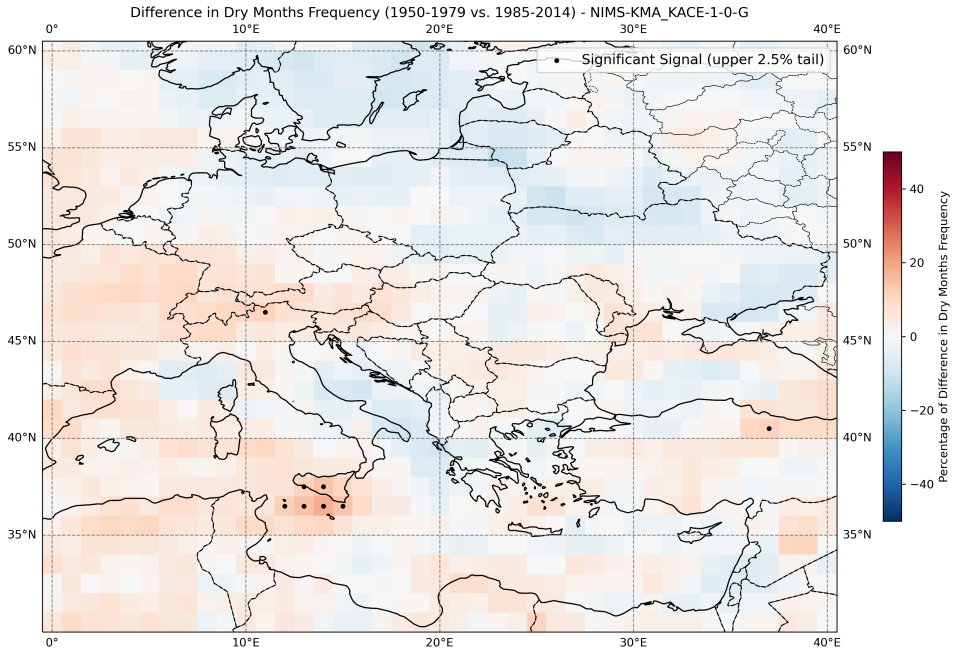

Figure A.29: Difference in dry months frequency for NIMS-KMA KACE-1-0-G.

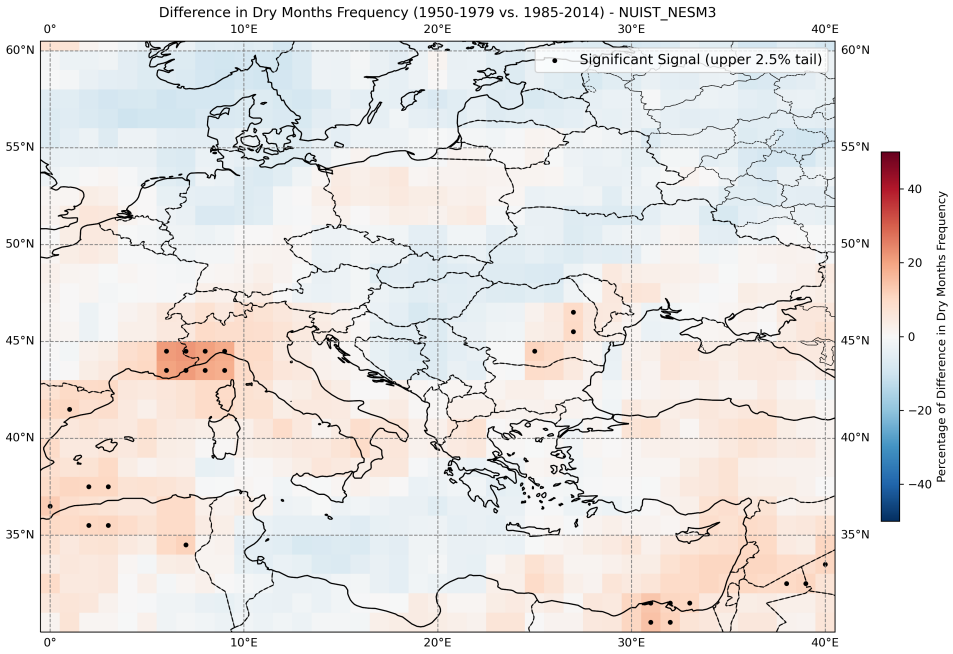

Figure A.30: Difference in dry months frequency for NUIST NESM3.

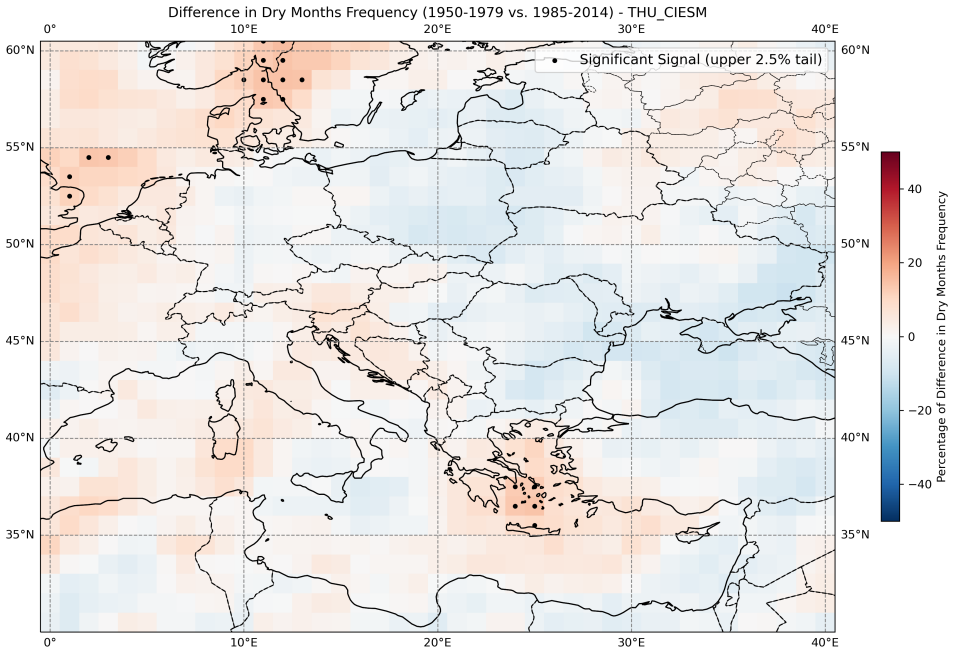

Figure A.31: Difference in dry months frequency for THU CIESM.

Appendix B

Future Projections

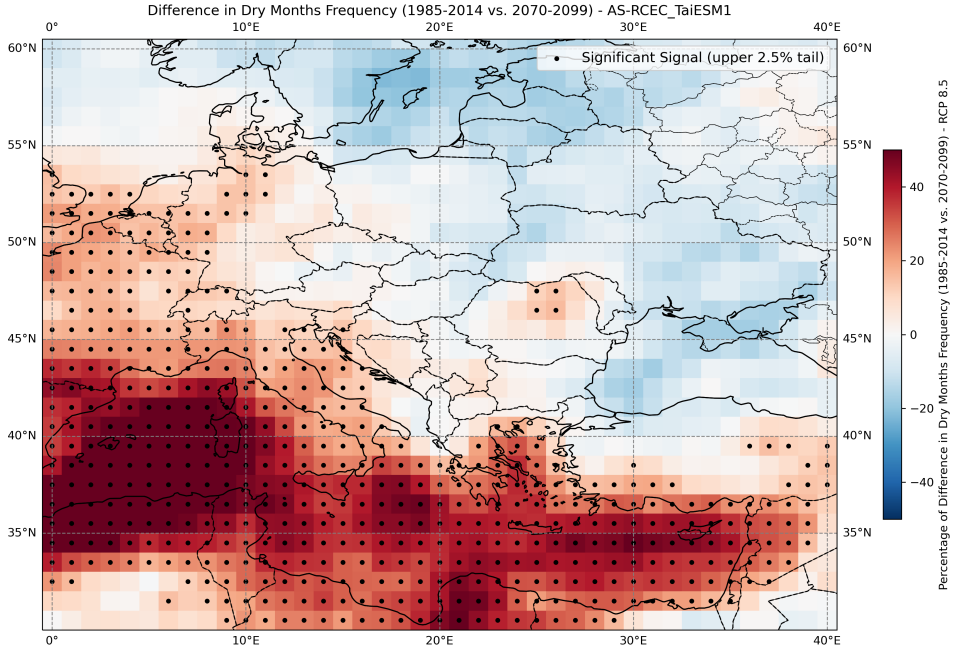

Figure B.1: Difference in dry months frequency for AS-RCEC TaiESM1.

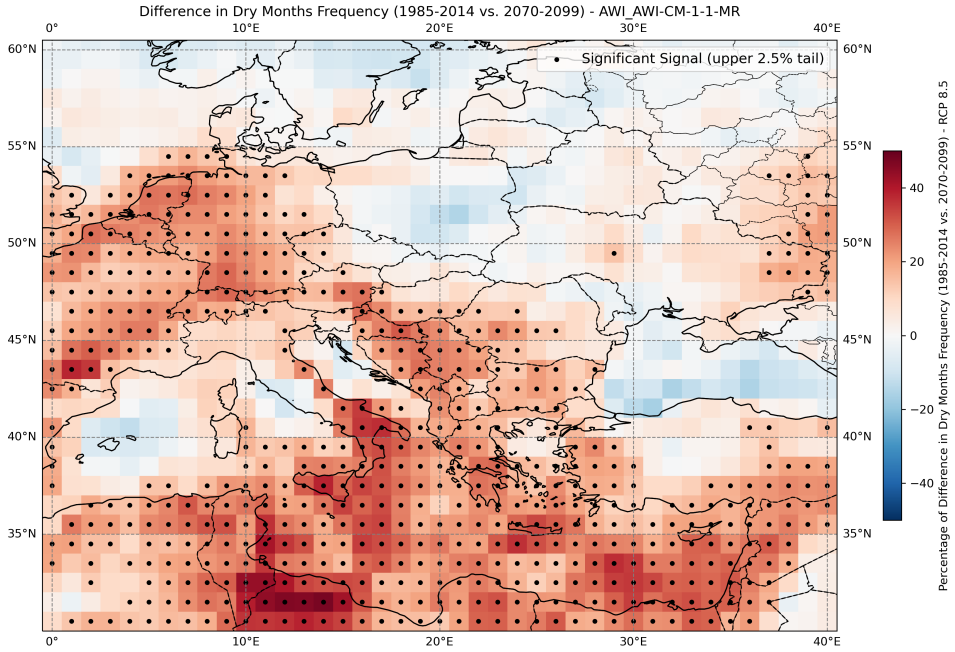

Figure B.2: Difference in dry months frequency for AWI AWI-CM-1-1-MR.

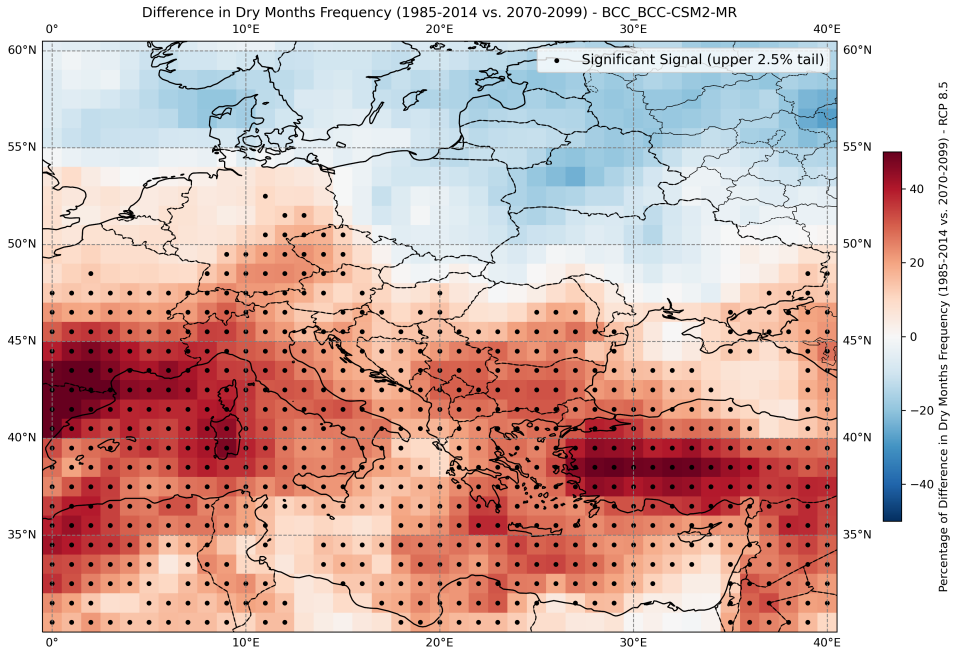

Figure B.3: Difference in dry months frequency for BCC BCC-CSM2-MR.

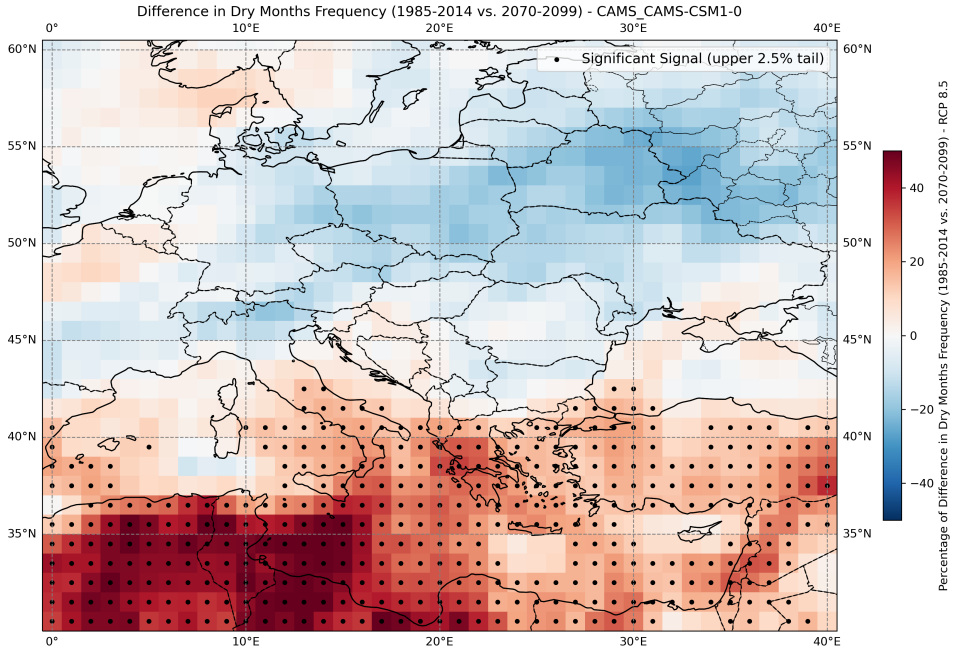

Figure B.4: Difference in dry months frequency for CAMS CAMS-CSM1-0.

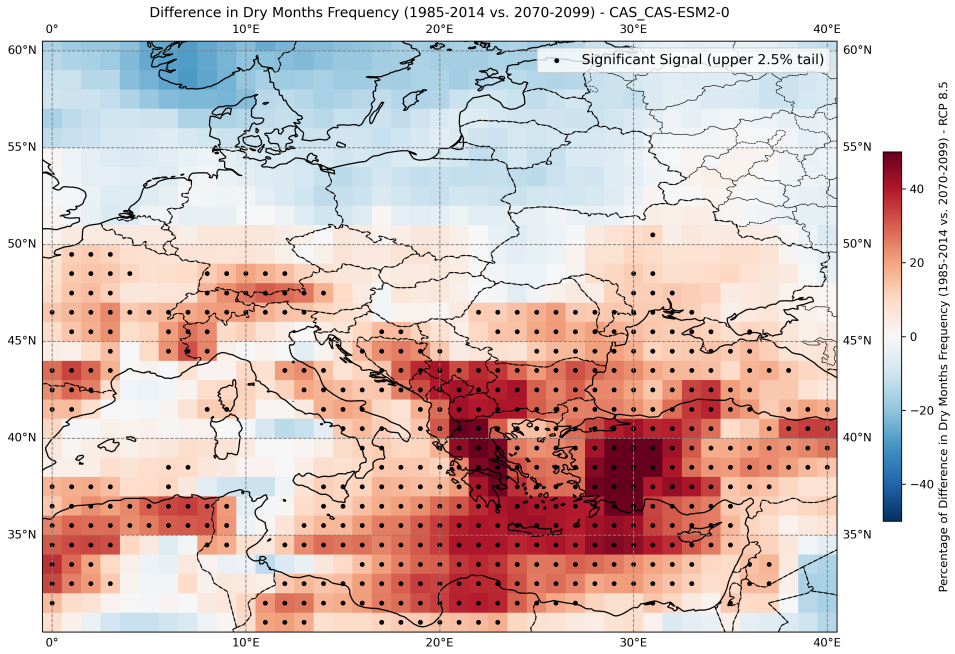

Figure B.5: Difference in dry months frequency for CAS CAS-ESM2-0.

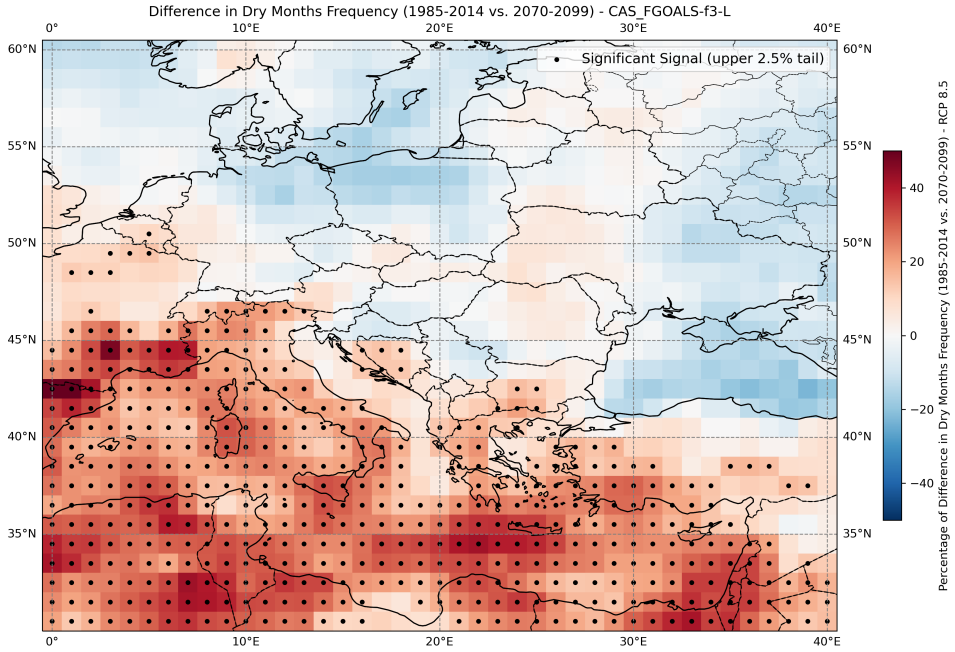

Figure B.6: Difference in dry months frequency for CAS FGOALS-f3-L.

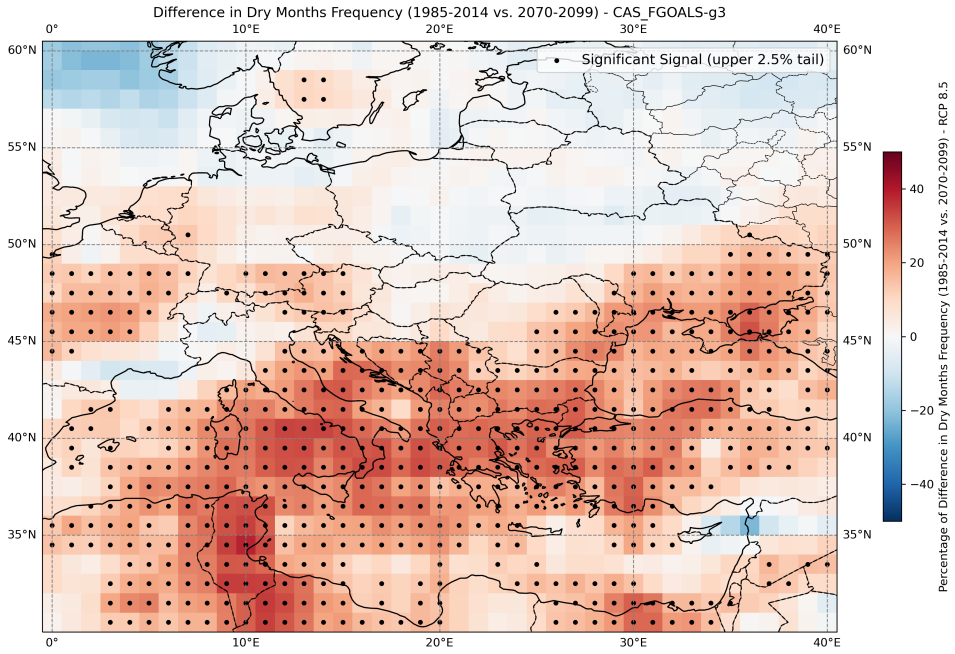

Figure B.7: Difference in dry months frequency for CAS FGOALS-g3.

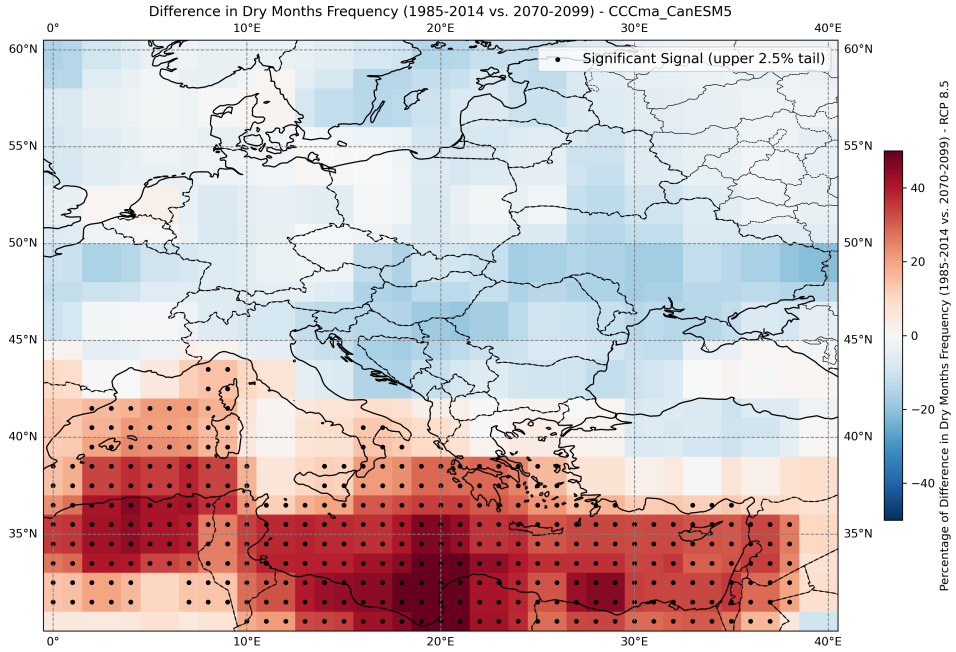

Figure B.8: Difference in dry months frequency for CCCma CanESM5.

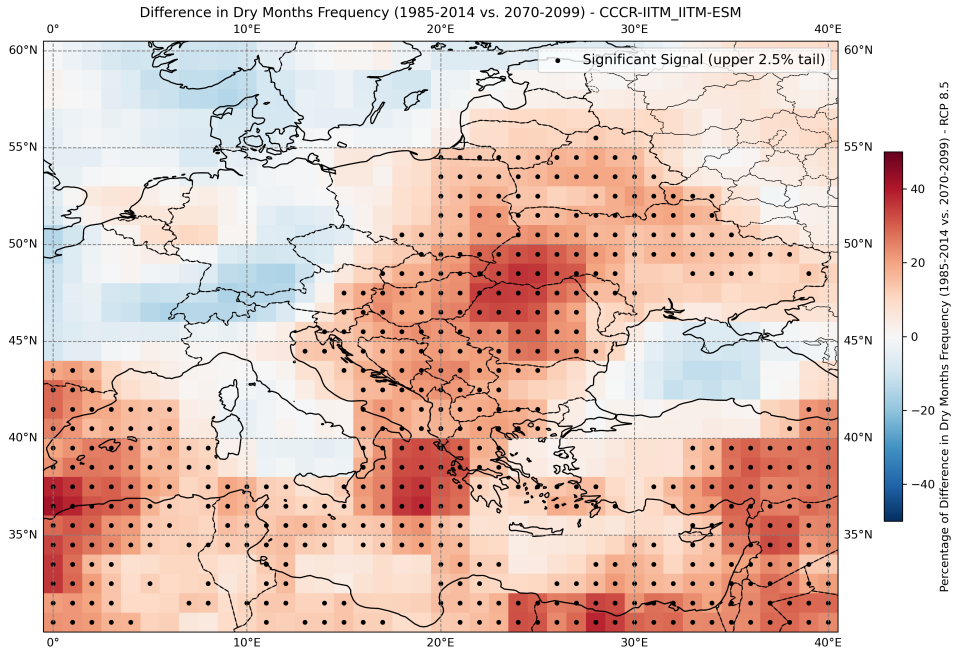

Figure B.9: Difference in dry months frequency for CCCR-IITM IITM-ESM.

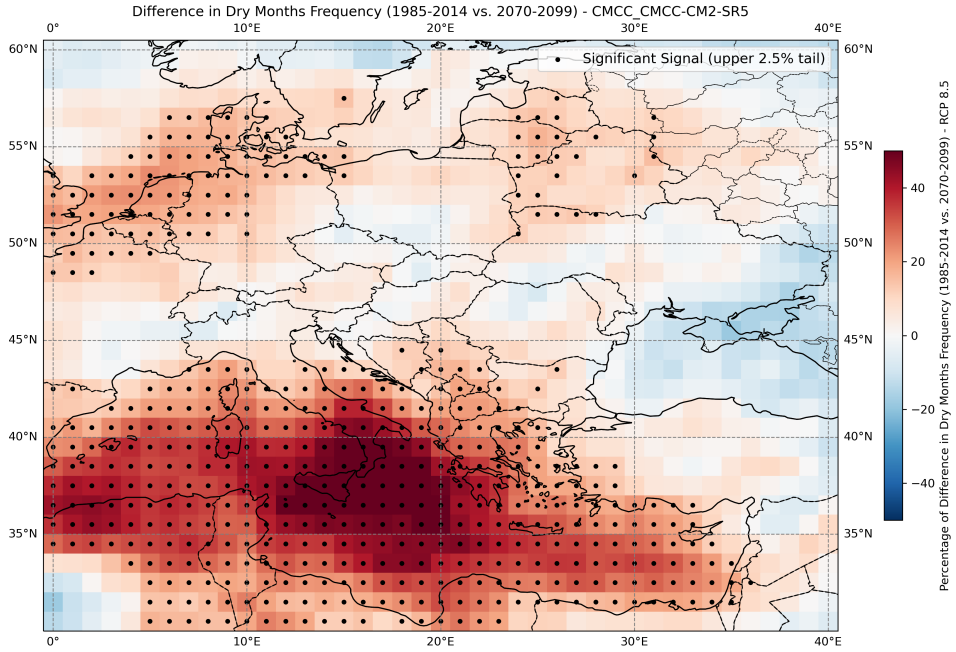

Figure B.10: Difference in dry months frequency for CMCC CMCC-CM2-SR5.

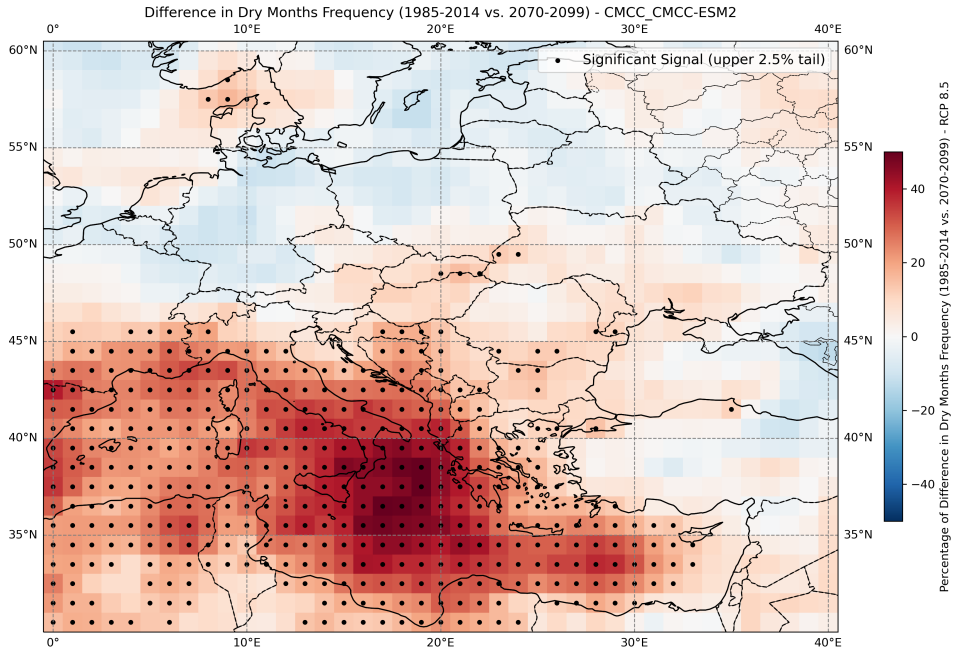

Figure B.11: Difference in dry months frequency for CMCC CMCC-ESM2.

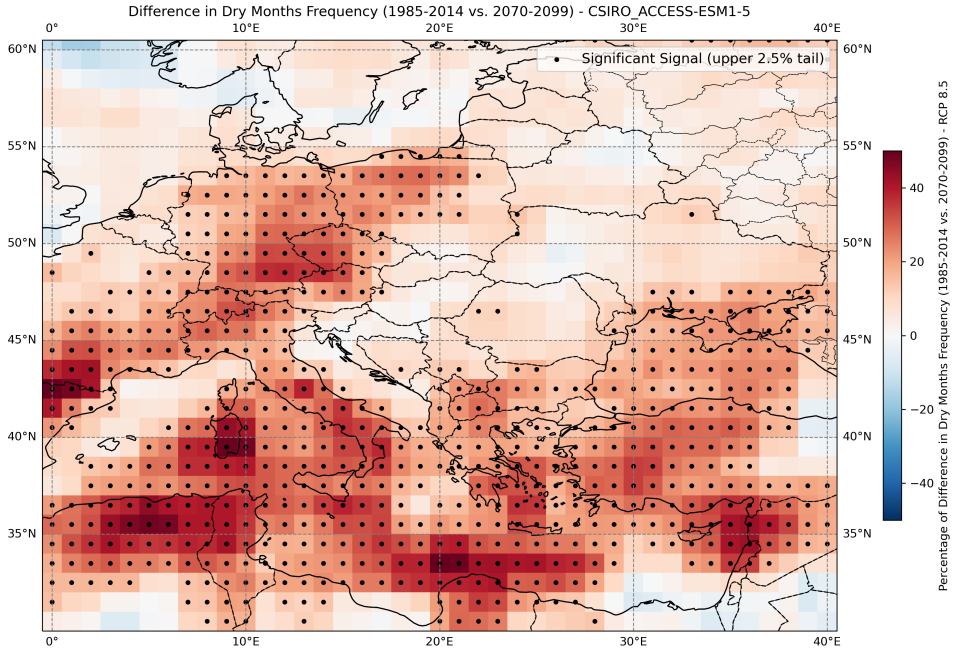

Figure B.12: Difference in dry months frequency for CSIRO ACCESS-ESM1-5.

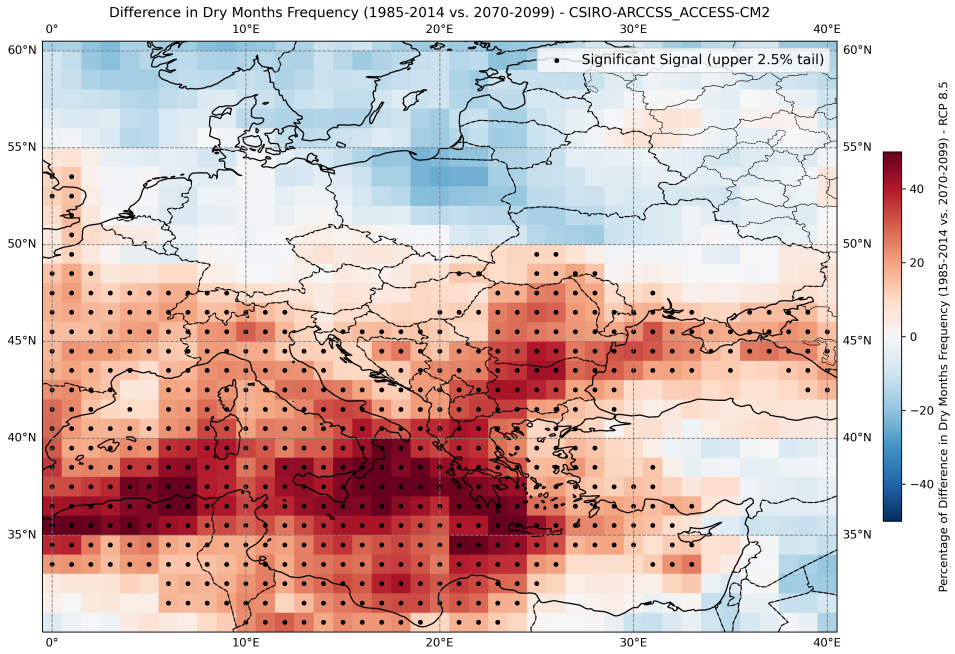

Figure B.13: Difference in dry months frequency for CSIRO-ARCCSS ACCESS-CM2.

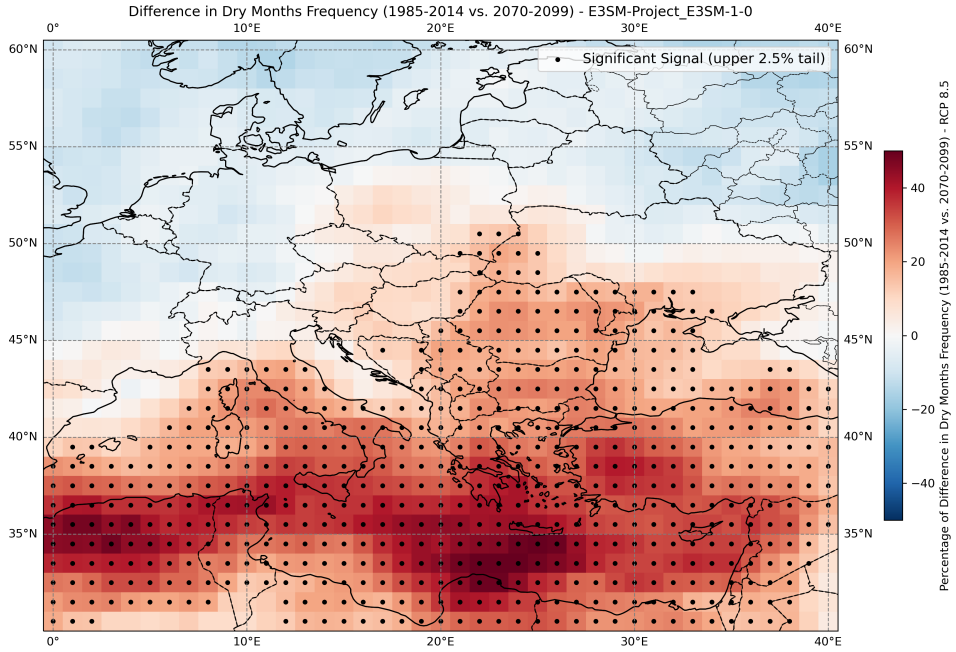

Figure B.14: Difference in dry months frequency for E3SM-Project E3SM-1-0.

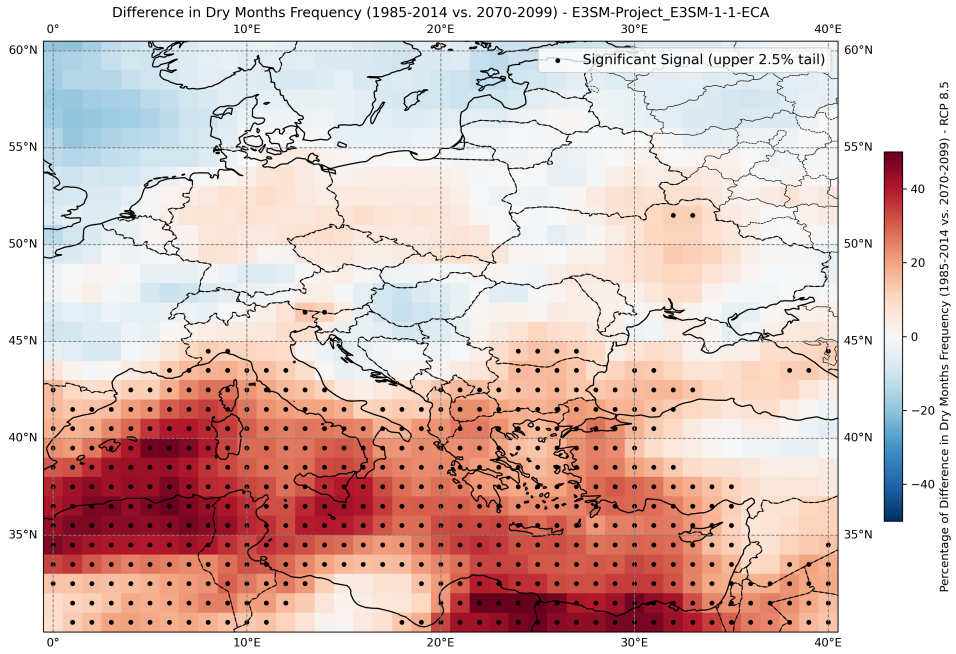

Figure B.15: Difference in dry months frequency for E3SM-Project E3SM-1-1-ECA.

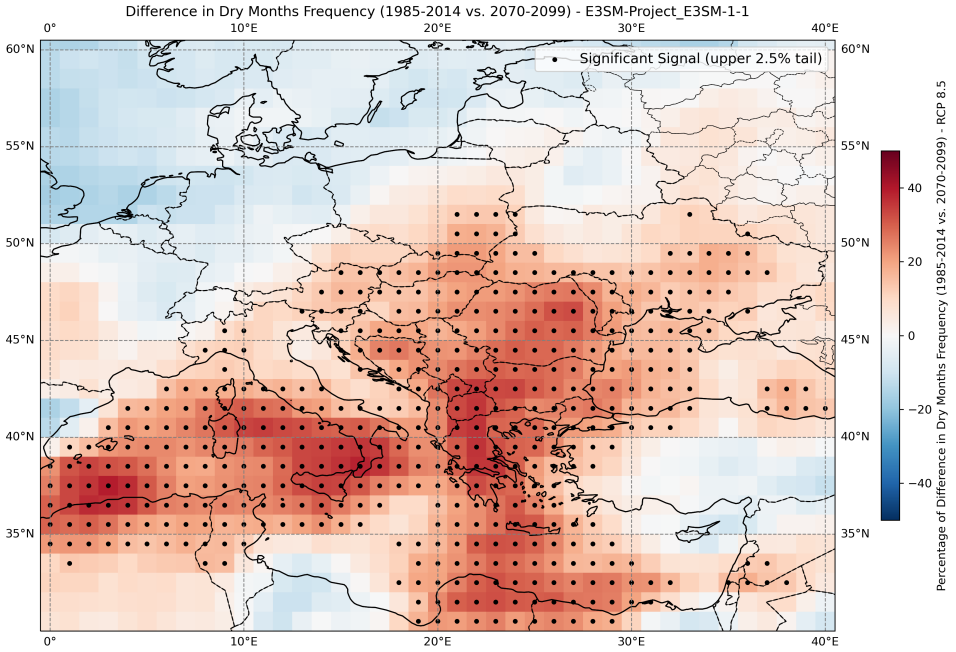

Figure B.16: Difference in dry months frequency for E3SM-Project E3SM-1-1.

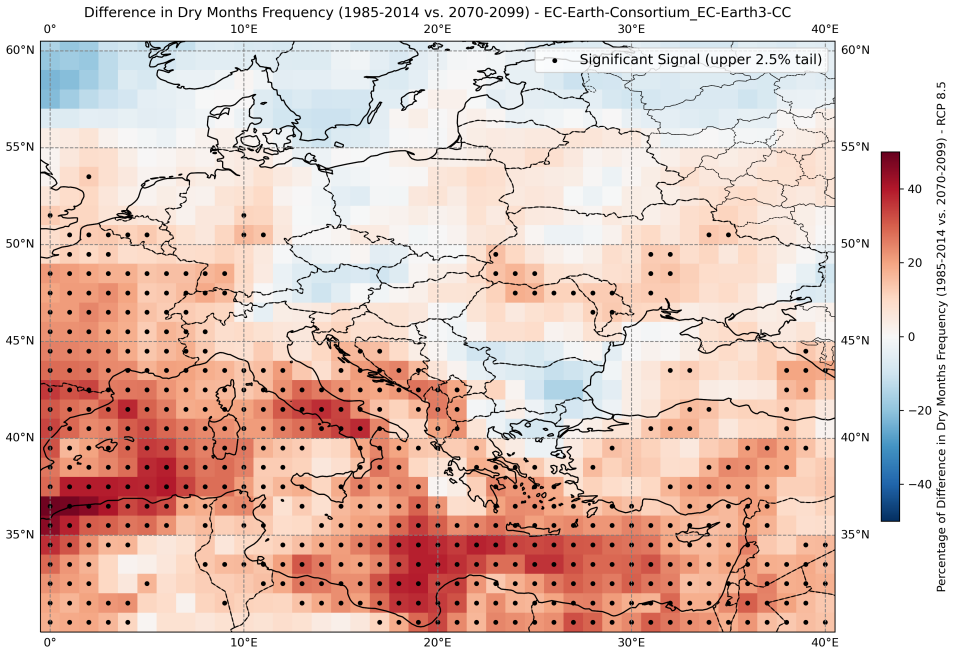

Figure B.17: Difference in dry months frequency for EC-Earth-Consortium EC-Earth3-CC.

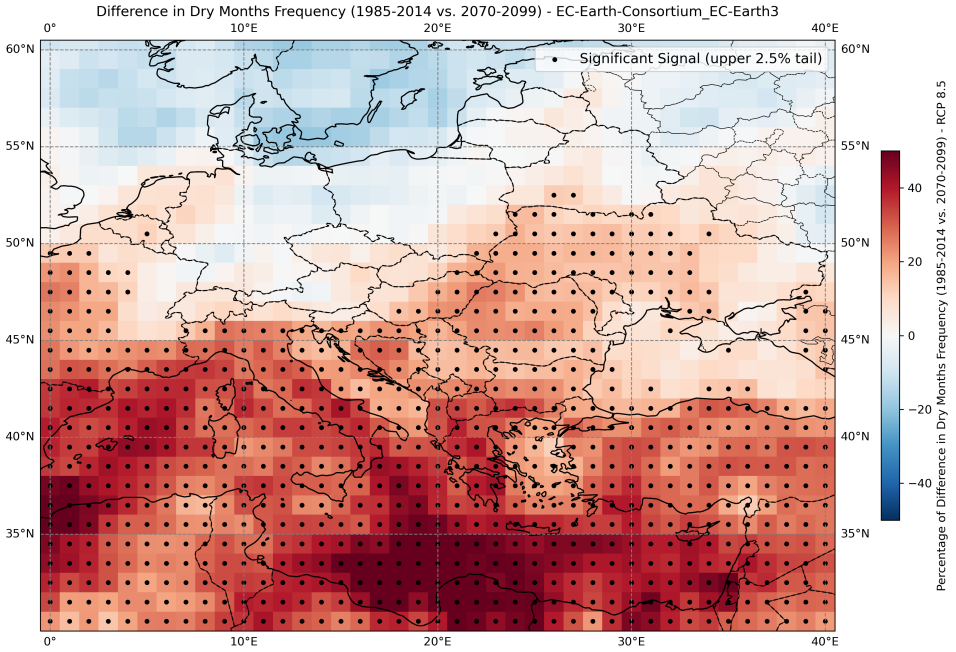

Figure B.18: Difference in dry months frequency for EC-Earth-Consortium EC-Earth3.

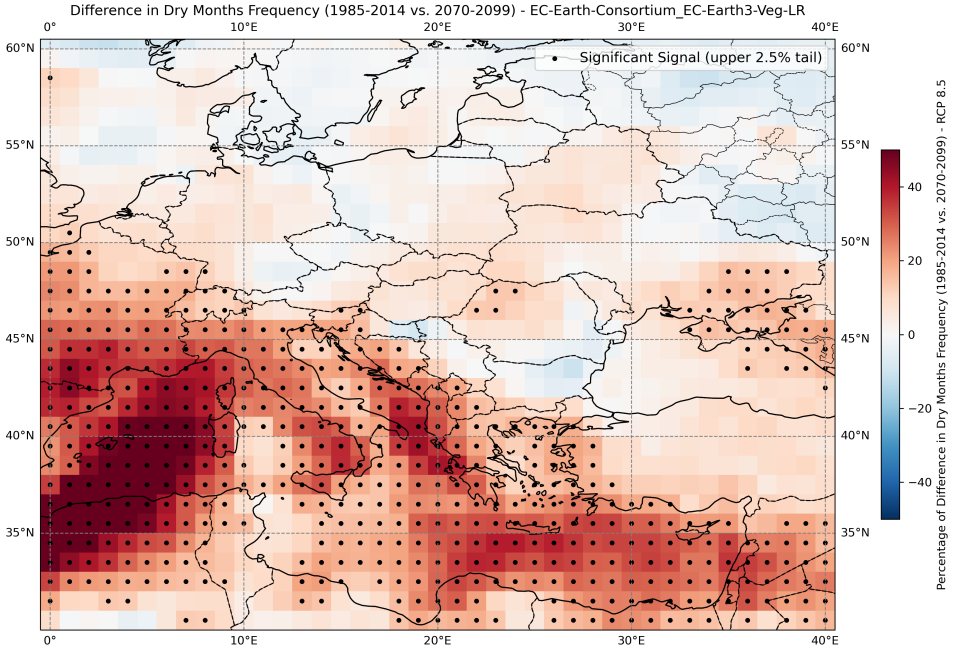

Figure B.19: Difference in dry months frequency for EC-Earth-Consortium EC-Earth3-Veg-LR.

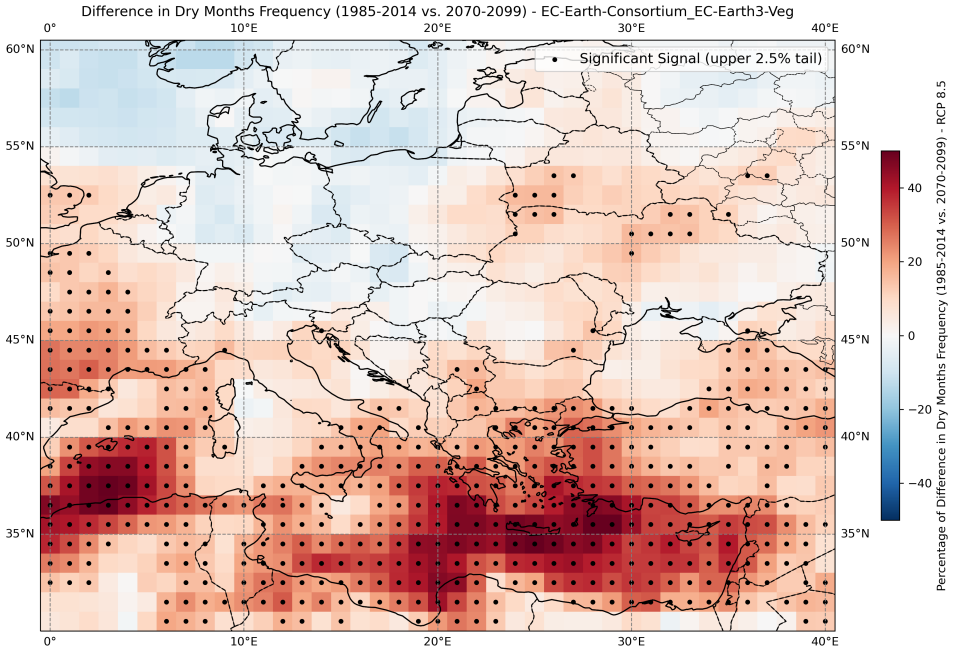

Figure B.20: Difference in dry months frequency for EC-Earth-Consortium EC-Earth3-Veg.

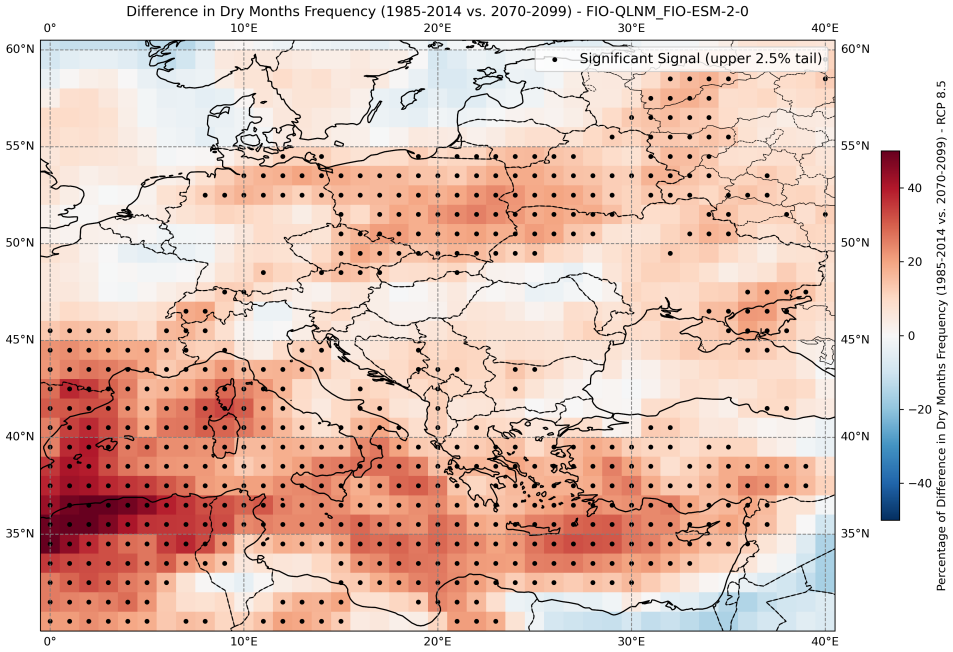

Figure B.21: Difference in dry months frequency for FIO-QLNM FIO-ESM-2-0.

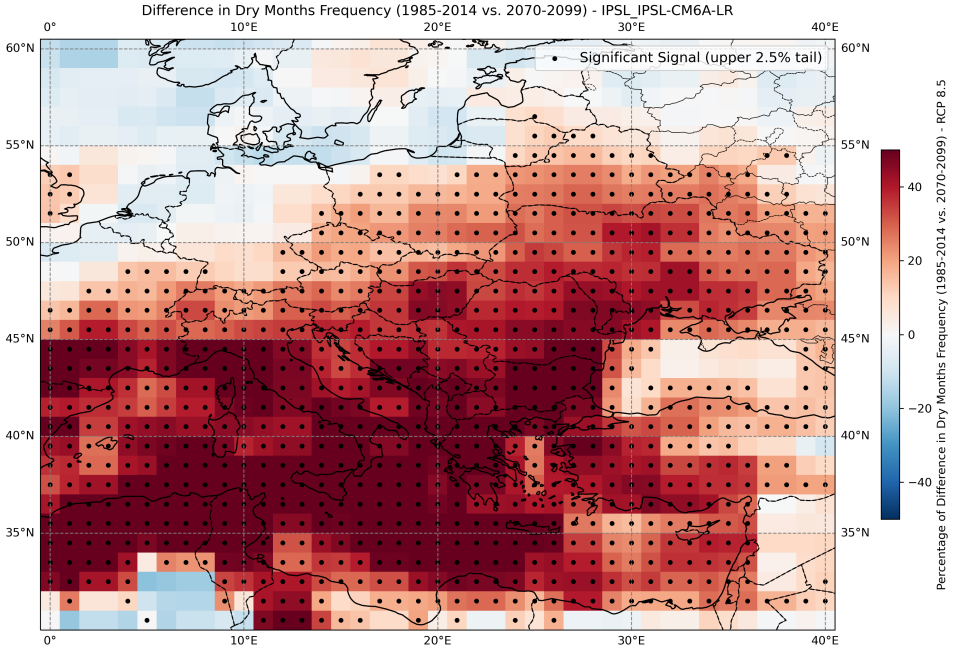

Figure B.22: Difference in dry months frequency for IPSL IPSL-CM6A-LR.

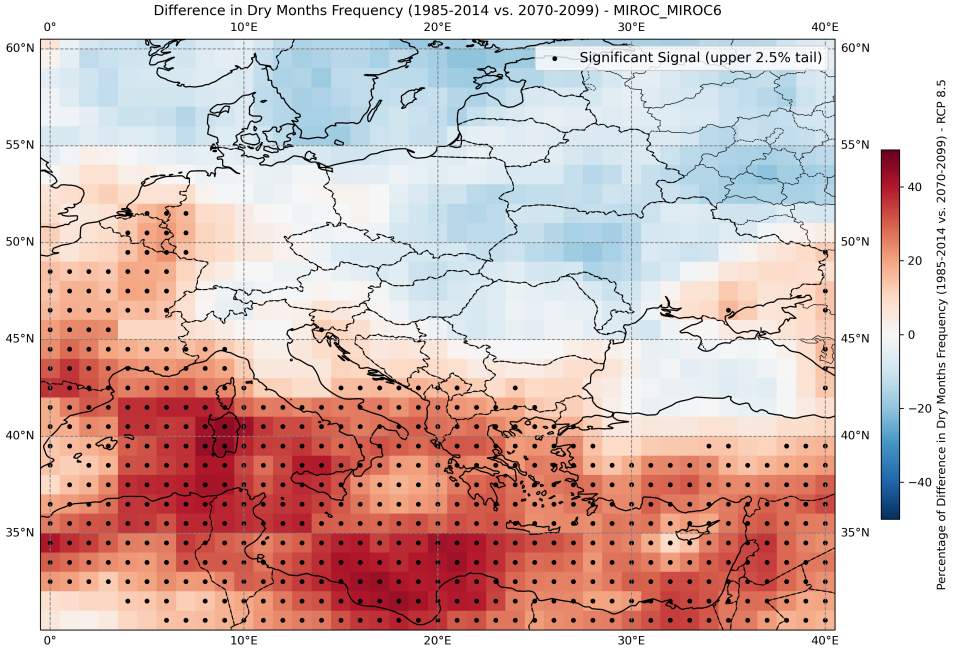

Figure B.23: Difference in dry months frequency for MIROC MIROC6.

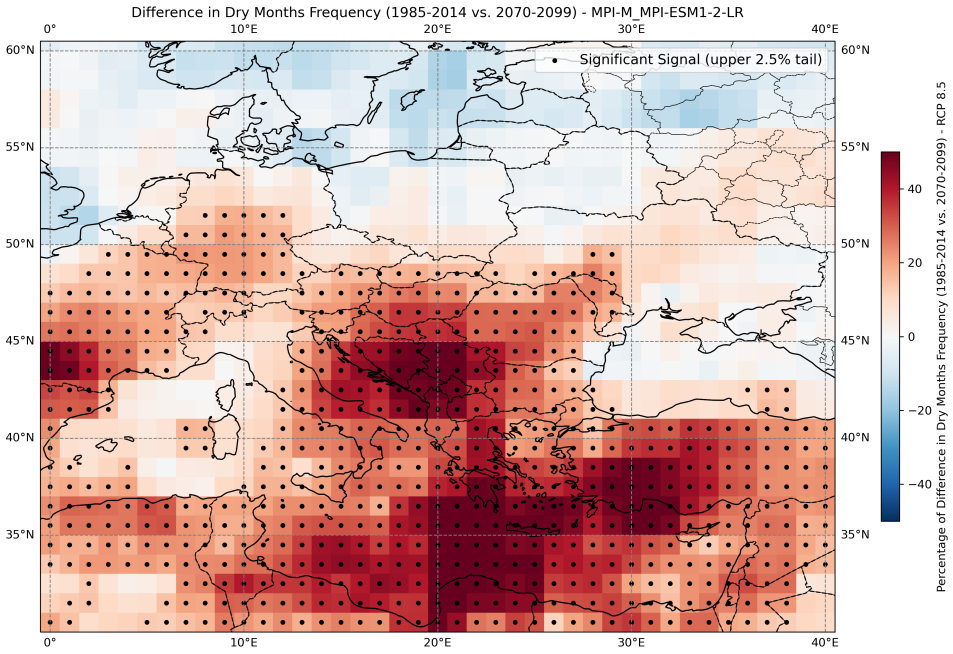

Figure B.24: Difference in dry months frequency for MPI-M MPI-ESM1-2-LR.

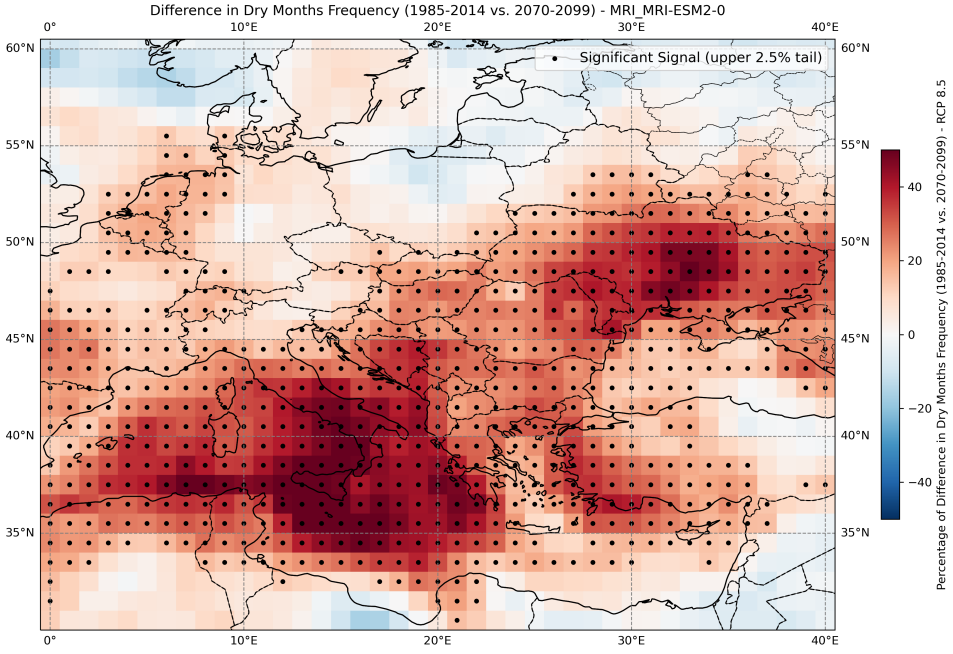

Figure B.25: Difference in dry months frequency for MRI MRI-ESM2-0.

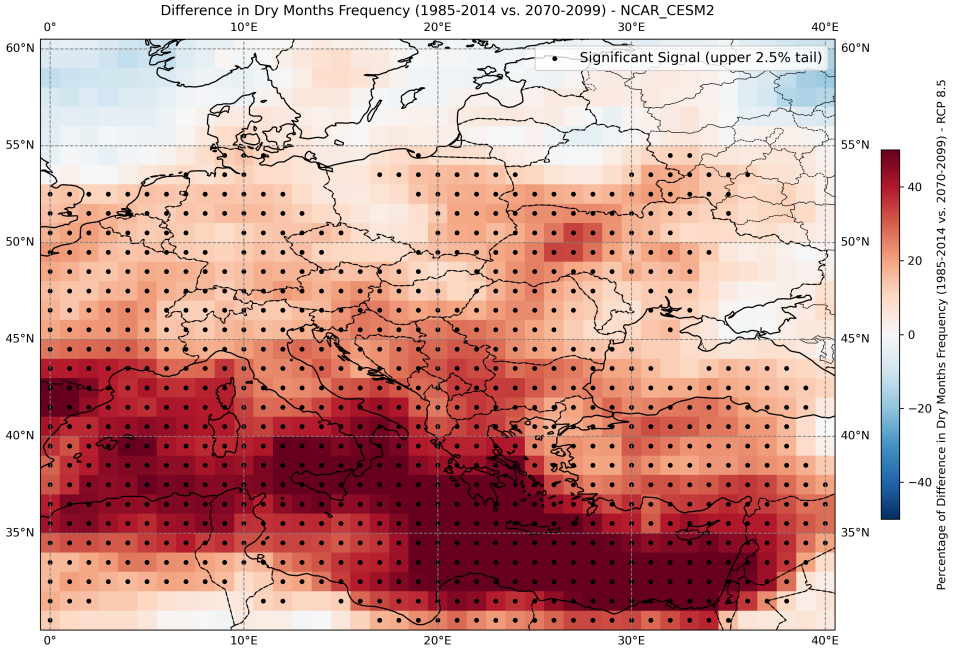

Figure B.26: Difference in dry months frequency for NCAR CESM2.

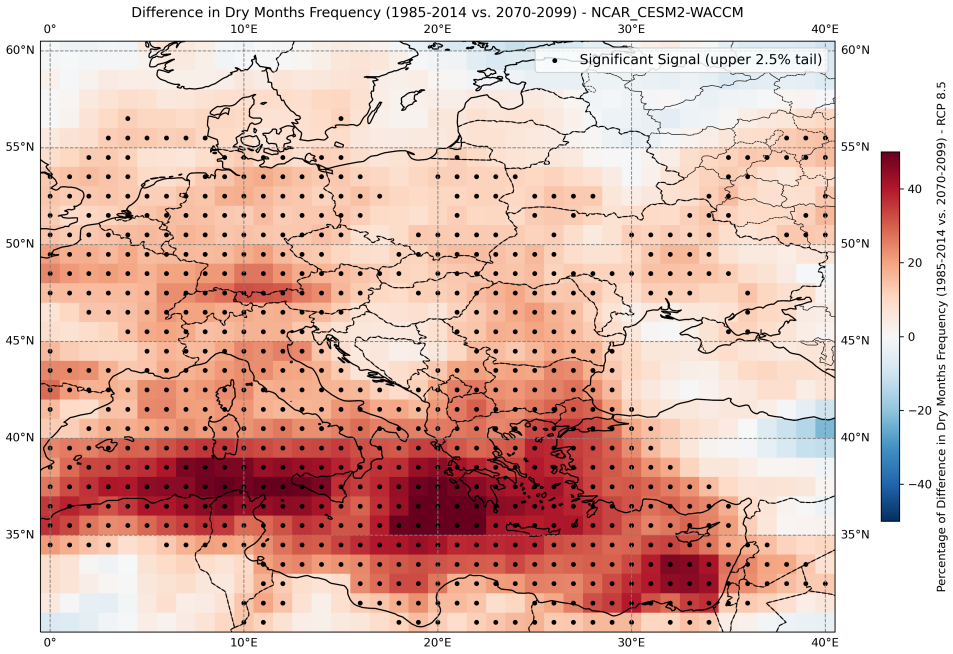

Figure B.27: Difference in dry months frequency for NCAR CESM2-WACCM.

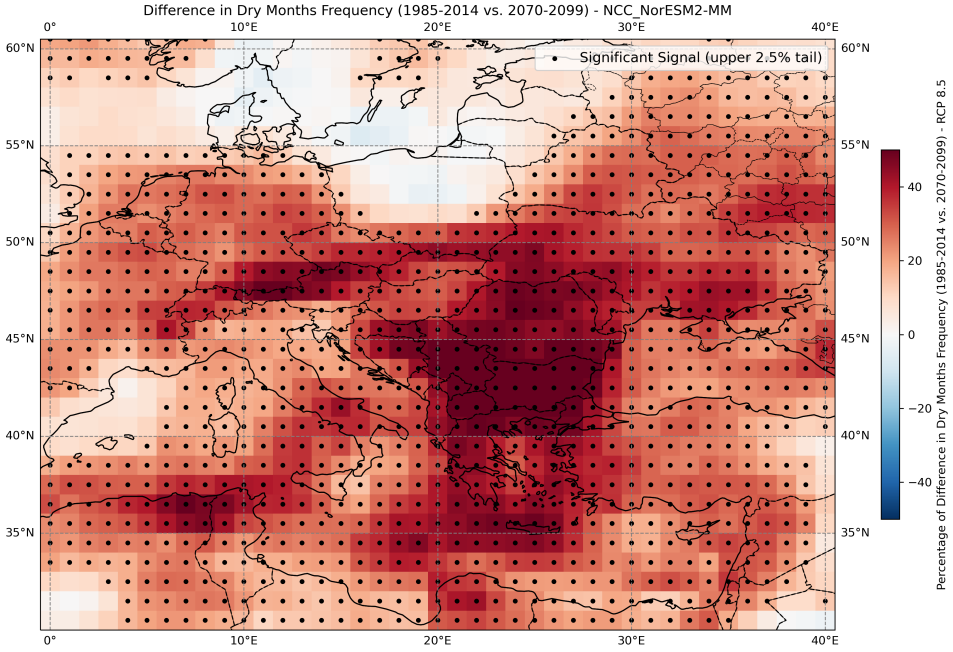

Figure B.28: Difference in dry months frequency for NCC NorESM2-MM.

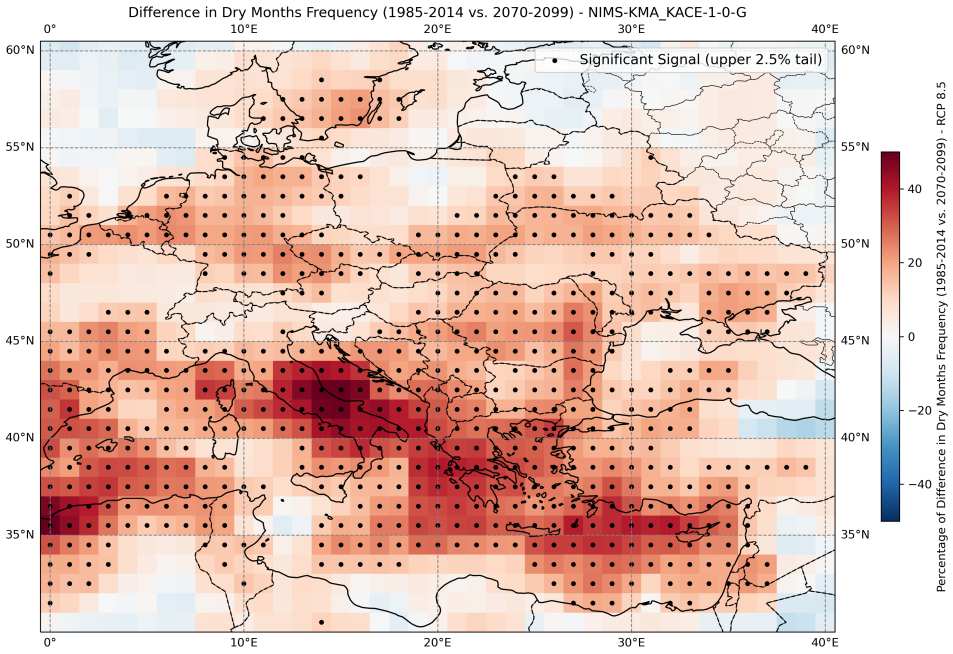

Figure B.29: Difference in dry months frequency for NIMS-KMA KACE-1-0-G.

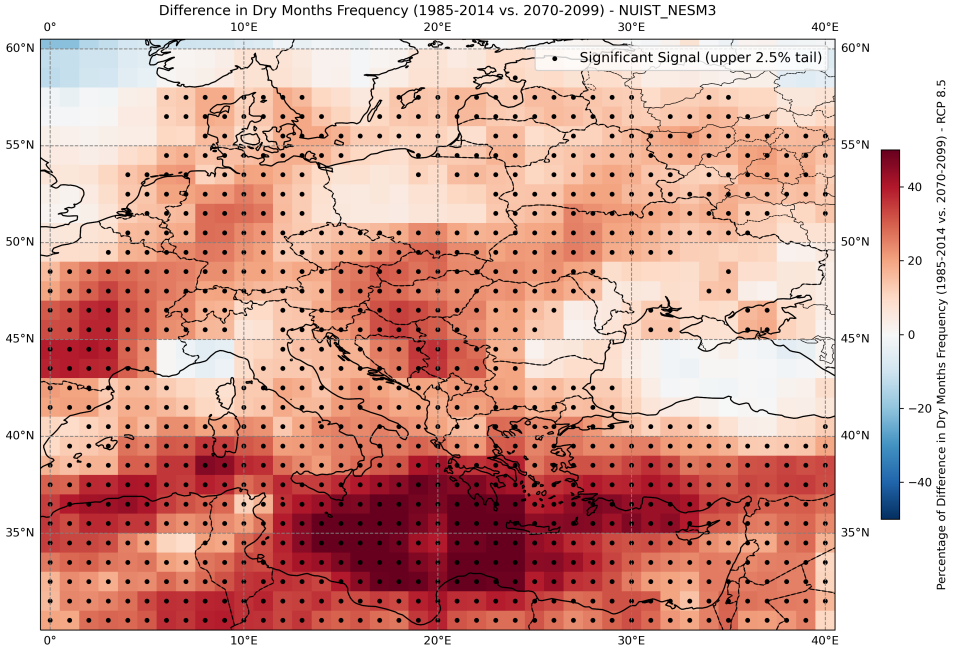

Figure B.30: Difference in dry months frequency for NUIST NESM3.

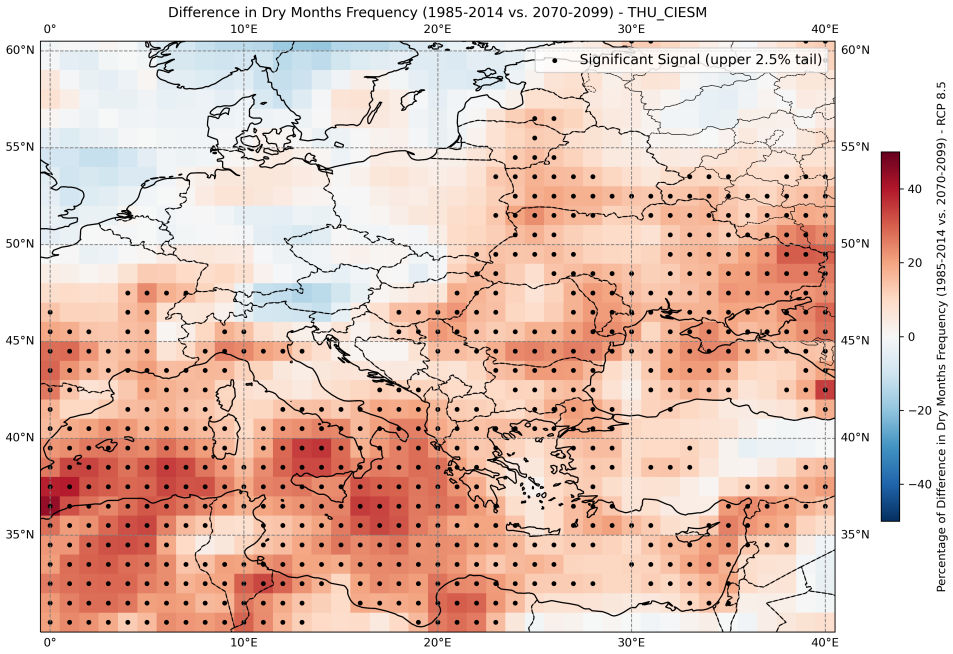

Figure B.31: Difference in dry months frequency for THU CIESM.